



Michigan Technological University
Create the Future Digital Commons @ Michigan Tech

Dissertations, Master's Theses and Master's
Reports - Open

Dissertations, Master's Theses and Master's
Reports

2011

Development and testing of an asymmetric capacitor with a nickel-carbon foam positive electrode

Wen Nee Yeo
Michigan Technological University

Follow this and additional works at: <https://digitalcommons.mtu.edu/etds>


 Part of the [Chemical Engineering Commons](#)

Copyright 2011 Wen Nee Yeo

Recommended Citation

Yeo, Wen Nee, "Development and testing of an asymmetric capacitor with a nickel-carbon foam positive electrode", Dissertation, Michigan Technological University, 2011.
<https://doi.org/10.37099/mtu.dc.etds/4>

Follow this and additional works at: <https://digitalcommons.mtu.edu/etds>

 Part of the [Chemical Engineering Commons](#)

DEVELOPMENT AND TESTING OF AN ASYMMETRIC CAPACITOR WITH A
NICKEL-CARBON FOAM POSITIVE ELECTRODE

By

Wen Nee Yeo

A DISSERTATION

Submitted in partial fulfillment of the requirements for the degree of

DOCTOR OF PHILOSOPHY

(Chemical Engineering)

MICHIGAN TECHNOLOGICAL UNIVERSITY

2011

© 2011 Wen Nee Yeo

This dissertation, "Development and Testing of an Asymmetric Capacitor with a Nickel-Carbon Foam Positive Electrode," is hereby approved in partial fulfillment of the requirements for the Degree of DOCTOR OF PHILOSOPHY IN CHEMICAL ENGINEERING.

Department of Chemical Engineering

Signatures:

Dissertation Advisor

Dr. Tony N. Rogers

Dissertation Co-Advisor

Dr. Bahne C. Cornilsen

Department Chair

Dr. Tony N. Rogers

Date

Table of Contents

List of Figures.....	vi
List of Tables	x
Acknowledgements	xi
Definitions.....	xiii
Abstract.....	xv
1.0 Introduction	1
1.1 Research Motivation / Objectives.....	1
1.2 Research Methodology	2
1.3 Organization of this Dissertation	3
2.0 An Overview of Asymmetric Capacitors with Emphasis on Nickel Hydroxide Asymmetric Capacitors.....	5
2.1 Abstract.....	6
2.2 Introduction.....	6
2.3 Nickel Electrode.....	12
2.4 Carbon Electrode	15
2.5 Electrolyte.....	16
2.6 Conclusions.....	17
3.0 Electrochemical Deposition of Nickel Hydroxide on Carbon Foam for Use as a Positive Electrode in an Asymmetric Capacitor	18
3.1 Abstract.....	19
3.2 Introduction.....	19
3.3 Experimental Setup.....	20
3.3.1 Preparation of a Nickel-Carbon Foam Positive Electrode.....	20
3.3.2 Materials Characterization	21
3.3.3 Electrochemical Characterization	21
3.3.3.1 Flooded Cell Capacitance Measurement	21
3.3.3.2 Fabrication of an Asymmetric Capacitor Cell	22
3.4 Results and Discussion	23
3.4.1 Nickel-Carbon Foam Positive Electrode	23

3.4.2	Materials Characteristics.....	25
3.4.3	Electrochemical Characteristics of the Nickel-Carbon Foam Positive Electrode	29
3.5	Conclusions.....	34
4.0	Examination of Various Carbon Electrodes Used in Aqueous Symmetric Capacitors.....	35
4.1	Abstract.....	36
4.2	Introduction.....	36
4.3	Experimental Setup.....	37
4.3.1	Electrode Preparation.....	37
4.3.2	Materials Characterization	37
4.3.3	Symmetric Capacitor Cell Preparation	38
4.4	Results and Discussion	38
4.4.1	Materials Characteristics.....	38
4.4.2	Cyclic Voltammetry.....	44
4.4.3	Galvanostatic Charge and Discharge	48
4.5	Conclusions.....	50
5.0	Optimization of the Performance of an Asymmetric Capacitor Based on a Nickel-Carbon Foam Positive Electrode.....	52
5.1	Abstract.....	53
5.2	Introduction.....	53
5.3	Experimental Setup.....	54
5.3.1	Preparation of Nickel-Carbon Foam Positive Electrode.....	54
5.3.2	Preparation of Negative Electrode	54
5.3.3	Materials Characterization	54
5.3.4	Preparation of Asymmetric Capacitor	54
5.4	Results and Discussion	55
5.4.1	Materials Characteristics.....	55
5.4.2	Electrochemical Characteristics.....	56
5.5	Conclusions.....	60

6.0 Comparison of Asymmetric Capacitors with Various Carbon Materials as the Negative Electrodes	62
6.1 Objective	62
6.2 Experimental Setup	62
6.3 Results and Discussion	62
6.4 Conclusions	63
7.0 Pouch Cell Design and Testing	64
7.1 Objectives	64
7.2 Experimental Setup	64
7.3 Results and Discussion	65
7.4 Conclusions	65
8.0 Conclusions and Future Work.....	68
8.1 Conclusions	68
8.2 Future Work	69
References	71
Appendix A Experimental Setup and Procedures.....	78
Appendix A1 Experimental Apparatus.....	78
Appendix A2 Experimental Procedures	78
Appendix B Electrode Morphology and Chemical Structure.....	82
Appendix B1 FE-SEM Images.....	82
Appendix B2 XRD Powder Patterns	89
Appendix B3 BET and Porosimetry.....	93
Appendix C Electrochemical Performance of Electrochemical Capacitors	96
Appendix C1 Symmetric Capacitors	96
Appendix C2 Asymmetric Capacitors.....	105
Appendix D Permission of Reprint.....	118

List of Figures

Figure 1.1.	Typical Swagelok [®] cell (open and assembled) and its cross-section.	3
Figure 2.1.	A generalized Ragone plot comparing energy storage and conversion devices.....	7
Figure 2.2.	Schematic of double layer on electrode (BDM model).....	8
Figure 2.3.	Schematic diagram of the charge/discharge process of asymmetric capacitors	12
Figure 2.4.	Bode diagram – two electrochemical cycles and their transformation via aging and overcharge process	13
Figure 2.5.	Modified Bode diagram – three electrochemical cycles and their transformation via aging and overcharge.....	14
Figure 3.1.	Schematic of the flooded cell for capacitance measurement.....	22
Figure 3.2.	A sealed cell using a PFA fitting. Left photo is the schematic view of the cell and the right photos are the unassembled and the assembled cell.	23
Figure 3.3.	Change in potential during constant current impregnation at 0.1 A/cm ² in 1.8 M Ni(NO ₃) ₂ and 0.26 M Co(NO ₃) ₂	24
Figure 3.4.	Voltage profile of the forming process for a nickel hydroxide electrode relative to a Hg/HgO reference electrode. Complete formation is defined when the last two cycles have the same capacity	25
Figure 3.5.	FE-SEM images of surface morphology of carbon foam taken at 50x and 100x magnifications.....	26
Figure 3.6.	FE-SEM image of the cross-section morphology of a carbon foam taken at 100x magnification.	27
Figure 3.7.	FE-SEM images of surface morphology of carbon foam impregnated with Ni(OH) ₂ taken at 100x and 1,000x magnifications.....	27
Figure 3.8.	FE-SEM images of cross-section morphology of carbon foam impregnated with Ni(OH) ₂ taken at 100x magnification. The left photo was taken near the edge of the foam and the right photo was taken near the center of the foam.	28
Figure 3.9.	XRD powder pattern of a POCOfoam [®]	28

Figure 3.10. XRD powder pattern of an as-deposited nickel-carbon foam electrode.....	29
Figure 3.11. Typical charge and discharge curves for nickel-carbon foam electrode relative to a Hg/HgO reference electrode cycled at 1 C-rate.	30
Figure 3.12. Specific capacitance at various discharge current densities.	31
Figure 3.13. CV of the nickel-carbon foam electrode relative to a Hg/HgO reference electrode at different scan rates in a T-cell.	32
Figure 3.14. CV of the nickel-carbon foam/AC asymmetric capacitor at different scan rates.	33
Figure 3.15. Charge and discharge behavior of the nickel-carbon foam/AC asymmetric capacitor at 10 mA/cm ²	33
Figure 3.16. Specific capacitance as a function of cycle number for a nickel-carbon foam/AC asymmetric capacitor cycled at 10 mA/cm ²	34
Figure 4.1. Schematic view and assembled symmetric capacitor cell. The cell body is constructed of a PFA fitting.	38
Figure 4.2. N ₂ adsorption/desorption isotherms of ACs. The upper graph contains the N ₂ adsorption/desorption isotherms for the three ACs, and the bottom graph shows RP-20 and YP-50F data only.	41
Figure 4.3. Mesopore size distributions of ACs. The upper graph exhibits the mesopore size distributions for the three ACs, and the bottom graph shows RP-20 and YP-50F data only. V is the pore volume and D is the pore diameter.	42
Figure 4.4. Comparison of XRD powder patterns of YP-50F, RP-20, and Ketjenblack EC-600JD.....	43
Figure 4.5. Comparison of XRD powder patterns of YP-50F, RP-20, and Ketjenblack EC-600JD, with background subtracted.	44
Figure 4.6. CV curves of RP-20 (top - 95 wt%, bottom - 90 wt%) at different scan rates.	45
Figure 4.7. CV curves of YP-50F (top - 95 wt%, bottom - 90 wt%) at different scan rates.	46

Figure 4.8. CV curves of Ketjenblack EC-600 JD (top - 95 wt%, bottom - 90 wt%) at different scan rates.	47
Figure 4.9. Charge and discharge curves of 95 wt% Ketjenblack EC-600JD symmetric capacitor.	49
Figure 4.10. Specific capacitances of a single electrode at various discharge current densities.....	49
Figure 4.11. Specific capacitance of a single electrode as a function of cycle number for various AC symmetric capacitors cycled at 20 mA/cm ²	50
Figure 5.1. FE-SEM images of surface morphology of carbon foam impregnated with Ni(OH) ₂ taken at 100x magnification. The left photo was of the carbon foam with full deposition and the right photo was of the carbon foam with partial deposition (deposition time: 51 and 25 minutes, respectively) ..	55
Figure 5.2. FE-SEM images of cross-section morphology of carbon foam (near the edge) impregnated with Ni(OH) ₂ at 100x magnification. The left photo was of the carbon foam with full deposition and the right photo was of the carbon foam with partial deposition.....	56
Figure 5.3. Specific capacitance as a function of discharge current density for an EDLC and six asymmetric capacitors with different mass ratios	57
Figure 5.4. Specific energy as a function of mass ratio cycling at a current density of 10 mA/cm ²	58
Figure 5.5. Ragone plot of asymmetric capacitors with various mass ratios at different current densities.	59
Figure 5.6. Specific capacitance and efficiency as a function of cycle number of an asymmetric capacitor with a mass ratio of 0.80 cycled at 10 mA/cm ²	60
Figure 5.7. CV of an asymmetric capacitor with a mass ratio of 3.71.....	61
Figure 6.1. Specific capacitance as a function of discharge current density for an EDLC and asymmetric capacitors with different mass ratios.....	63
Figure 7.1. Symmetric pouch cell based on Ketjenblack EC-600JD electrodes. Left photo is the completed cell and right photo is the completed cell compressed between two PTFE plates.....	65

Figure 7.2. Charge and discharge behavior of the 95 wt% Ketjenblack EC-600JD symmetric capacitor (pouch cell) at 5 mA/cm ²	66
Figure 7.3. Specific capacitance of single electrode versus cycle number. The pouch cell was cycled at 5 mA/cm ²	67

List of Tables

Table 2.1. Differences between rechargeable batteries and ECs.	9
Table 3.1. Conditions for electrochemical deposition.	21
Table 4.1. Pore characteristics of ACs.....	40
Table 4.2. Pore characteristics of carbon/PTFE electrodes.	40

ACKNOWLEDGMENTS

I would like to thank all people who have helped and encouraged me during my study at Michigan Technological University.

I especially want to thank Dr. Tony N. Rogers, the advisor, for his guidance and support he provided throughout my study. He was always accessible and willing to help his students with their research and treated them like his buddies. I also would like to express appreciations to Dr. Cornilsen, the co-advisor, for his guidance and suggestions in my experiments and dissertation writing.

I would like to extend my appreciations to Dr. Jason M. Keith and Dr. Wenzhen Li for their instruction and service as my committee members. I also wish to express my thanks to the consultants, Dr. Ralph J. Brodd for his suggestions and inputs in my experiment and discussion in electrochemistry, Dr. Steven M. Lipka from University of Kentucky for his technical support on making the negative electrodes, Dr. Joseph H. Holles for his input in my oral defense, Dr. Faith A. Morrison for letting me to work in her laboratory during my study, Mr. Edward A. Laitila for training me to operate the powder diffractometer, Dr. Julia A. King for giving me the Ketjenblack EC-600JD carbon black, and Dr. Matthew B. Chye, Ms. Jinjin Wang, and Mr. Daniel R. Woldring for their helps in my experiments.

I would like to thank Dr. Michael E. Mullins, Dr. Komar Kawatra, the Department of Material Science and Engineering, and the Department of Chemistry for letting me use their apparatus, equipment, and facilities throughout my study.

I also would like to thank Mr. Jerry A. Norkol, Mr. Tim P. Gasperich, Mr. David W. Caspary, Ms. Alexis Snell, and Ms. Felicia R. Nip. Jerry provided me the technical need on my experiment and also helped me in fixing the ASAP 2020 apparatus. Tim helped me to move and set-up the Arbin instrument. David enhanced my teaching experience by giving me an opportunity to teach in summer youth program and unit operation laboratory. Alexis assisted me with all the paperwork throughout my study. Felicia helped me in performing the FE-SEM. Thanks also goes to the colleagues in the

Department of Chemical Engineering and Malaysian Students Association, especially to Cho Hui Lim, Felix Adom, Edward Ng, Shu Wei Goh, Su Ting Lau, and Chee Huei Lee, for their friendship and kind assistance.

Thanks also go to Michigan Universities Commercialization Initiative (MUCI) and U.S. DOE (Contract DE-FG36-08GO88104) through the Michigan Tech Center for Nanostructured and Lightweight Materials (CNLM) for sponsoring this research and the opportunity for me to work in the project. I also would like to thank JME Capacitor, Inc. for their technical guidance, Celgard, LLC for donating their separators, and the Department of Chemical Engineering for the financial support.

I would like to express my deepest appreciations to my family, my boyfriend (Mr. Phie Theng Lee), and friends for their mental support and encouragements throughout my study. They always cheered me up and kept me motivated. This day would not occur without them.

Last but not least, I would like to thank everybody who assisted me before, as well as forgiving me that I could not mention personally one by one.

Definitions

active mass or

active material.

The electrode substance in which the electrochemical reaction takes place (half-cell reaction) during charging and discharging processes. For example, nickel hydroxide in the positive electrode is the active mass.

capacity.

It is defined as the total number of ampere-hours that can be withdrawn from a fully charged cell under specified discharge conditions. The capacity can be calculated by multiplying the constant discharge current by the time it takes to discharge.

C-rate.

It is defined as the rate to charge or discharge the rated capacity of the battery. For instance, a 1000 mAh battery gives 1000 mA for 1 hour if it discharges at a 1 C-rate or 500 mA for 2 hours if it discharges at a 0.5 or C/2 C-rate.

conductive holder.

It is a substance that is used to serve as a current collector which holds the active mass in position.

counter electrode.

It is an electrode that links the electrolyte to the working electrode in order for the current to flow to the working electrode.

electrode charging.

It is defined as the process of electrically storing energy in an electrode. The charging can be done either at a constant current or a controlled voltage.

electrode discharging.

It is defined as the process of electrically consuming energy stored in an electrode. The discharging can be done either at a constant current or a controlled voltage.

electrolyte.

A substance which behaves as an electrically conductive medium, connecting the positive and the negative electrodes in the cell.

formation process.	Deposited nickel hydroxide is a poor conductor and exhibits poor capacity. The formation process charges and discharges the material and “forms” or changes it into an electrochemically active material.
reference electrode.	It is an electrode which has a stable and well-known electrode potential.
specific capacitance.	The charge required to cause unit potential difference per unit mass of active material in a conductor. The units of specific capacitance are farads per gram (F/g) or coulombs per volt per gram.
specific energy.	It is also known as gravimetric energy density. It is used to indicate the amount of energy a cell can contains per unit mass of active material (W.h/kg).
specific power.	It is used to reflect the rate capability or the amount of current that can be delivered per unit mass of active material (W/kg).
working electrode.	It is the electrode where the reaction of interest takes place.

ABSTRACT

Electrochemical capacitors (ECs), also known as supercapacitors or ultracapacitors, are energy storage devices with properties between batteries and conventional capacitors. EC have evolved through several generations. The trend in EC is to combine a double-layer electrode with a battery-type electrode in an asymmetric capacitor configuration. The double-layer electrode is usually an activated carbon (AC) since it has high surface area, good conductivity, and relatively low cost. The battery-type electrode usually consists of PbO_2 or Ni(OH)_2 .

In this research, a graphitic carbon foam was impregnated with Co-substituted Ni(OH)_2 using electrochemical deposition to serve as the positive electrode in the asymmetric capacitor. The purpose was to reduce the cost and weight of the ECs while maintaining or increasing capacitance and gravimetric energy storage density. The XRD result indicated that the nickel-carbon foam electrode was a typical $\alpha\text{-Ni(OH)}_2$. The specific capacitance of the nickel-carbon foam electrode was 2641 F/g at 5 mA/cm^2 , higher than the previously reported value of 2080 F/g for a 7.5% Al-substituted $\alpha\text{-Ni(OH)}_2$ electrode.

Three different ACs (RP-20, YP-50F, and Ketjenblack EC-600JD) were evaluated through their morphology and electrochemical performance to determine their suitability for use in ECs. The study indicated that YP-50F demonstrated the better overall performance because of the combination of micropore and mesopore structures. Therefore, YP-50F was chosen to combine with the nickel-carbon foam electrode for further evaluation.

Six cells with different mass ratios of negative to positive active mass were fabricated to study the electrochemical performance. Among the different mass ratios, the asymmetric capacitor with the mass ratio of 3.71 gave the highest specific energy and specific power, 24.5 W.h/kg and 498 W/kg, respectively.

1.0 Introduction

1.1 Research Motivation / Objectives

Electrochemical capacitors (ECs), also called supercapacitors or ultracapacitors, store electrical charge within the electrochemical double layer at the electrode/electrolyte interface. In 1957, Becker obtained the first patent for ECs using a porous carbon electrode.¹ In 1966, SOHIO patented a device that utilized the double layer interface for energy storage.² ECs filled the gap between batteries and conventional capacitors. ECs have a higher power density compared to batteries and a higher energy density compared to capacitors. In addition, they have a longer cycle life compared to batteries because only a physical charge is involved. In recent years, this has created a focus on ECs in the market because of the need for high power and long cycle life energy storage devices.

There are three generations of ECs.³ The first generation is called symmetric capacitors (having the same electrode material for both positive and negative electrodes; usually, a high surface area carbon is used) with an aqueous electrolyte. The second generation is symmetric carbon capacitors but with a nonaqueous electrolyte. This type of capacitor can achieve higher voltages, up to 2.7 V, which increases the energy density over earlier ECs. The third generation is called asymmetric capacitors. In asymmetric capacitors, a rechargeable battery-type electrode (faradaic) is combined with a double-layer type of electrochemical capacitor electrode (non-faradaic).⁴ Asymmetric capacitors are more favorable compared to symmetric capacitors because they have higher capacitance and power density due to the battery-type electrode.⁵

The common types of asymmetric capacitors are $\text{PbO}_2|\text{H}_2\text{SO}_4|\text{C}$ and $\text{NiOOH}|\text{KOH}|\text{C}$. The $\text{NiOOH}|\text{KOH}|\text{C}$ system is of particular interest because nickel electrodes are well known in the battery industry since they can operate at low temperatures and are capable of a high rate of discharge. For the past few years, Michigan Technological University (MTU) has performed cycling tests using a nickel-carbon foam positive electrode in flooded cells.⁶ The capacity and cycle life of these cells at a variety of discharge rates are competitive with those batteries currently required by consumer electronics and power

tools. Operating prototype sealed cells with this new positive electrode and a carbon negative electrode are needed to understand the electrochemical performance relative to other asymmetric capacitors with NiOOH|KOH|C system. Studying the morphology and chemical structure will allow for a better understanding of the electrochemical behavior observed in the sealed cells.

The objectives of this research are:

- (i) To determine the specific capacitance and the material characteristics of the nickel-carbon foam electrode.
- (ii) To examine different carbon-based materials to serve as the negative electrode in an asymmetric capacitor through the study of an electric double layer capacitor (EDLC) and the carbon-based materials' morphology.
- (iii) To determine the optimum mass ratio (negative to positive active mass) for maximum specific energy through the study of electrochemical performance of the asymmetric capacitors assembled with different mass ratios. Research has shown that employment of the nickel hydroxide electrode in an asymmetric capacitor required determination of the optimum mass ratio.⁷

1.2 Research Methodology

Commercially, nickel hydroxide is deposited or pasted on a conductive support to make the nickel electrodes.^{8,9} The conductive support serves as a current collector which holds the active mass in position. In recent years, a graphitic carbon foam was impregnated with nickel hydroxide to make a nickel-carbon foam electrode and was tested in flooded cells. These have shown promising results.⁶ A sealed cell with a nickel-carbon foam positive electrode is needed to ascertain the possibility of replacing the nickel metal current collector with carbon foam.

The most commonly studied sealed cells in the laboratory are coin cells and “Swagelok[®] cells”. A “Swagelok[®] cell” is a sealed cell with limited electrolyte that is constructed using a compression tube fitting as a cell casing. Figure 1.1 shows a typical “Swagelok[®]

cell”. All the sealed cells in this research are constructed similar to this “Swagelok[®] cell” because this design has the following advantages:

- (i) Flexibility: The cell can be assembled and disassembled easily. This enables easy modifications and permit observations of any physical changes in the electrodes.
- (ii) Large electrodes: The size of electrodes can be thicker compared to those in coin cells which makes preparation of the electrodes simpler.
- (iii) Reusability: The cell can be reused multiple times.

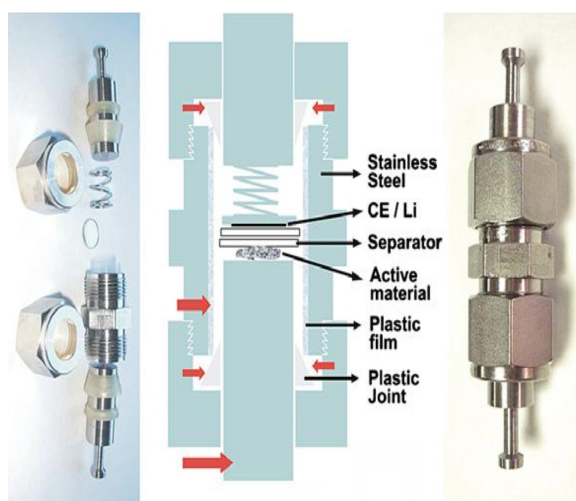


Figure 1.1. Typical Swagelok[®] cell (open and assembled) and its cross-section.¹⁰ CE is defines as counter electrode. The permission of reprint is provided in Appendix D.

1.3 Organization of this Dissertation

This dissertation consists of eight sections. The first section discusses the reasons for conducting this research, the approach of the research, and the organization of this dissertation. The next four sections consist of four papers. Section 2 is an overview of the asymmetric capacitor focusing on the nickel hydroxide system. Section 3 is about the performance of an asymmetric capacitor with a nickel-carbon foam that serves as the positive electrode. Section 4 is about examining different carbon materials through the study of symmetric capacitors. Section 5 is about optimizing the performance of an asymmetric capacitor by changing the mass ratio. Section 6 is about comparing

asymmetric capacitors using different negative electrodes. Section 7 is about assembling a pouch cell to demonstrate commercialization viability. The last section summarizes the conclusions and suggested future work. This dissertation also includes appendices containing the details of experimental procedures, additional data, graphs, and reprint permissions.

2.0

An Overview of Asymmetric Capacitors with Emphasis on Nickel Hydroxide Asymmetric Capacitors

Wen Nee Yeo ¹, Tony N. Rogers ^{1,3}, Bahne C. Cornilsen ²

¹ Department of Chemical Engineering, Michigan Technological University, 1400 Townsend Drive, Houghton, MI 49931-1295

² Department of Chemistry, Michigan Technological University, 1400 Townsend Drive, Houghton, MI 49931-1295

³ To whom correspondence should be addressed: Telephone: 906-487-2210, Fax: 906-487-3213, Email: tnrogers@mtu.edu, Postal address: 1400 Townsend Drive, Houghton, MI 49931-1295

Manuscript in preparation

2.1 Abstract

ECs also known as supercapacitors, are energy storage devices with properties between batteries and conventional capacitors. Similar to batteries, ECs must be series connected in order to meet operating voltage requirements. Single cell voltage of ECs typically ranges from 1 to 3 V, depending on the electrolyte used. Fundamental principles, characteristics, and a brief history of ECs are discussed in this paper. A discussion of the third generation of ECs, especially the NiOOH|KOH|C system is also included. Third generation ECs, asymmetric capacitors, combine a rechargeable battery-type electrode (faradaic) and a double-layer type of electrochemical capacitor electrode (non-faradaic).

2.2 Introduction

ECs also known as supercapacitors or ultracapacitors, are energy storage devices which utilize the double layer formed at the electrode/electrolyte interface.¹¹ The first patent, US 2,800,616, describing ECs using a porous carbon electrode was by Becker in 1957.¹ A device was patented in 1966 by SOHIO to store energy in the double layer interface (US 3,288,641).² ECs have been used as a backup power source for volatile computer and appliance memories for many years.¹² In the 1990s, ECs became popular because of the application in hybrid electric cars. In this case, ECs obtained energy from the regenerative braking is used as a temporary energy storage device with high power capability. This stored energy is then redistributed in the following phase of acceleration of the vehicle.¹³

It is a known fact that batteries have a higher energy density whereas capacitors have a higher power density. This makes batteries a better choice for the storage of energy and capacitors a better choice for applications where energy needs to be expended or stored in quick powerful repetitive pulses. ECs fill in the gap between batteries and capacitors and this has made them draw attention in recent years. This niche can be represented in the Ragone plot in Figure 2.1. As illustrated in Figure 2.1, ECs have a higher specific energy than capacitors and have a higher specific power than most batteries. In addition, ECs are

believed to have long cycle life because no, or negligible, chemical reactions are involved. The storage mechanism is based on physical charge storage.

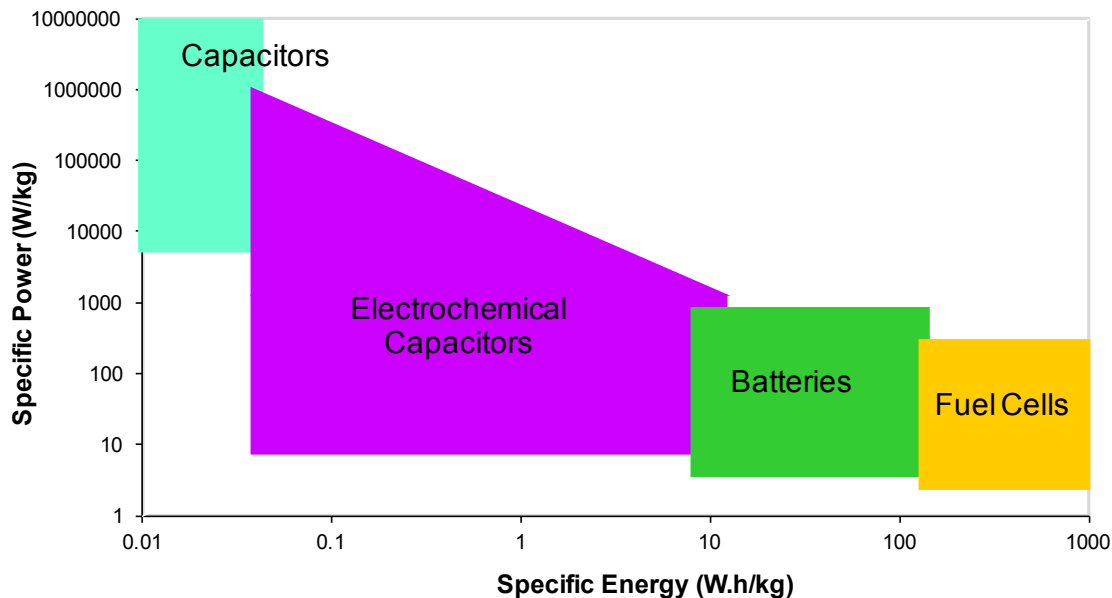


Figure 2.1. A generalized Ragone plot comparing energy storage and conversion devices.

The principle of energy storage for ECs utilizes the double layer, also known as the Helmholtz layer, formed at the electrode/electrolyte interface. It was first described in the work of Hermann von Helmholtz in 1853. His work focused on a “physical model in which a single layer of ions is adsorbed at the surface”.¹⁴ Louis Georges Gouy and David Leonard Chapman extended the model by proposing a diffuse electrical double layer. However, this model is not suitable for highly charged double layers.¹⁴ Therefore, Stern combined Helmholtz and Gouy-Chapman models to overcome this limitation.¹⁴ The most recent model is by Bockris, Devanathan, and Muller (BDM’s model). This model shows the presence and orientation of solvent dipole (Figure 2.2).¹⁴

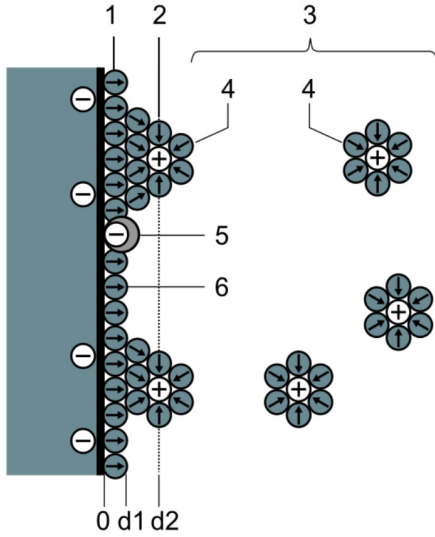


Figure 2.2. Schematic of double layer on electrode (BDM model). 1 and 2 denote the inner and outer Helmholtz layers, respectively. 3 is the diffuse layer. 4 is the solvated ions and 5 is the peculiar adsorbed ions. Lastly, 6 is the solvent molecule. Figure reproduced from reference ¹⁴.

Capacitance (C) is defined as the ability to hold an electrical charge. Capacitance can be expressed as the ratio of a charge (q) to the inter-plate voltage (V) as shown in equation 2.1. The unit of capacitance is the farad (F) or coulombs per volt.

$$C = \frac{q}{V} \quad (2.1)$$

The common type is the parallel-plate capacitor.¹⁵ Its capacitance depends on the area of the contact plates (A) and the distance between the plates (d) as show in equation 2.2. For a smooth electrode in a solution with high electrolyte concentration, the capacitance is about $10\text{-}20 \mu\text{F}/\text{cm}^2$.¹³ However, a higher capacitance can be achieved for a porous electrode with a large internal effective area (1000 or more m^2/g).

$$C \propto \frac{A}{d} \quad (2.2)$$

“Capacitance is also a measure of the amount of electrical energy stored (or separated) for a given electric potential.”¹⁵ As shown in equation 2.3, the stored energy in ECs directly proportional to the capacitance and increases as the square of the cell voltage as charge is accumulated.

$$Energy = \frac{1}{2} CV^2 \quad (2.3)$$

Similar to batteries, ECs must be series connected in order to meet operating voltage requirements. This is because the operating voltage of ECs is limited by the breakdown potential of the electrolyte and therefore much lower than that of conventional capacitors. There are differences between batteries (rechargeable) and ECs, even though both serve as energy storage devices. The main difference between the two is batteries use chemical charge storage whereas ECs use physical charge storage. The power density for batteries is lower because it is limited by reaction kinetics and mass transport. When charging or discharging most batteries, the operating voltage is relatively constant, whereas there is consistently an intrinsic increase of voltage on charge or decrease on discharge for ECs. The cycle life of batteries is usually has several hundreds of cycles but ECs can endure millions of cycles. This is because the storage mechanism of ECs is a highly reversible electrostatic charge whereas batteries involve electrochemical conversions of active mass.¹⁶ Table 2.1 summarizes the differences between the two.

Table 2.1.
Differences between rechargeable batteries and ECs.

Property	Secondary Batteries	Electrochemical Capacitors
Storage mechanism	Chemical	Physical
Power density	Lower, slower	Higher, faster
Energy limitation	Electrode mass (bulk)	Electrode surface area
Output voltage	Approximate constant value	Sloping value
Charge rate	Kinetic reaction, mass transport limited	Very high, same as discharge rate
Cycle life	Up to several hundreds	Up to millions
Life limitation	Thermodynamic stability	Side reactions

ECs have evolved through several generations. The first generation is the symmetric construction with an aqueous electrolyte. Symmetric construction means the same type of

electrode material has been used for both positive and negative electrodes of the ECs device. Therefore, this type of capacitor is also called EDLC. High surface area carbon usually serves as the electrode material. It was originally produced with stored energy up to ten joules.¹² Besides high surface area carbon, ruthenium dioxide was the favored electrode material in early ECs, especially in the space and military applications.¹⁷ These capacitors gave high specific power, but never reached commercial scale production because the cost for the electrode material was high.

The second generation is the symmetric carbon capacitors but with a nonaqueous electrolyte. This type of capacitor can achieve higher voltage, up to 2.7 V, and hence increases in energy density over earlier ECs. The cell voltage is limited by the water content of the electrolyte.¹³ The disadvantage of this second generation ECs in the early stage is that it is lower in power performance due to the use of the low conductivity electrolyte. However, with the electrolyte changed to acetonitrile (higher conductivity), the power performance can compete with those with aqueous electrolyte ECs.

The third generation of ECs, introduced in 1997, is called an asymmetric capacitors.^{18,19} The beginning of asymmetric capacitors development was by a Russian company, ESMA. This capacitor used a nickel (NiOOH) positive electrode with a high surface area carbon negative electrode in a potassium hydroxide (KOH) electrolyte.¹⁸ In asymmetric capacitors, a rechargeable battery-type electrode (faradaic) is combined with a double-layer type of electrochemical capacitor electrode (non-faradaic).⁴ Therefore, this cell has a higher capacitance because the faradaic positive electrode has a much larger capacitance ($C_{+ve} \gg C_{-ve}$, refer to equation 2.4, C_{Cell} = total capacitance of the cell, C_{+ve} = capacitance of the positive electrode, C_{-ve} = capacitance of the negative electrode).⁵ In addition, the capacity of the positive electrode is much larger than the negative electrode, which reduces the depth of discharge of the positive. As a result, the positive electrode has a longer cycle life which allows the asymmetric capacitor to have a high cycle life.

$$\frac{1}{C_{Cell}} = \frac{1}{C_{+ve}} + \frac{1}{C_{-ve}} \quad (2.4)$$

The most common systems for the faradaic electrode are the $\text{PbO}_2/\text{PbSO}_4$ and the $\text{NiOOH}/\text{Ni}(\text{OH})_2$ materials.^{19,20} The faradaic electrode has advantages and disadvantages relative to the non-faradaic electrode. The advantages are listed below:⁴

- a. It has higher energy density.
- b. It has a relatively constant voltage profile; except for Li-intercalation electrodes.
- c. It is more stable as the potentials are thermodynamically based. This can help the self-discharge of the asymmetric capacitor cell become less, as it is determined by only one electrode rather than two electrodes (potentials in opposite directions) in the symmetric cell.

The disadvantages are listed below:⁴

- a. It has lower power density.
- b. It has less cycle life.
- c. Its cycle life depends on the charge and discharge rates and the depth of discharge.
- d. The performance of the faradaic electrode under different temperatures is different from the non-faradaic electrode because involves different activation energies and temperature-dependent degradation processes.
- e. It is less reversible and can only be cycled at lower C-rates due to phase changes (not a problem with NiOOH).

This paper is focused on the asymmetric capacitors in which a nickel (NiOOH) positive electrode and a high surface area carbon negative electrode are used in a potassium hydroxide electrolyte ($\text{NiOOH}|\text{KOH}|\text{C}$). This system is one of the oldest and well-studied electrochemical systems with industrial production and mass application.²¹ The use of this system is for starting internal combustion engines and electric transport.²² The principles on which asymmetric capacitors operate are based on charge and discharge at a constant current. During charging, the faradaic electrode undergoes a change in the oxidation state, while the non-faradaic electrode physically absorbs hydrated K^+/H^+ ions at the interface.⁷ During the discharge, the opposite behavior occurs. Figure 2.3 shows the schematic diagram of the reactions that occur at both electrodes.

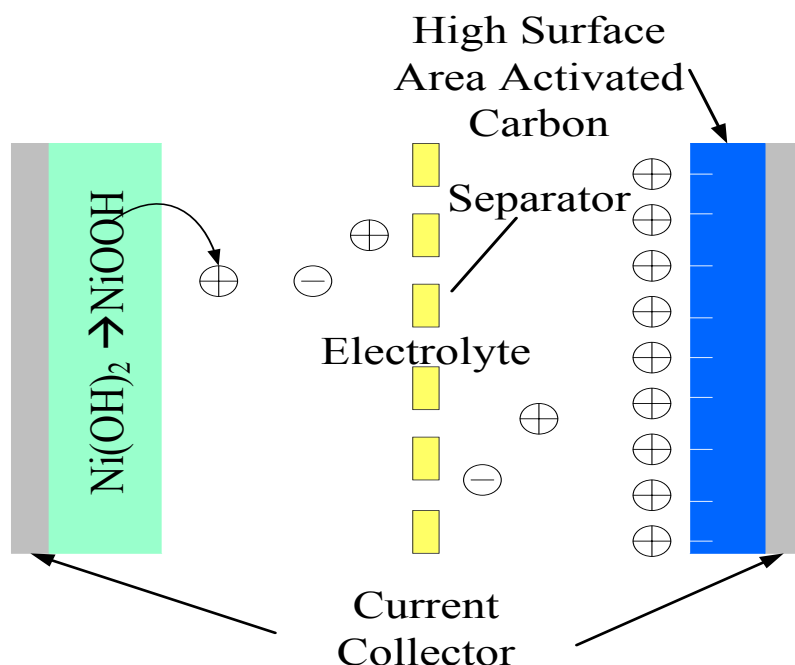


Figure 2.3. Schematic diagram of the charge/discharge process of asymmetric capacitors.

2.3 Nickel Electrode

The nickel electrode is the positive electrode for all nickel-based batteries. The first nickel-based battery, Ni-Cd battery, was built in 1900 by Waldemar Junger and Karl Berg.²³ This battery dominated the market for a long period due to its long cycle life and wide range of operating temperatures. The efficiency of nickel batteries significantly depends on the nickel electrode. Commercially, nickel hydroxide is deposited or pasted on a conductive holder to make the nickel electrodes.^{8,9} The conductive holder serves as a current collector which holds the active mass in position. Improvement on the positive electrode therefore becomes the highest priority in increasing the performance of the nickel-based energy storage systems. Over the years, different types of nickel electrode, such as a pocket electrode, pressed electrode, and sintered electrode, have been developed to improve the performance, lower the manufacturing cost, and reduce emission of waste materials.

The primary attraction of ECs is that the charge and discharge processes are reversible. This means the energy consumed during the discharge can be replaced by recharging the

EC. The nominal redox reaction that takes place in the nickel electrode is given in equation 2.5. Nickel oxyhydroxide (NiOOH) is the active mass of the nickel electrode in the charged state. During the charging process, nickel hydroxide (Ni(OH)₂) is oxidized to NiOOH. During the discharge process, NiOOH is reduced to Ni(OH)₂. A consequence of charge and discharge is a change in the structure of the active mass. Over the years, research has been done to further understand and improve the properties of nickel electrodes by studying the charge and discharge processes of nickel electrode.



Bode, *et al.* proposed the reaction in terms of four phases (see Figure 2.4): (i) an anhydrous phase termed β -Ni(OH)₂, (ii) a hydrated phase termed α -Ni(OH)₂, (iii) an oxidized phase termed β -NiOOH, and (iv) an oxidized phase termed γ -NiOOH.²⁴ Oxidation or charging of α -Ni(OH)₂ forms γ -NiOOH and the oxidation of β -Ni(OH)₂ forms β -NiOOH. The β -phase converts to γ -phase on overcharge and takes the active materials to the α - γ cycle. In concentrated alkali, the α -phase ages to the β -phase and back to the β - β cycle.

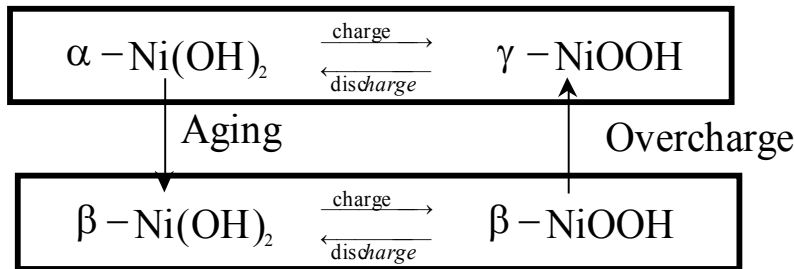


Figure 2.4. Bode diagram – two electrochemical cycles and their transformation via aging and overcharge process.

Nickel active material is considered to be a layered structure of NiO₂. Each layer is composed of a sandwich of two close packed oxygen layers (AB) with nickel cations filling the octahedral interstices. These NiO₂ layers can then be stacked in either close (ABAB) or non-close (ABBCCA) packed structures. β -Ni(OH)₂ has an ABAB close packed structure, while γ -NiOOH has the ABBCCA non-close packed structure.²⁵ It was

initially thought that α -Ni(OH)₂ had the ABAB close packed structure as well.²⁵ However, Cornilsen and co-workers showed that these four active materials all have an ABBCCA non-close packed structure.^{9,25,26} Note that β and 2β differ in structure. Figure 2.5 summarizes these results.

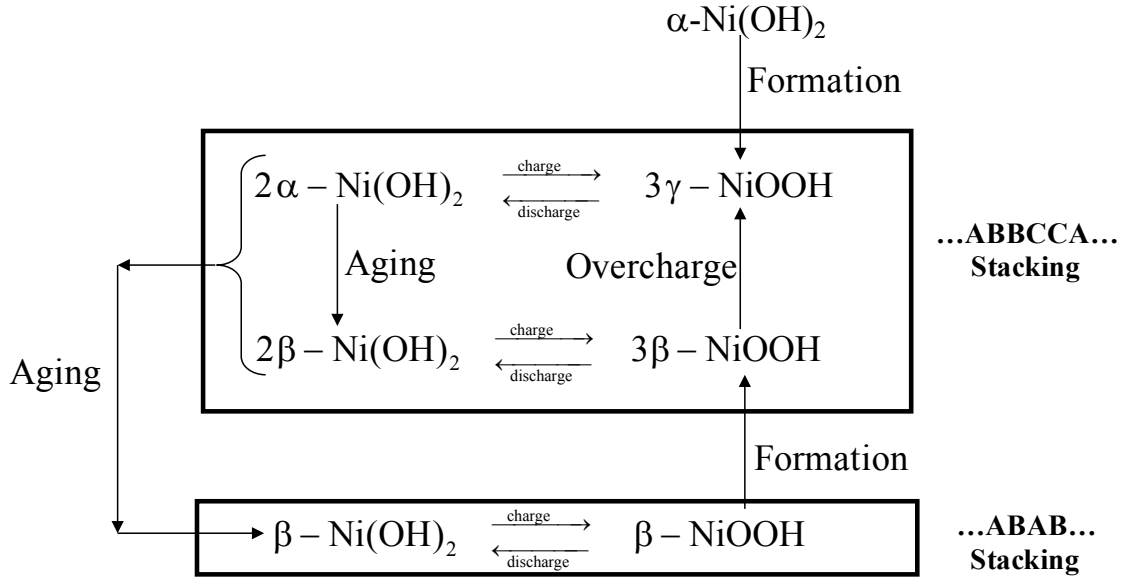
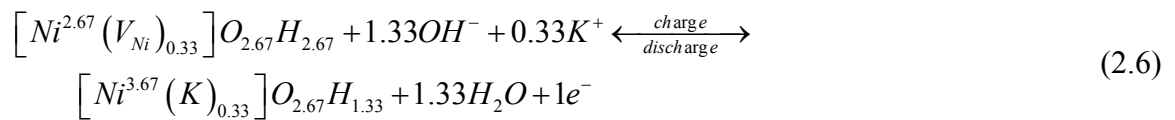


Figure 2.5. Modified Bode diagram – three electrochemical cycles and their transformation via aging and overcharge.²⁷ The permission of reprint is provided in Appendix D.

The $2\alpha/3\gamma$ and $2\beta/3\beta$ cycles have the non-close packed structure and therefore there is no phase change during the reaction.⁹ A structural change is involved as the 2α and 2β age because true β materials are close packed. Cornilsen and co-workers also showed that the nickel hydroxides in active mass are nonstoichiometric, containing point defects.^{9,25-27} During “forming” and cycling the nickel electrode nonstoichiometry can and does change (see equation 2.6).²⁷ Most importantly this nonstoichiometry controls the oxidation states of the 2α (2.67), 3γ (3.67), 2β (2.25), and 3β (3.25) phases.⁹



2.4 Carbon Electrode

Carbon, especially activated carbon (AC), is commonly used as the electrode for energy storage devices. The reasons include (i) availability, (ii) low cost, (iii) high surface area, (iv) high conductivity, and (v) established electrode production technologies.^{28,29}

Carbon from different precursors can be activated using a thermal or chemical process to increase the surface area and the porosity. Thermal activation is a gasification process to modify the precursor at temperatures between 700 and 1100 °C. The common gases used are steam, carbon dioxide, air, and mixtures of these gases. Chemical activation activates the carbon by dehydrating phosphoric acid, zinc chloride or potassium hydroxide at temperatures between 400 and 700 °C. Post-activation is needed for this process to remove the residue from the reactants and also from the carbon precursors. A high surface area of up to 3000 m²/g can be achieved from the activation process. In general, the larger the surface area of carbon, the higher the ability for charges to accumulate at the electrode/electrolyte interfaces and hence the higher the capacitance.^{30, 31} However, not all the ACs follow this trend perfectly. This is because not all the micropores are electrochemically accessible for the electrolyte ions.^{32, 33} For AC, the capacitance is between 100 to 200 F/g in aqueous solution and 50 to 150 F/g in organic solution.³¹ The reasons for the higher value in aqueous solution are the smaller size of the solvated ions and higher dielectric constant compared to organic solution.

As seen in the above, the pore structure on carbon plays a vital role in the performance of the capacitor. For a high power application, large pore size is more favorable because better ion diffusion can occur. However, this will in turn decrease the surface area. A carbon with wide pore size distribution and random connected pores will limit the charge storage capacity and rate capability. In addition, the electrolyte may not reach those isolated or closed pores and ions are difficult to move when the pore network is irregular. Therefore, to assure good charge distribution and delivery, the carbon should have micropores of narrow pore size interconnected with a regular network. In addition, a

sufficient amount of mesopores are also needed for a rapid mass transport of electrolyte ions to the electrode.^{30,34,35}

Another factor to take into consideration when choosing an appropriate carbon to use in ECs is the functional groups, such as oxygen, nitrogen, sulfur, and hydrogen, that are present in the carbon. A variable amount of foreign elements can be present in carbon due to different precursors and processing conditions. These foreign elements can modify the electrochemical interfacial state of the carbon surface and its double-layer properties (e.g. absorption of ions and wettability).³⁰ Among the common functional groups, nitrogen is the most studied element in the literature.³⁶⁻³⁸

In the future, the development of carbon electrodes should focus on tailor-made pore size distribution with foreign elements to yield electrodes with high capacitance and also maintain low cost.

2.5 Electrolyte

The electrolyte use in asymmetric capacitors can be categorized into solid and liquid. An example of a solid electrolyte is polyacids (e.g. isopolyacids and heteropolyacids) but it is not preferred due to high corrosion.³⁹ Liquid electrolytes can be either organic or aqueous. An organic electrolyte allows the cell voltage of the ECs to be above 2 V, whereas an aqueous electrolyte limits the cell voltage to < 1.2 V. Thus, aqueous electrolytes have a lower stored energy compared to organic electrolytes according to equation 2.3. A Japanese company plans to increase the voltage window to 3.2 V by applying extreme purification procedures on the organic electrolyte and reducing the corrosion of carbon electrodes by special protective coatings.⁴⁰ This will further increase the stored energy of EC.

The disadvantage of an organic electrolyte is it has lower power performance (at least lower by 20 times) compared to a concentrated aqueous electrolyte.¹³ In addition, an aqueous electrolyte usually has the advantages of low cost and non-flammability compared to an organic electrolyte. This makes it the preferred electrolyte.

One important thing, the concentration of the electrolyte has to be high to avoid degradation problems during the cycling of the ECs. This is extremely important for an organic electrolyte where the electrolyte solubility is low.⁴¹ For a nickel hydroxide asymmetric capacitor, the preferred electrolyte is KOH with a typical concentration between 25 and 45 weight percent.⁴²

2.6 Conclusions

ECs have evolved through three generations. The first and second generations are symmetric capacitors with different electrolytes. The third generation is called asymmetric capacitors. It has higher capacitance and energy density compared to conventional capacitors due to the use of faradaic electrode as the positive electrode.

The NiOOH|KOH|C system is discussed in this paper. NiOOH is the active mass of the nickel electrode in the charged state. The charge and discharge processes involve a change in the oxidation state or defect content. In addition, the nickel hydroxides in active mass are nonstoichiometric, containing point defects that control the oxidation states. Carbon materials are commonly used as the negative electrodes in asymmetric capacitors. When choosing a suitable carbon electrode, surface area, pore size, and the functional groups attached to the carbon need to be taken into consideration. Aqueous electrolyte is preferred even though it lowers the stored energy in the capacitor. This is because it has cost and safety advantages. The electrolyte used in nickel asymmetric capacitor is KOH with a typical concentration between 25 and 45 weight percent.

ECs, especially the NiOOH|KOH|C system, may well be the next generation of energy storage for certain applications requiring high cycle life and high rate capabilities as it combines the advantages of both capacitors and rechargeable batteries. More research and development is needed in order to further reduce the manufacturing cost and increase the cell voltage.

3.0

Electrochemical Deposition of Nickel Hydroxide on Carbon Foam for Use as a Positive Electrode in an Asymmetric Capacitor

Wen Nee Yeo ¹, Tony N. Rogers ^{1,3}, Bahne C. Cornilsen ²

¹ Department of Chemical Engineering, Michigan Technological University, 1400 Townsend Drive, Houghton, MI 49931-1295

² Department of Chemistry, Michigan Technological University, 1400 Townsend Drive, Houghton, MI 49931-1295

³ To whom correspondence should be addressed: Telephone: 906-487-2210, Fax: 906-487-3213, Email: tnrogers@mtu.edu, Postal address: 1400 Townsend Drive, Houghton, MI 49931-1295

Manuscript in preparation

3.1 Abstract

Carbon foam impregnated with nickel hydroxide via an electrochemical deposition method was prepared for the positive electrode of an asymmetric capacitor. In this application, carbon foam was chosen to serve as the current collector due to its electrical conductivity, pore size, connectivity, nominal cost, and light weight. The surface morphology and chemical structure of the positive electrode were studied through FE-SEM and XRD. The FE-SEM results demonstrated that the positive electrode has uniform particles and a loose packed structure. The XRD results indicated that the deposited positive electrode is a typical α -Ni(OH)₂. The specific capacitance of this nickel-carbon foam electrode was found to be 2641 F/g at 5 mA/cm², which was higher than the reported literature value of 2080 F/g for a 7.5% Al-substituted α -Ni(OH)₂ electrode. The nickel-carbon foam electrode was then combined with a commercial AC to become an asymmetric capacitor. The average specific capacitance and specific energy of the cell for a cell voltage between 1.4 to 0.8 V were 129.2 F/g and 19.9 W.h/kg, respectively.

3.2 Introduction

ECs, also known as supercapacitors or ultracapacitors, have drawn attention in recent years because they can store and deliver energy at relatively high rates. The energy storage mechanism of ECs is the ion double layer formed at the electrode/electrolyte interface.¹¹ In addition, ECs have a higher power density compared to batteries. This makes ECs a better choice for applications where energy needs to be expended or stored in quick, powerful repetitive pulses. Currently, the most promising application is to use ECs in electric hybrid vehicles. Another advantage of ECs is they provide a longer cycle life than batteries. This is because no volume change (unlike a faradaic electrode) is observed in the highly-reversible electrostatic charge storage mechanism in the ECs.¹⁶

ECs have evolved through several generations. The first and second generations are symmetric capacitors with aqueous and organic electrolytes, respectively. The third generation is called asymmetric capacitors. They were introduced in 1997 and developed

by a Russian company, ESMA.^{18,19} In asymmetric capacitors, a rechargeable battery-type electrode (faradaic) is combined with a double-layer type of electrochemical capacitor electrode (non-faradaic).⁴ Therefore, this cell has a higher capacitance because the faradaic positive electrode has a much large capacitance ($C_{+ve} \gg C_{-ve}$, refer to equation 2.4).⁵

Two common types of asymmetric capacitors are $PbO_2|H_2SO_4|C$ and $NiOOH|KOH|C$. The $NiOOH|KOH|C$ system is of particular interest because it can operate at low temperatures and is capable of high rates of discharge.

In this work, a carbon foam (conductive support) impregnated with nickel hydroxide using an electrochemical deposition method serves as the faradaic electrode in the EC. Carbon foam is used as the conductive support due to its electrical conductivity, pore size, and connectivity.^{6,43} In addition, the low material cost and light weight of carbon foam overcome two of the disadvantages of the nickel electrode. Electrochemical deposition was chosen because it gave the highest level of loading compared to chemical and thermal impregnation.⁶ Furthermore, the electrode loading and pore filling can be controlled precisely by changing the deposition bath temperature and the deposition potential.⁴⁴

3.3 Experimental Setup

3.3.1 Preparation of a Nickel-Carbon Foam Positive Electrode

Carbon foam from Poco Graphite, Inc. was studied as an alternative positive electrode support. The carbon foam was washed with a deionized water/ethanol solution in a sonicator bath for 30 minutes to remove any loose particles and then dried under vacuum prior to use. The entire deposition process was maintained at 70°C in a heating bath and conducted using the Arbin MSTAT electrochemical testing system.⁶ Table 3.1 summarizes the conditions for the electrochemical deposition. The reagents were all of AR grade and the water used in the synthesis was deionized. In addition, the nickel hydroxide solution contained 45 vol% denatured ethanol, which serves as a wetting agent.

The advantages of adding ethanol are to lower the deposition temperature, increase the loading level, and reduce electrode swelling.⁶

Table 3.1.
Conditions for electrochemical deposition.

Step	Counter Electrode	Ni(NO ₃) ₂ Conc. (M)	Co(NO ₃) ₂ Conc. (M)	Temperature (°C)	Current Density (A/cm ²)	Time (min)
Pre-deposition Deposition	Ni	1.8	0.26	70	0.055 0.100	45 (variable)

After deposition, the nickel-carbon foam electrode was washed with deionized water to remove excess Ni(NO₃)₂ and the electrode was formed to convert the nickel hydroxide into active mass. The formation process occurred as the nickel hydroxide underwent 5 cycles of charge and discharge in a flooded cell. The aqueous electrolyte contained 26 wt% of KOH. The first cycle was charged for 60 minutes at 70 mA/cm² and discharged at 70 mA/cm² to 0 V (relative to Hg/HgO). The next 4 cycles were charged for 45 minutes at 20 mA/cm² and discharged at 20 mA/cm² to 0.15 V.

3.3.2 Materials Characterization

The morphologies of carbon foam (as-received) and nickel-carbon foam positive electrodes were investigated using field emission scanning electron microscope (FE-SEM) (Hitachi S-4700). X-ray diffraction (XRD) was performed on a Scintag XDS2000 powder diffractometer with Cu K α radiation ($\lambda = 1.5406 \text{ \AA}$) operating at 45 kV and 35 mA to characterize the structure of carbon foam (as-received) and Ni(OH)₂ active materials.

3.3.3 Electrochemical Characterization

3.3.3.1 Flooded Cell Capacitance Measurement

After the formation process, the nickel-carbon foam electrode was transferred to a flooded cell to measure its capacitance. A schematic of the flooded cell is shown in Figure 3.1. The cell was a 250 ml sample jar with four components: two counter electrodes (nickel foil plates), a working electrode (nickel-carbon foam electrode), and a

Hg/HgO reference electrode. The aqueous electrolyte contained 26 wt% of potassium hydroxide (KOH).

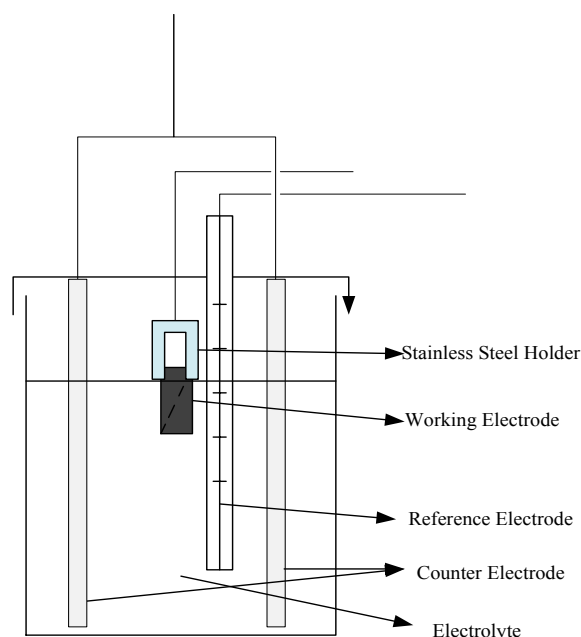


Figure 3.1. Schematic of the flooded cell for capacitance measurement.

3.3.3.2 Fabrication of an Asymmetric Capacitor Cell

After the formation process, the nickel-carbon foam electrode was transferred to a sealed cell, which acts as an asymmetric capacitor, for cycling to examine its electrochemical properties. The sealed cell consisted of a clear perfluoroalkoxy fluorocarbon (PFA) compression tube coupling (body, nuts, and ferrules) for $\frac{3}{4}$ -in ID tubing from McMaster-Carr, along with two $\frac{3}{4}$ -in OD SS plungers. The two gripping rings were poly(ethylene-co-tetrafluoroethylene) (ETFE). The nickel-carbon foam positive electrode was placed against a nickel mesh to ensure good connectivity with one of the plungers. Two layers of separator membrane made of microporous polypropylene were soaked with electrolyte solution (26 wt% KOH) and then placed against the positive electrode. A commercial carbon negative electrode was placed against the separators to complete the electrode stack. Before placing the negative electrode into the PFA cell, the negative electrode was soaked for days in the electrolyte to allow electrolyte uptake within the pores. A nickel mesh was placed against the negative electrode for good connectivity. Then, a plunger

was inserted on the negative electrode side. The nuts compressed the ferrules to hold the plungers in place and to provide a seal. Figure 3.2 shows the schematic view, unassembled and assembled sealed cell.

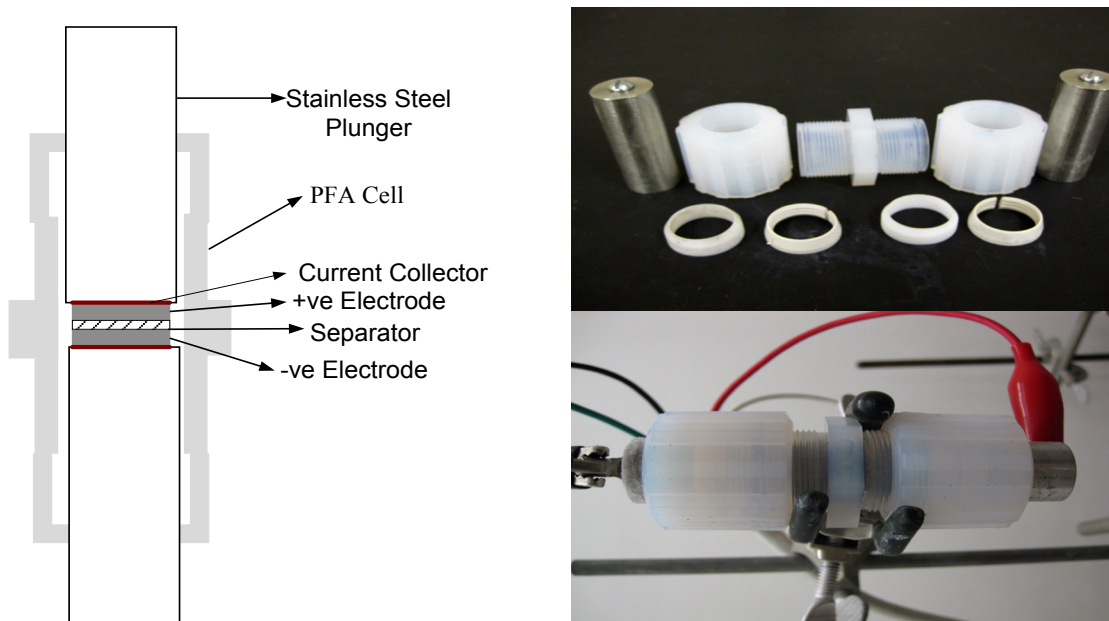


Figure 3.2. A sealed cell using a PFA fitting. Left photo is the schematic view of the cell and the right photos are the unassembled and the assembled cell.

3.4 Results and Discussion

3.4.1 Nickel-Carbon Foam Positive Electrode

During the deposition, cobalt hydroxide was deposited along with the nickel hydroxide to produce a solid solution.^{45,46} The addition of the cobalt is believed to enhance the electrical conductivity of the electrode, raise the oxygen evolution potential, and prolong the cycle life of the electrodes.⁴⁷⁻⁴⁹ The deposition involves 2 steps at a constant current and 70°C. These optimized conditions were based on observations of the performance of the nickel-carbon foam positive electrode.⁵⁰ The first step is called pre-deposition. Based on previous experience in flooded cells, carbon foams that underwent this treatment performed better during charge/discharge cycling. This step is believed to have modified the surface structure of the carbon foams and therefore improved the active mass loading.⁵⁰ The second step is the deposition, where active mass is deposited into the pores

of the carbon foam. Figure 3.3 shows the change in potential during a constant current deposition. At about -2.9 V (where it was fully loaded), the pores were filled and green $\text{Ni}(\text{OH})_2$ began to deposit on the surface. Since each electrode behaved differently, the voltage was monitored to determine when surface deposition began to take place.

Before the electrode is able to undergo charge/discharge cycling, the electrode must be subjected to a forming process to convert the nickel hydroxide into active mass. This activation changes the electrode structure, increasing conductivity, and achieves stable charge and discharge behavior (refer to Figure 3.4). The number of cycles required for the forming process must be kept to a minimum to reduce the cost of manufacturing a positive electrode.

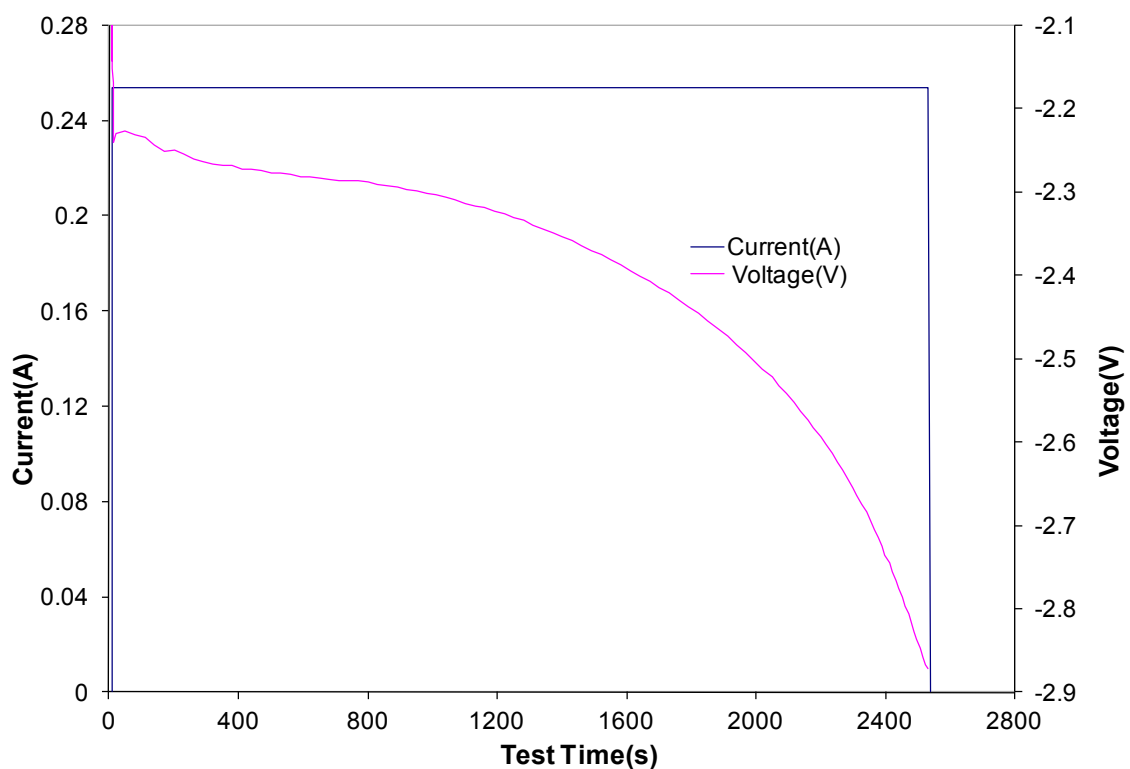


Figure 3.3. Change in potential during constant current impregnation at 0.1 A/cm^2 in $1.8 \text{ M Ni}(\text{NO}_3)_2$ and $0.26 \text{ M Co}(\text{NO}_3)_2$.

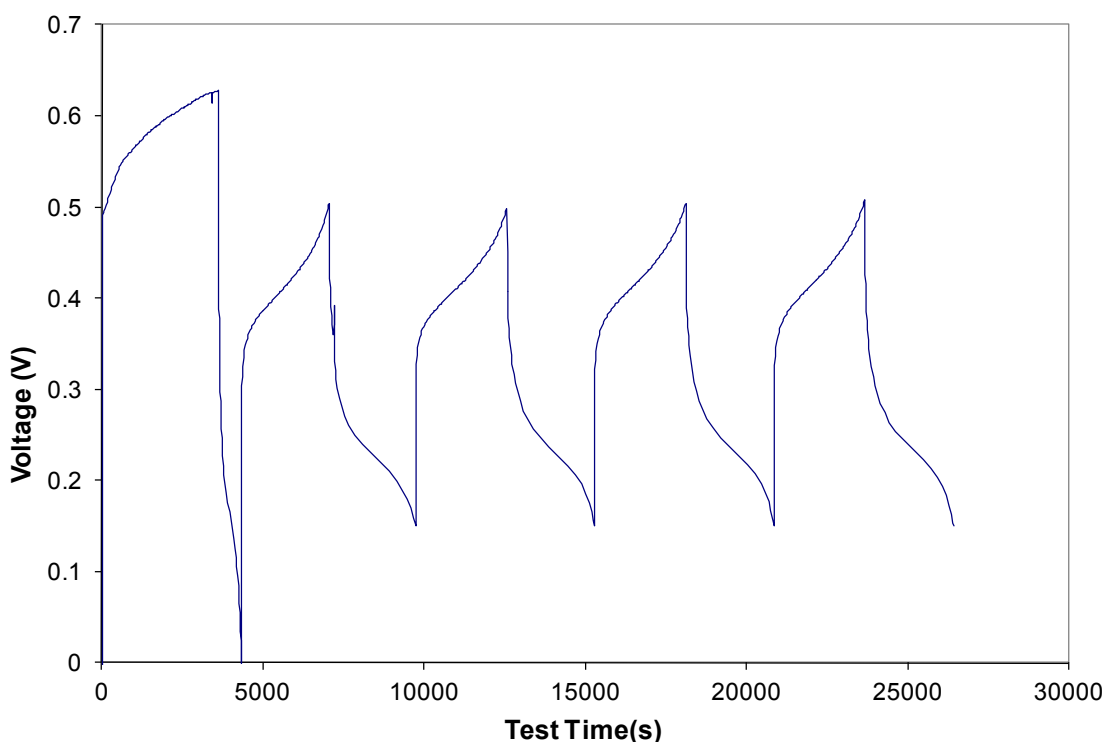


Figure 3.4. Voltage profile of the forming process for a nickel hydroxide electrode relative to a Hg/HgO reference electrode. Complete formation is defined when the last two cycles have the same capacity.

3.4.2 Materials Characteristics

The morphologies of a carbon foam and of a nickel-carbon foam positive electrode were investigated by FE-SEM. Figures 3.5 and 3.6 show the FE-SEM images of the surface and cross-section of a carbon foam sample. As indicated in these figures, this carbon foam shows cell wall integrity with small pore size and uniform pore shape, which indicates good conductivity and hence suitability to serve as the current collector in electrochemical applications.^{6,43} Figure 3.7 shows FE-SEM images of the surface of a nickel-carbon foam electrode. Uniform particles and a loose packed structure are apparent. This may make it easier for electrolyte ions to access the $\text{Ni}(\text{OH})_2$ active material. As a result, good capacitive performance would be expected. The cross-section of the electrode (Figure 3.8) illustrates the extent of deposition in the inner pores of the carbon foam. As demonstrated in Figure 3.8, the $\text{Ni}(\text{OH})_2$ almost fully loads the carbon foam and is well distributed in the pores.

The structures of carbon foam (as-received) and a nickel-carbon foam electrode were characterized using powder XRD measurements. Figure 3.9 shows the XRD powder pattern of the carbon foam. The pattern can be indexed on a hexagonal cell with lattice constants of $a = 2.461 \text{ \AA}$ and $c = 6.705 \text{ \AA}$. These lattice constants agree with the literature.⁵¹ The sharp diffraction peak at (002) of carbon foam implies a high degree of crystallinity and a highly ordered plane. Figure 3.10 shows the XRD powder pattern of a nickel-carbon foam electrode. The pattern can be indexed on a hexagonal cell with lattice constants of $a = 3.091 \text{ \AA}$ and $c = 24.184 \text{ \AA}$. The characteristic peaks, at 11.0° , 22.0° , 34.1° , 60.0° , and 61.1° 2-theta, indicate the nickel-carbon foam electrode has a crystal structure of $\alpha\text{-Ni(OH)}_2$. The diffraction peak indexed at (002) belongs to the carbon foam. The broadened diffraction peaks at (003) and (006) of $\alpha\text{-Ni(OH)}_2$ imply a disordered plane. Powder patterns based on the above lattice constants were calculated using the program available at the Database of Zeolite Structures.⁵² The information used to calculate the patterns and the calculated patterns for both the carbon foam and the nickel-carbon foam electrode can be found in Appendix B2.

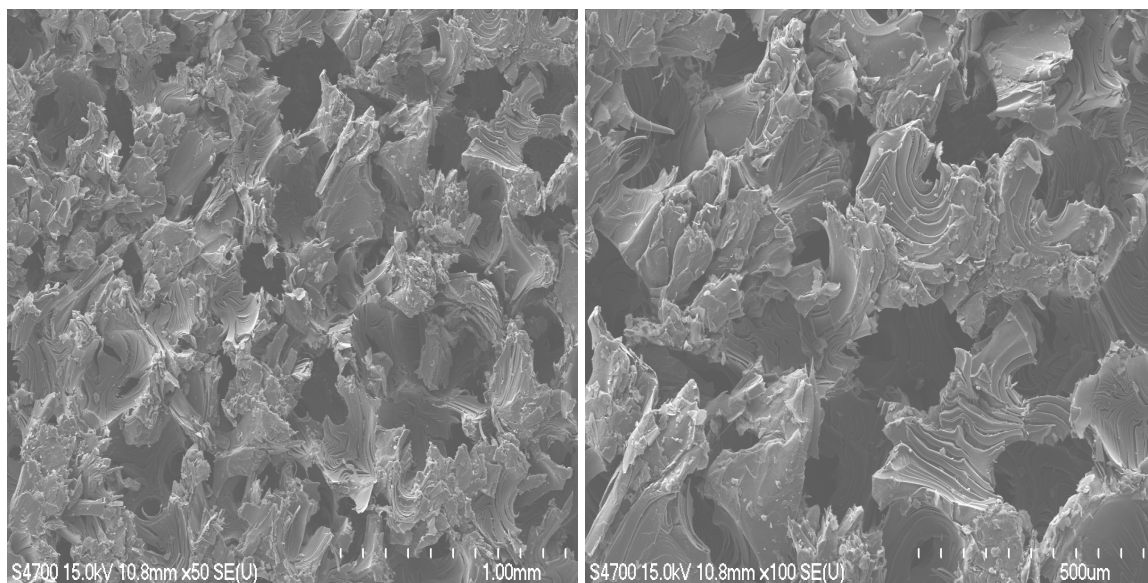


Figure 3.5. FE-SEM images of surface morphology of carbon foam taken at 50x and 100x magnifications.

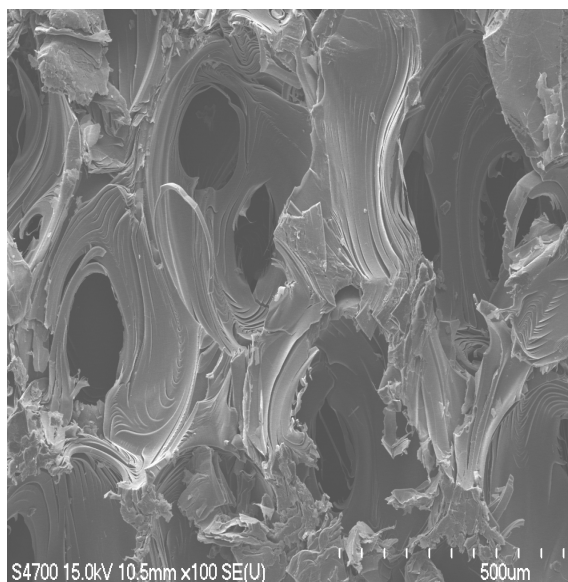


Figure 3.6. FE-SEM image of the cross-section morphology of a carbon foam taken at 100x magnification.

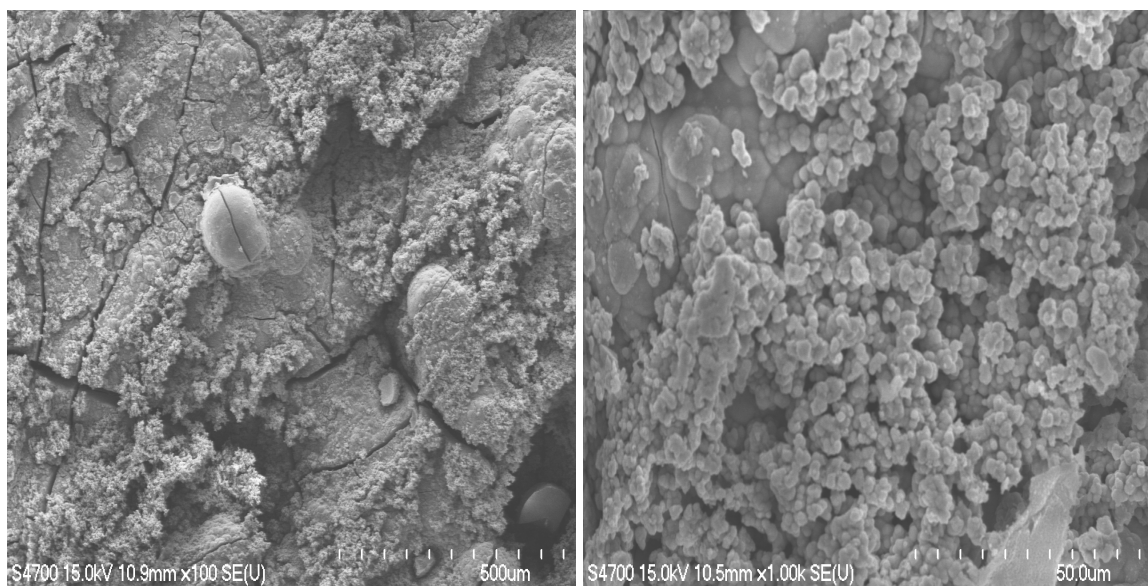


Figure 3.7. FE-SEM images of surface morphology of carbon foam impregnated with Ni(OH)_2 taken at 100x and 1,000x magnifications.

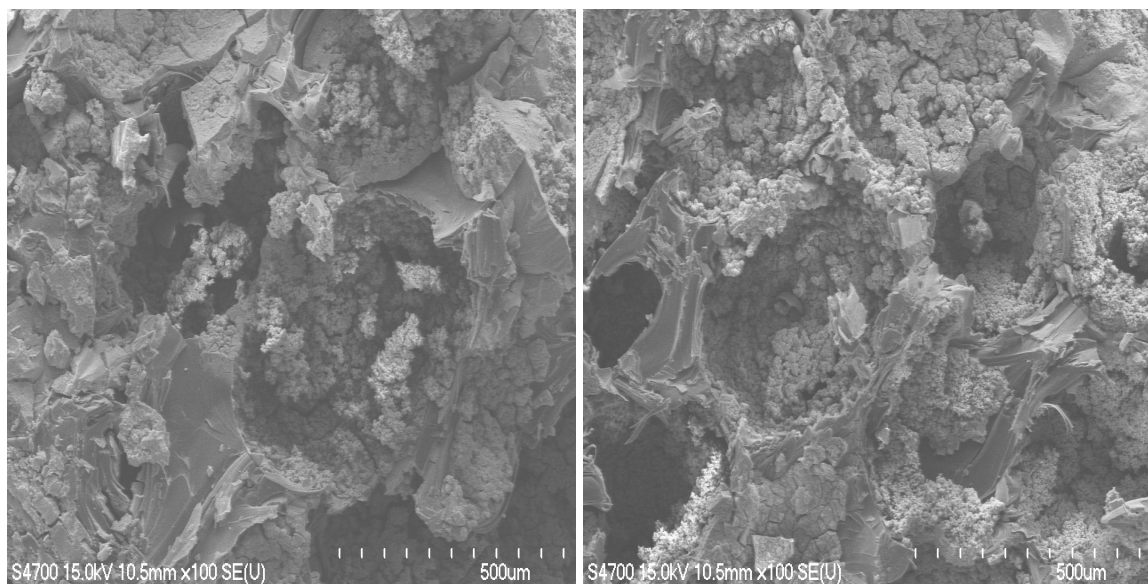


Figure 3.8. FE-SEM images of cross-section morphology of carbon foam impregnated with $\text{Ni}(\text{OH})_2$ taken at 100x magnification. The left photo was taken near the edge of the foam and the right photo was taken near the center of the foam.

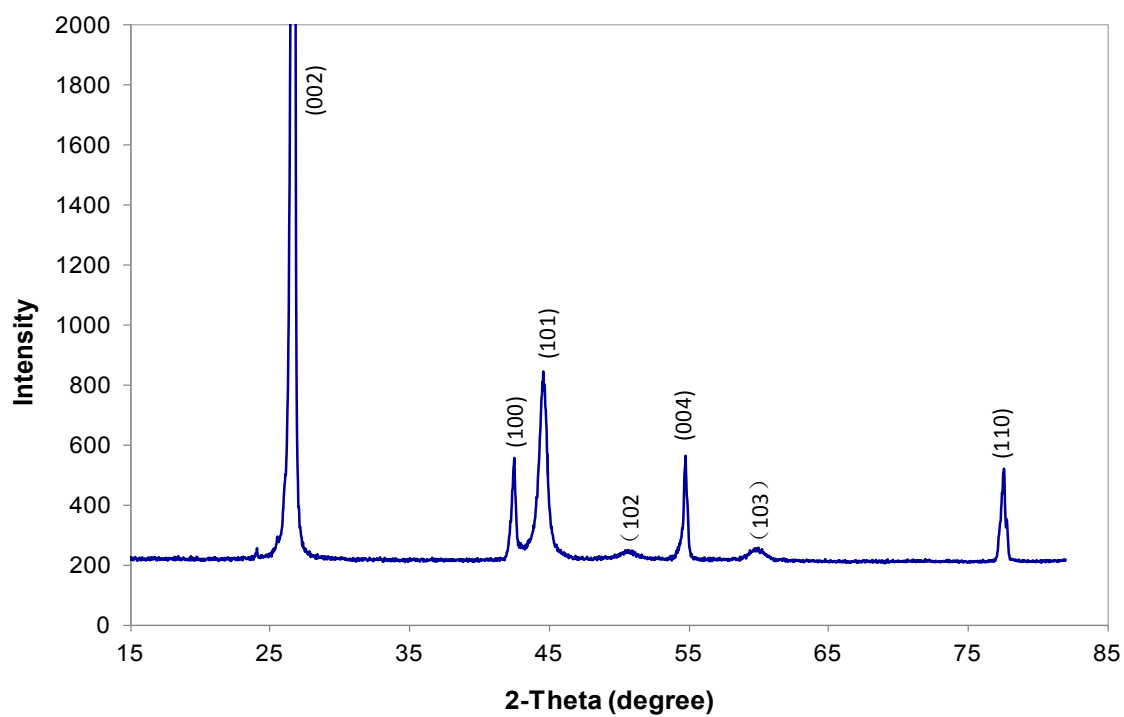


Figure 3.9. XRD powder pattern of a POCOfoam®.

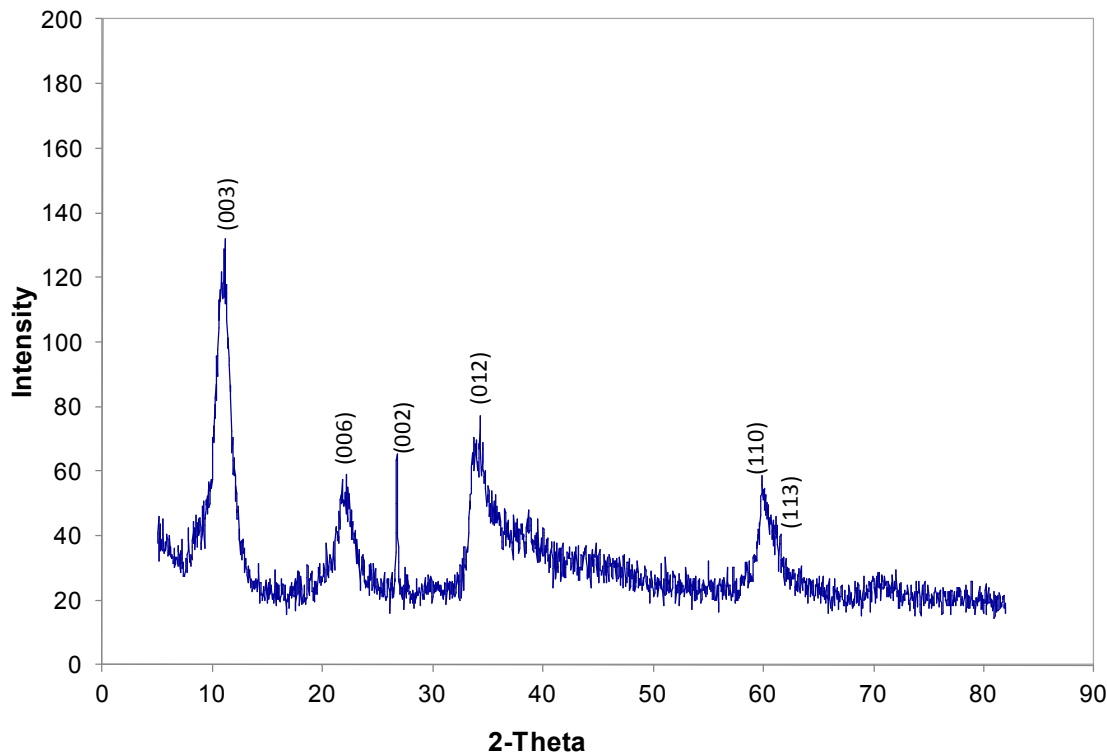


Figure 3.10. XRD powder pattern of an as-deposited nickel-carbon foam electrode.

3.4.3 Electrochemical Characteristics of the Nickel-Carbon Foam

Positive Electrode

The electrochemical capacitance behavior of the nickel-carbon foam positive electrode was evaluated in a flooded cell that contained 26 wt% KOH via a galvanostatic charge and discharge technique. The explanation for the advantage of this KOH concentration is reported by Lim and Loyselle.^{53,54} Figure 3.11 shows the voltage profile for the nickel-carbon foam electrode during the charge and discharge processes. The first 4000 seconds represents the profile for the charge process. The profile for the discharge process is from 4000 to 7800 seconds. The shape of the profile suggests pseudo-capacitance behavior, which results from the redox reaction at the electrode/electrolyte interface.⁵⁵ (This behavior is substantiated in the upcoming discussion of Figure 3.13.)

The nickel- carbon foam electrode was cycled at different current densities (1, 5, 10, 20, and 50 mA/cm²) to determine the corresponding specific capacitances. Specific capacitance is calculated using equation 3.1.

$$C = \frac{I \times \Delta t}{m \times V} \quad (3.1)$$

where C = specific capacitance (F/g)

I = constant discharging current (A)

Δt = discharging time (s)

m = mass of active material (Ni(OH)₂), estimated by Faraday's law with a deposition efficiency of 37.5%⁵⁶

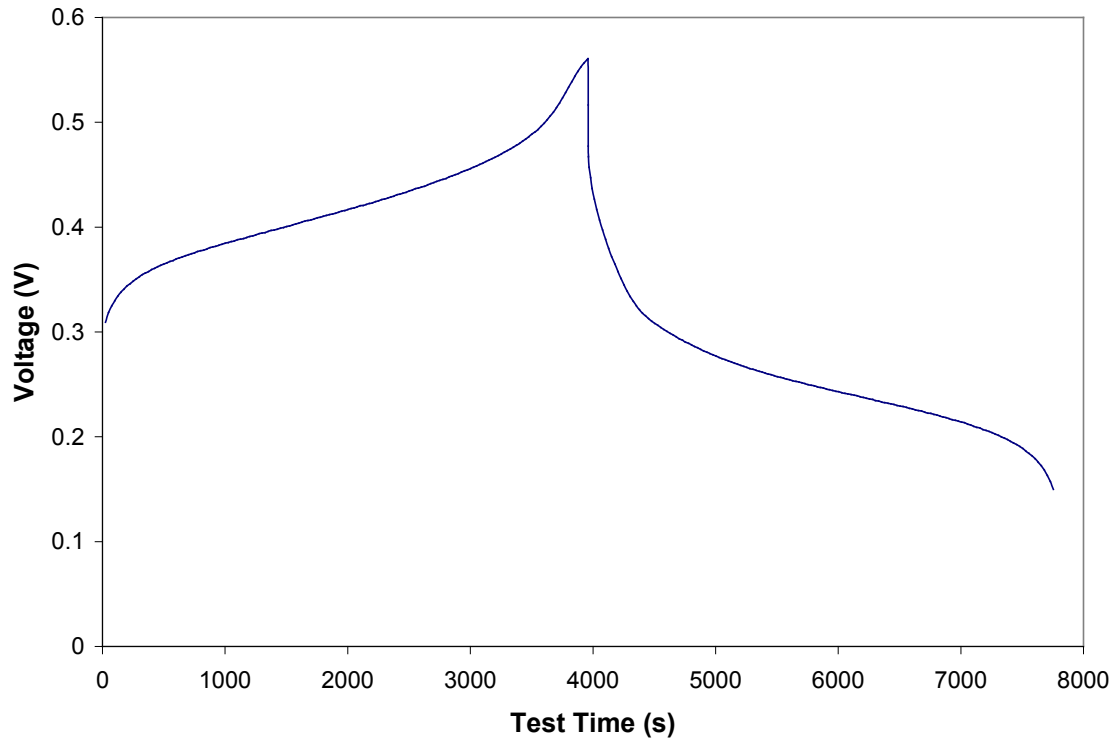


Figure 3.11. Typical charge and discharge curves for a nickel-carbon foam electrode relative to a Hg/HgO reference electrode cycled at 1 C-rate.

The calculated specific capacitance values at discharge current densities of 1, 5, 10, 20, and 50 mA/cm² were 2935, 2641, 2537, 1873, and 1182 F/g, respectively (see Figure 3.12). These capacitance values demonstrate that this nickel-carbon foam electrode has

excellent electrochemical performance. The specific capacitance at 5 mA/cm² (2641 F/g) is higher than the reported literature value of 2080 F/g.⁵⁷ This suggests that the nickel-carbon foam electrode could serve as the faradaic electrode in an asymmetric capacitor to achieve a high power density.

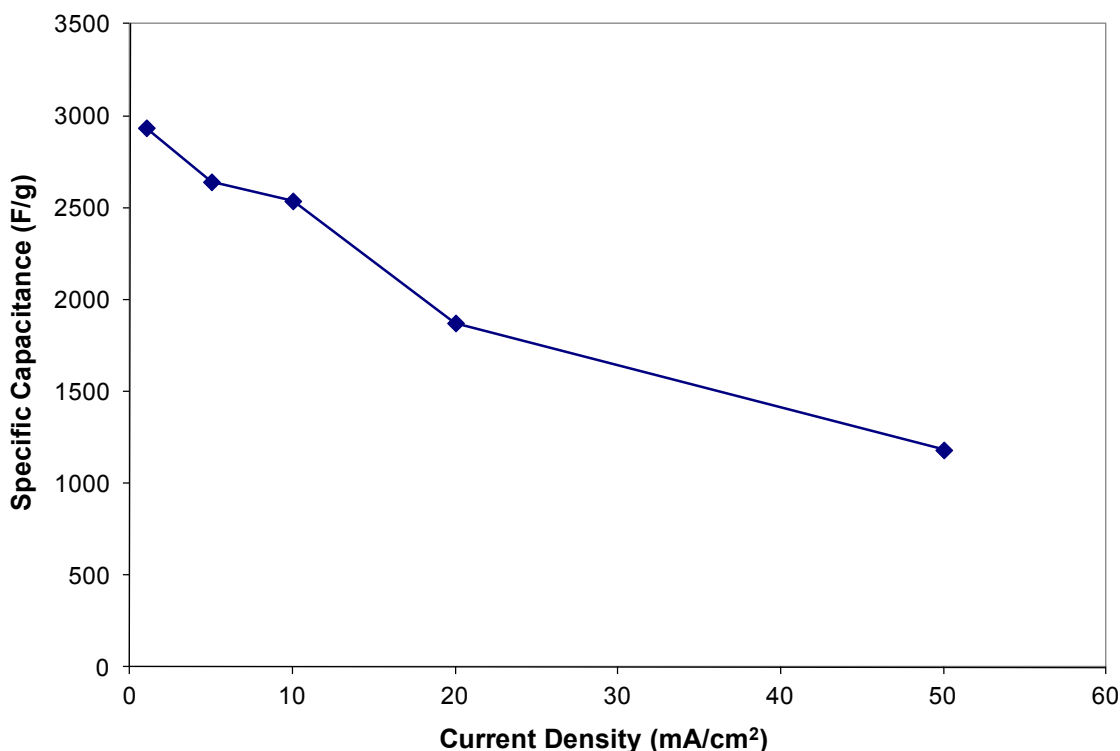


Figure 3.12. Specific capacitance at various discharge current densities.

To further evaluate the nickel-carbon foam electrode, an asymmetric capacitor using this electrode and a commercial carbon electrode was assembled. Cyclic voltammetry (CV) and galvanostatic charge and discharge measurements were used to evaluate the asymmetric capacitor cell. Figure 3.13 shows the CV curves of the nickel-carbon foam electrode relative to a Hg/HgO reference electrode at different scan rates. As indicated by the curves, there are two redox peaks observed. Typical CV curves of the asymmetric capacitor at different scan rates are presented in Figure 3.14. The CV curves have a smaller area or capacitance at a high scan rate (*i.e.*, 25 mV/s) as compared to a low scan rate (*i.e.*, 5 mV/s). This may be caused by the high scan rate, where not all of the active surface area is accessible for charge storage. Large concentration polarization could also

appear easily.⁵⁸ Figure 3.15 shows the charge and discharge behavior of the nickel-carbon foam/AC asymmetric capacitor. In the figure, the voltage profile varies linearly with time, which demonstrates that the cell has good capacitive behavior. Equation 3.1 was used to determine the specific capacitance of the asymmetric capacitor, with m being equal to the total mass of the active material for both nickel-carbon foam and AC electrodes. Over 1,000 cycles, the average specific capacitance and specific energy of the cell, for a cell voltage between 1.4 and 0.8 V, were 129.2 F/g and 19.9 W.h/kg, respectively.

The stability of the nickel-carbon foam/AC asymmetric capacitor was observed through repeated charge and discharge processes. The cell was cycled at a current density of 10 mA/cm², between 1.4 and 0.8 V. Figure 3.16 shows the specific capacitance over 1,000 cycles. The results demonstrated a 15% decrease in the specific capacitance after 1,000 cycles compared to its initial value, probably due to degraded performance of the faradaic electrode (nickel-carbon foam electrode).

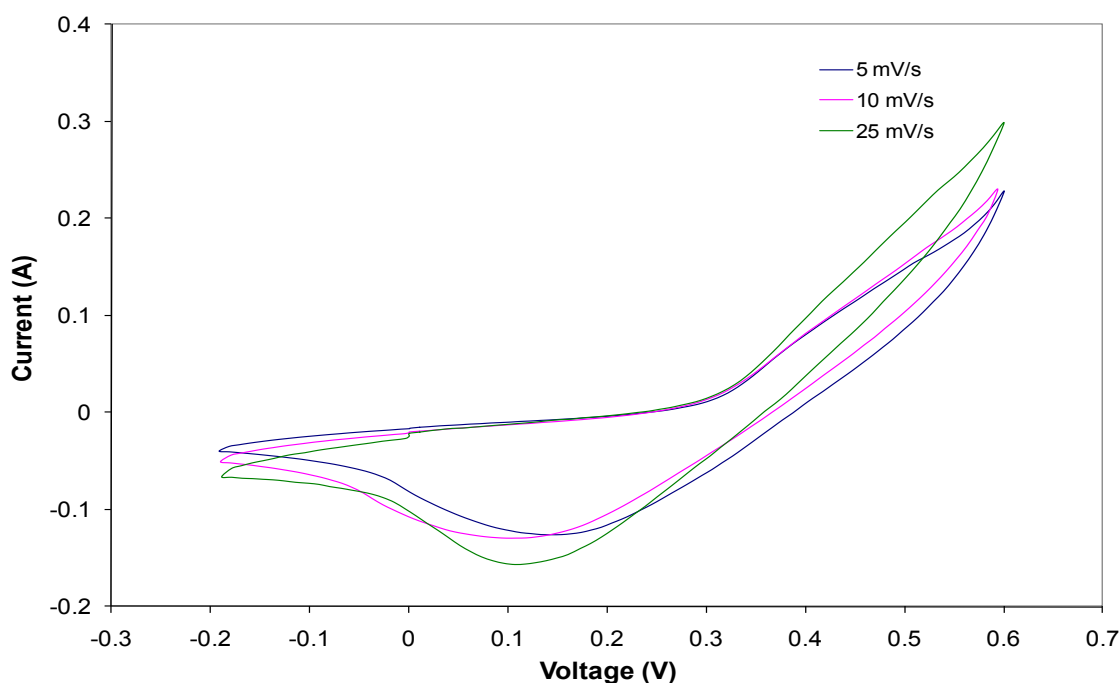


Figure 3.13. CV of the nickel-carbon foam electrode relative to a Hg/HgO reference electrode at different scan rates in a T-cell.

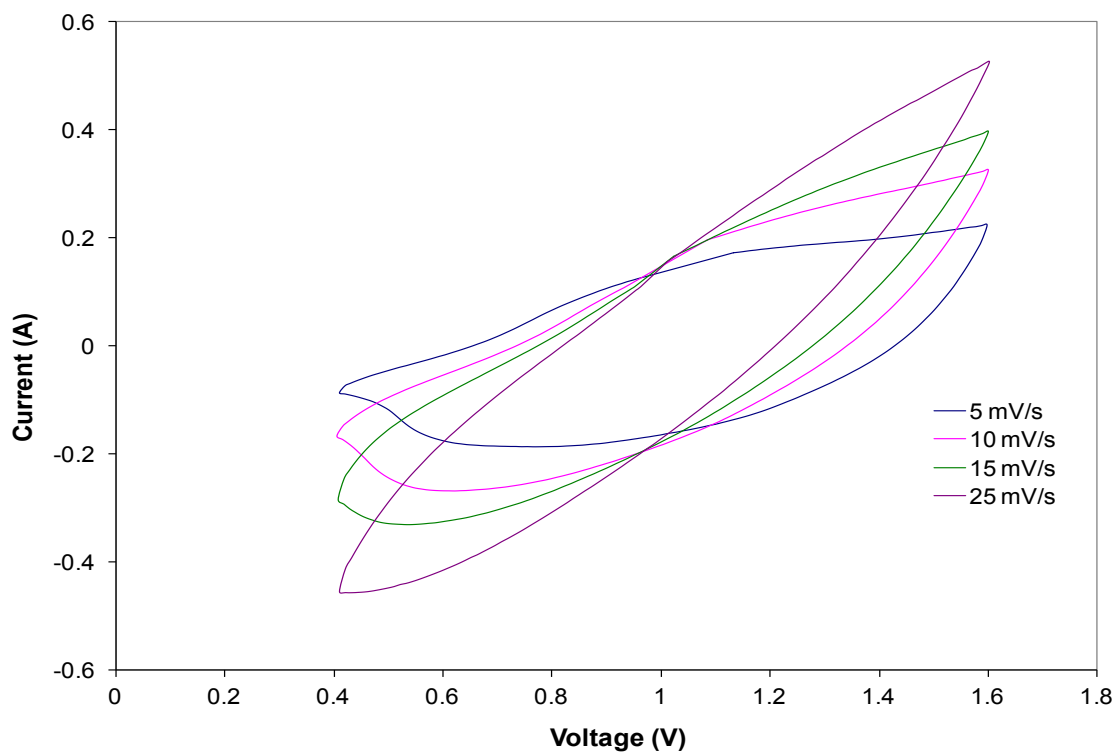


Figure 3.14. CV of the nickel-carbon foam/AC asymmetric capacitor at different scan rates.

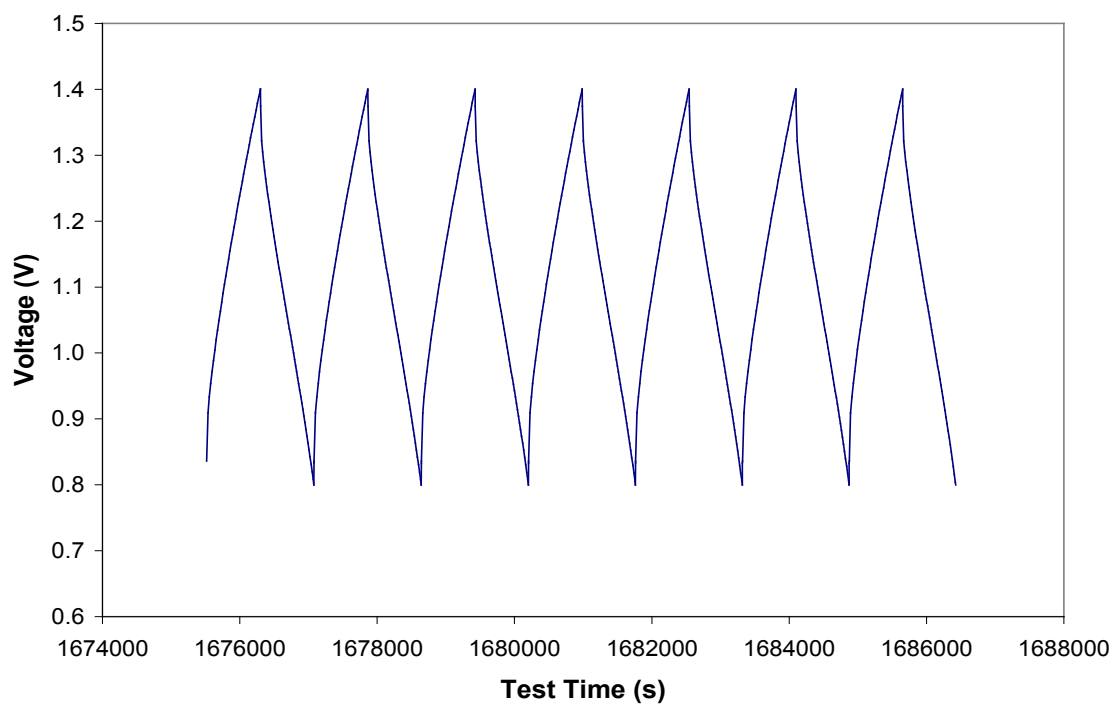


Figure 3.15. Charge and discharge behavior of the nickel-carbon foam/AC asymmetric capacitor at 10 mA/cm².

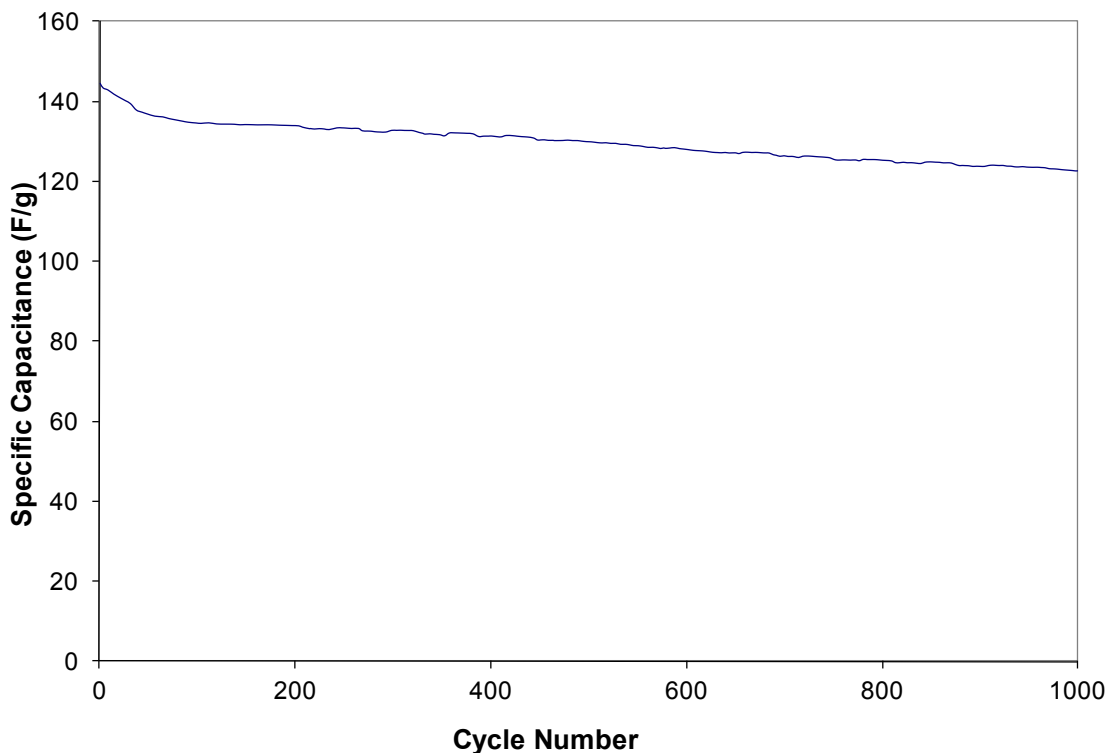


Figure 3.16. Specific capacitance as a function of cycle number for a nickel-carbon foam/AC asymmetric capacitor cycled at 10 mA/cm².

3.5 Conclusions

Nickel hydroxide was impregnated within carbon foam via electrochemical deposition to determine its specific capacitance in flooded cell tests. The specific capacitance at different current densities indicated the nickel-carbon foam electrode is suitable to serve as the faradaic electrode in the asymmetric capacitor. The specific capacitance at 5 mA/cm² is higher than the reported value for a similar electrode (2641 vs. 2080 F/g).⁵⁷ The electrochemical behavior of the nickel-carbon foam electrode was further evaluated by assembling an asymmetric capacitor. The results from the cell indicated good capacitive behavior. The average specific capacitance and specific energy of the asymmetric cell for a cell voltage between 1.4 to 0.8 V were 129.2 F/g and 19.9 W.h/kg, respectively.

4.0

Examination of Various Carbon Electrodes Used in Aqueous Symmetric Capacitors

Wen Nee Yeo ¹, Tony N. Rogers ^{1,3}, Bahne C. Cornilsen ²

¹ Department of Chemical Engineering, Michigan Technological University, 1400 Townsend Drive, Houghton, MI 49931-1295

² Department of Chemistry, Michigan Technological University, 1400 Townsend Drive, Houghton, MI 49931-1295

³ To whom correspondence should be addressed: Telephone: 906-487-2210, Fax: 906-487-3213, Email: tnrogers@mtu.edu, Postal address: 1400 Townsend Drive, Houghton, MI 49931-1295

Manuscript in preparation

4.1 Abstract

Three ACs (RP-20, YP-50F, and Ketjenblack EC-600JD) were used without further treatment as electrode materials for symmetric capacitors. The structures were characterized by XRD and N₂ adsorption/desorption isotherms at 77 K. The electrochemical performance was evaluated in symmetric aqueous capacitors. The study indicated that these ACs were suitable to use in ECs depending on the application. In general, RP-20 and YP-50F are suitable to employ in high energy applications because of the combination of micropore and mesopore structures, whereas Ketjenblack EC-600JD is more suitable to employ in high power applications due to its high mesopore structure.

4.2 Introduction

ECs have drawn attention recently because they have higher specific power compared to batteries and higher specific energy compared to conventional capacitors. Moreover, ECs have the advantages of much longer cycle life and rapid discharge characteristics compared to batteries. ECs with the same type of electrode material for the positive and negative electrodes are called symmetric capacitors. Charge and discharge processes are carried out without involving chemical reactions (faradaic reactions). The energy is stored in the electric double layers (inner and outer Helmholtz layers). Therefore, this type of capacitor is also called EDLC.

There are two types of electrolyte in symmetric capacitors, aqueous and non-aqueous. An aqueous electrolyte is preferred even though it has a lower stored energy because of low cost and safety advantages. Carbons, especially ACs, are commonly used in ECs because they are commercially available, inexpensive and have good electrochemical properties. Various ACs have been investigated to use in ECs.^{31,33,35,38} In general, the larger the surface area of the carbon, the greater the ability for ions to accumulate in the electrode/electrolyte interface, and hence the higher the capacitance.^{30,31} In addition, the pore structure of the carbon also affects the performance of the capacitors.^{32,33}

In this work, the electrochemical performance of three different ACs was evaluated using symmetric aqueous capacitors. In addition, the morphologies of these ACs were compared.

4.3 Experimental Setup

4.3.1 Electrode Preparation

RP-20 and YP-50F (Kuraray Chemical) and Ketjenblack EC-600JD (Akzo Nobel) were used without further treatment. Two batches of electrodes (90 and 95 wt% carbon) were prepared from each of the carbon black powders. This process was developed by Professor Stephen M. Lipka at the University of Kentucky.⁵⁹ The binder used in this work was a PTFE solution from Aldrich (60 wt% in water). Normally, the electrodes were made on a 1.5 g carbon weight basis. The carbon black powder and PTFE were weighed according to the formulation, then mixed and ground together using a mortar and pestle for about an hour or until the PTFE was well-dispersed in the carbon black powder. Next, the mixture was heated at 120°C in an oven for an hour, followed by 20 minutes of further grinding in the mortar. The heating and grinding process was repeated three times. Then, the mixture was removed from the mortar and placed into a beaker. The mixture was pressed using a glass rod to form dough with the addition of isopropyl alcohol. The rod was used to roll the dough to the desired film thickness (0.6 mm), and it was subsequently air dried for a few hours to evaporate the isopropyl alcohol. The prepared film was cut into a circular shape with a diameter of 0.75 inches (1.9 cm) and heated at 80°C in an oven for an hour.

4.3.2 Materials Characterization

Measurements of N₂ adsorption/desorption isotherms were made at 77K using an ASAP2020 apparatus made by Micromeritics Instrument Corporation. For each carbon black and prepared electrode, the specific surface area and pore structure parameters were determined from the N₂ isotherms by the Brunauer-Emmett-Teller (BET) and the t-plot methods, respectively. The mesopore size distributions were analyzed by the

Barrett-Joyner-Halenda (BJH) method.⁶⁰ Powder XRD was also used to compare the structures of these ACs. The operating conditions are listed in Section 3.3.2 of Chapter 3.

4.3.3 Symmetric Capacitor Cell Preparation

A symmetric capacitor was made of five components: (i) compression tube fitting as the cell body, (ii) plungers to hold the electrode stack and connect the cell to an Arbin MSTAT electrochemical testing system, (iii) carbon electrodes, (iv) two layers of separator membrane made of microporous polypropylene filled with electrolyte solution (26 wt% KOH), and (v) nickel mesh current collectors located between each electrode and the SS plunger. Figure 4.1 shows a schematic view and an assembled symmetric capacitor cell.

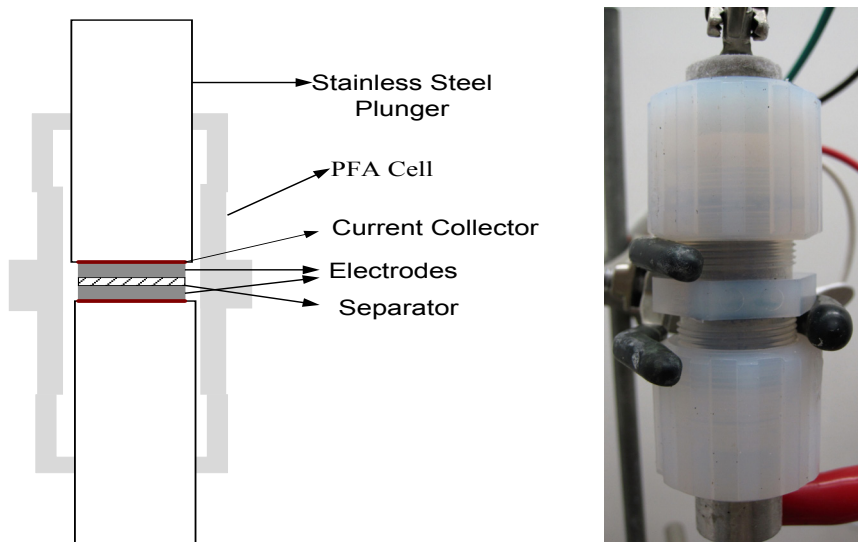


Figure 4.1. Schematic view and assembled symmetric capacitor cell. The cell body is constructed of a PFA fitting.

4.4 Results and Discussion

4.4.1 Materials Characteristics

The N₂ adsorption/desorption isotherms of the ACs are shown in Figure 4.2. For both RP-20 and YP-50F, a major N₂ uptake occurs at low relative pressures (<0.1) and reaches a plateau at high relative pressures. This is a Type I isotherm, indicating both ACs are microporous.^{61,62} In addition, the isotherm of YP-50F also contains a hysteresis loop that

occurs at a relative pressure of ~ 0.45 , which indicates the presence of some mesopores. Ketjenblack EC-600JD has a Type IV isotherm based on its adsorption and desorption curves.⁶¹ The hysteresis loop has a closure at a relative pressure of ~ 0.45 indicating the presence of mesopores. This hysteresis is also characteristic of a Type IV isotherm. Table 4.1 summarizes the pore characteristics of ACs. All ACs have a BET surface area above $1300 \text{ m}^2/\text{g}$. As illustrated in Table 4.1, the majority of the pores for Ketjenblack EC-600JD are mesopores, and hence it has the largest average pore diameter. Figure 4.3 shows BJH mesopore size distributions of the ACs. As shown in Figure 4.3, RP-20 and YP-50F mainly contain micropores whereas Ketjenblack EC-600JD mainly contains mesopores.

The pore characteristics of the prepared electrodes were also determined and are summarized in Table 4.2. The carbon/PTFE electrodes show isotherm behavior for N_2 adsorption/desorption similar to each individual AC (and, therefore, these are not reproduce here). The reduction in surface area, micropore, and mesopore for each of the electrode was likely caused by some of the area and pores being filled or blocked by the PTFE binder.

Table 4.1.
Pore characteristics of ACs.

Acs	BET (m²/g)	Micropore Area (m²/g)	Mesopore Area (m²/g)	Single Point Pore Volume 10⁻⁶ m³/g	BJH Adsorption Average Pore Diameter (nm)	BJH Desorption Average Pore Diameter (nm)
RP-20	1333	1139	194	0.69	3.76	3.46
YP-50F (YP-17)	1314	1085	229	0.68	3.82	3.48
Ketjenblack EC-600JD	1422	44	1378	2.42	8.74	7.69

Table 4.2.
Pore characteristics of carbon/PTFE electrodes.

Electrodes	BET (m²/g)	Micropore Area (m²/g)	Mesopore Area (m²/g)	Single Point Pore Volume 10⁻⁶ m³/g	BJH Adsorption Average Pore Diameter (nm)	BJH Desorption Average Pore Diameter (nm)
95 wt% RP-20	1093	892	201	0.61	3.91	3.75
95 wt% YP-50F	1096	862	234	0.63	3.98	3.51
95 wt% Ketjenblack EC-600JD	1029	30	999	1.99	9.71	8.52
90 wt% RP-20	933	711	222	0.52	3.66	3.70
90 wt% YP-50F	932	718	214	0.54	4.07	3.67
90 wt% Ketjenblack EC-600JD	967	10	957	1.92	9.26	8.15

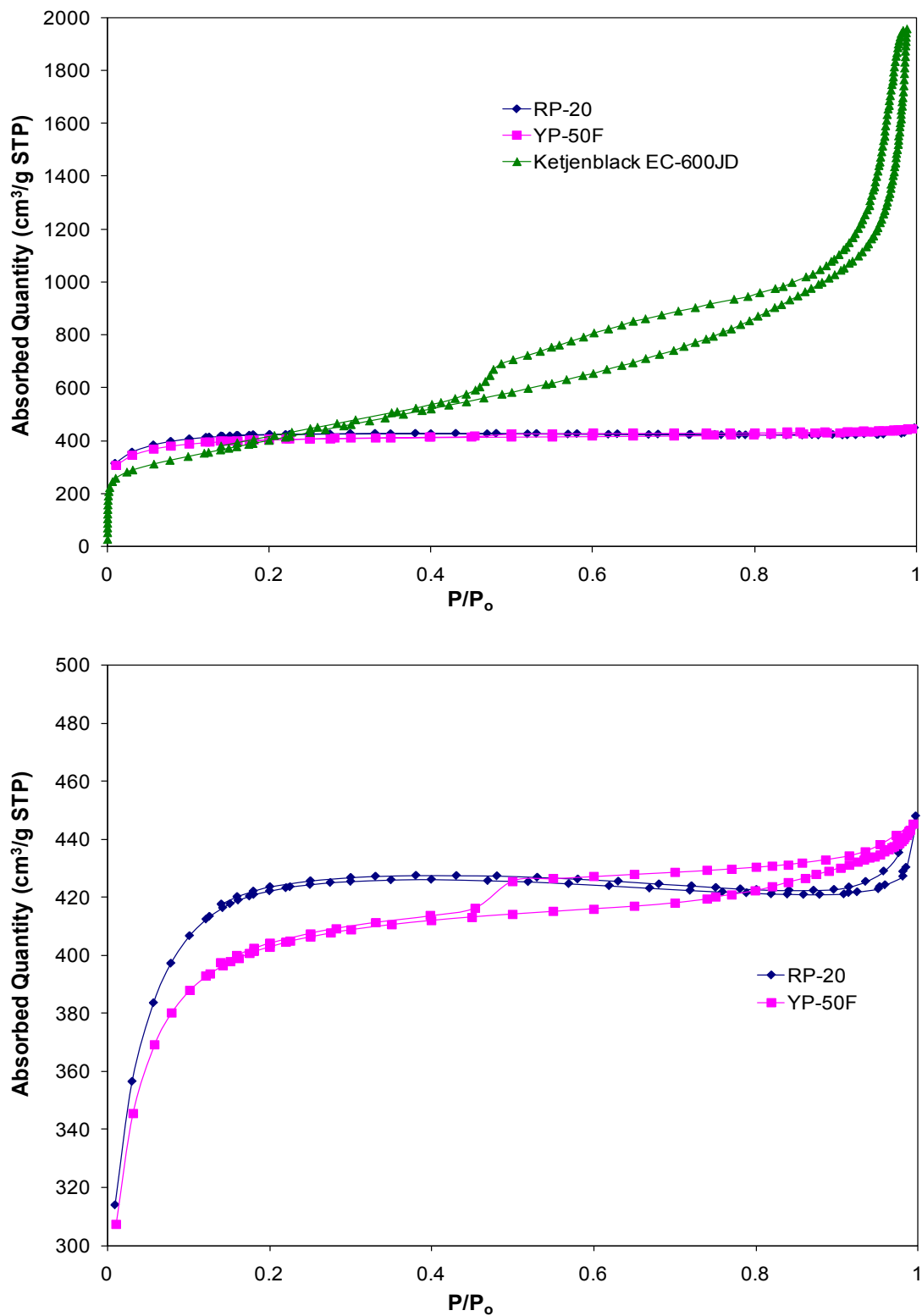


Figure 4.2. N₂ adsorption/desorption isotherms of ACs. The upper graph contains the N₂ adsorption/desorption isotherms for the three ACs, and the bottom graph shows RP-20 and YP-50F data only.

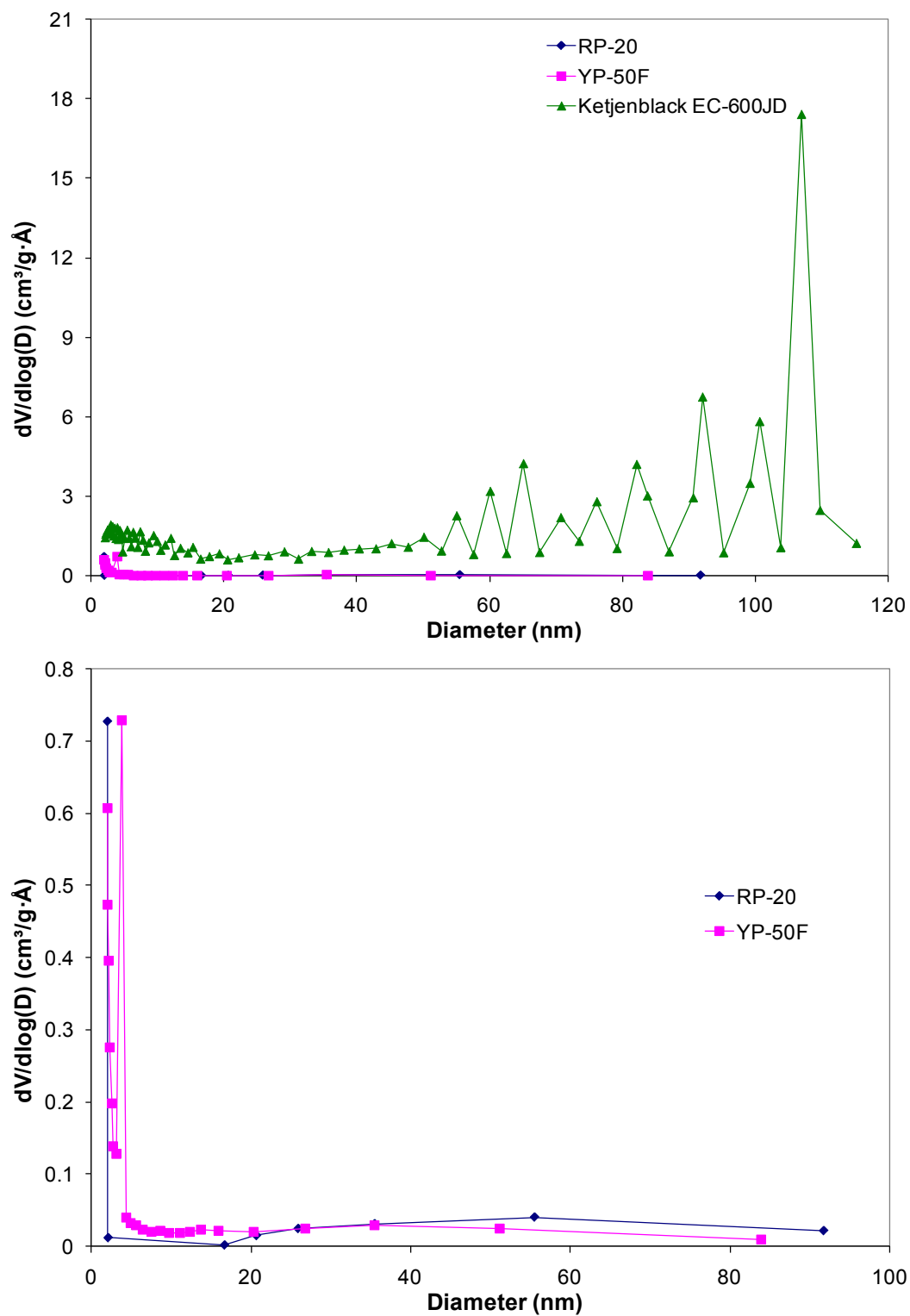


Figure 4.3. Mesopore size distributions of ACs. The upper graph exhibits the mesopore size distributions for the three ACs, and the bottom graph shows RP-20 and YP-50F data only. V is the pore volume and D is the pore diameter.

The structures of the three ACs were characterized through powder XRD measurements. Figure 4.4 shows the comparison of XRD powder patterns of the three ACs studied. According to JCPDS, No 75-1621, the diffraction peak near 24° 2-theta can be indexed as (002), and the two diffraction peaks near 44° 2-theta can be indexed as overlap of (100) and (101). The broad peak at (002) indicates that these ACs are amorphous carbons. Ketjenblack EC-600JD has the sharpest peak, and therefore it is the most ordered.

The specific capacitance of an AC is related to the sum of the capacitance of the basal planes and the capacitance of the edge planes.⁶³ Figure 4.5 shows the diffraction peaks with the background subtracted. Among the three ACs, RP-20 has the largest basal plane (002) and edge plane ((100) and (101)) peak areas, followed by YP-50F and Ketjenblack EC-600JD. Therefore, RP-20F should have the highest specific capacitance, followed by YP-50F and Ketjenblack EC-600JD.

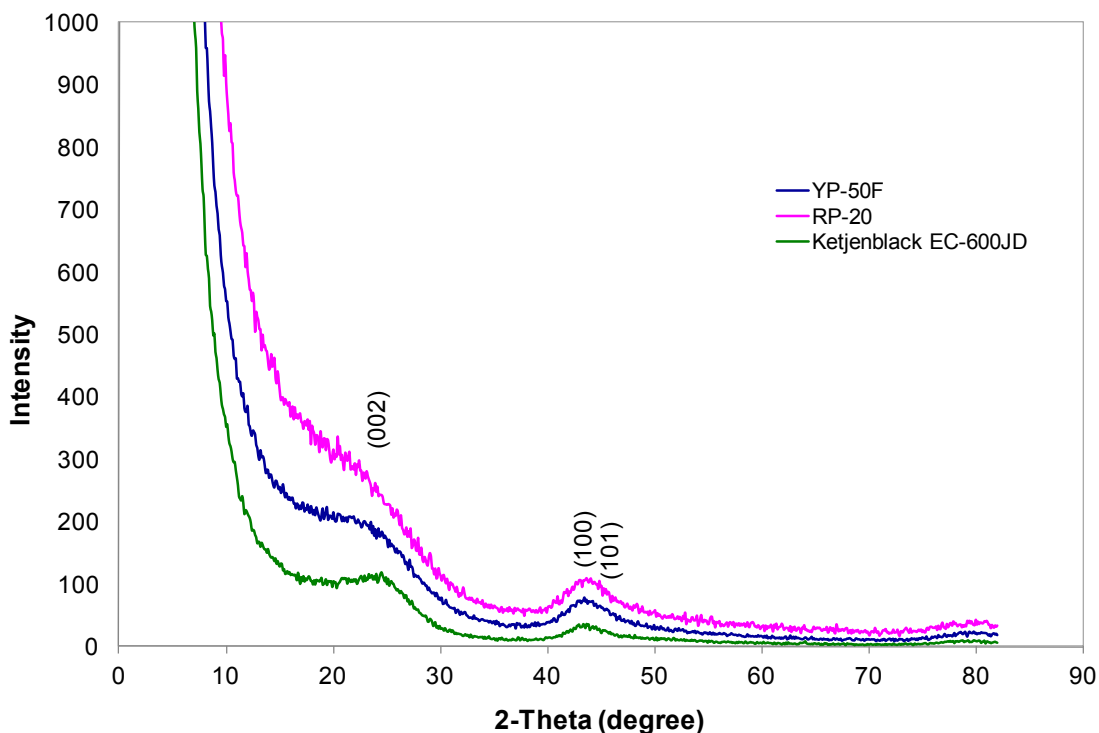


Figure 4.4. Comparison of XRD powder patterns of YP-50F, RP-20, and Ketjenblack EC-600JD.

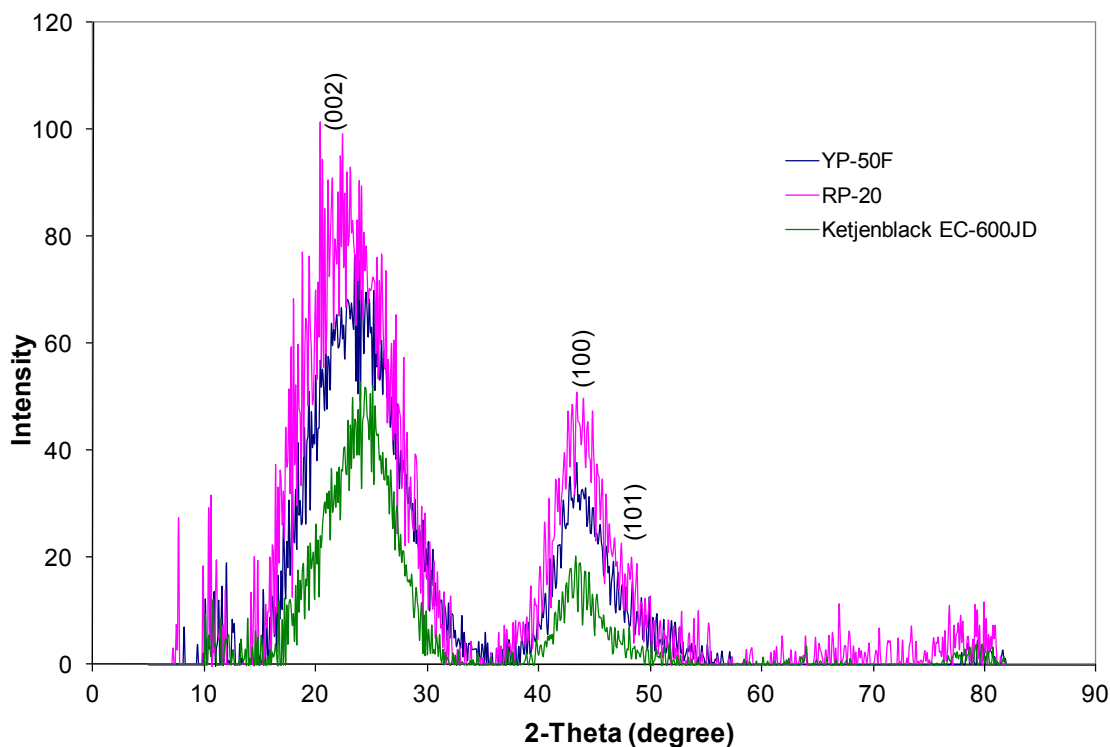


Figure 4.5. Comparison of XRD patterns of YP-50F, RP-20, and Ketjenblack EC-600JD, with background subtracted.

4.4.2 Cyclic Voltammetry

CV was applied to check the charge and discharge reversibility of these symmetric capacitors. For an ideal symmetric capacitor, the shape of the CV is a rectangular shape. This means there is no significant oxidation and reduction peaks on the CV as there are no redox reactions involved during the charge and discharge processes. Figures 4.6, 4.7, and 4.8 show the CVs for the three AC electrodes. The CVs were carried out for scan rates of 1, 5, 10, and 25 mV/s, and the voltage window was controlled from 0 to 1 V. As demonstrated in these figures, the CV curves lose their rectangular shape as the scan rate is increased due to more rapid ion transport. This means that these carbon materials are capable of rapid charge and discharge.⁶⁴

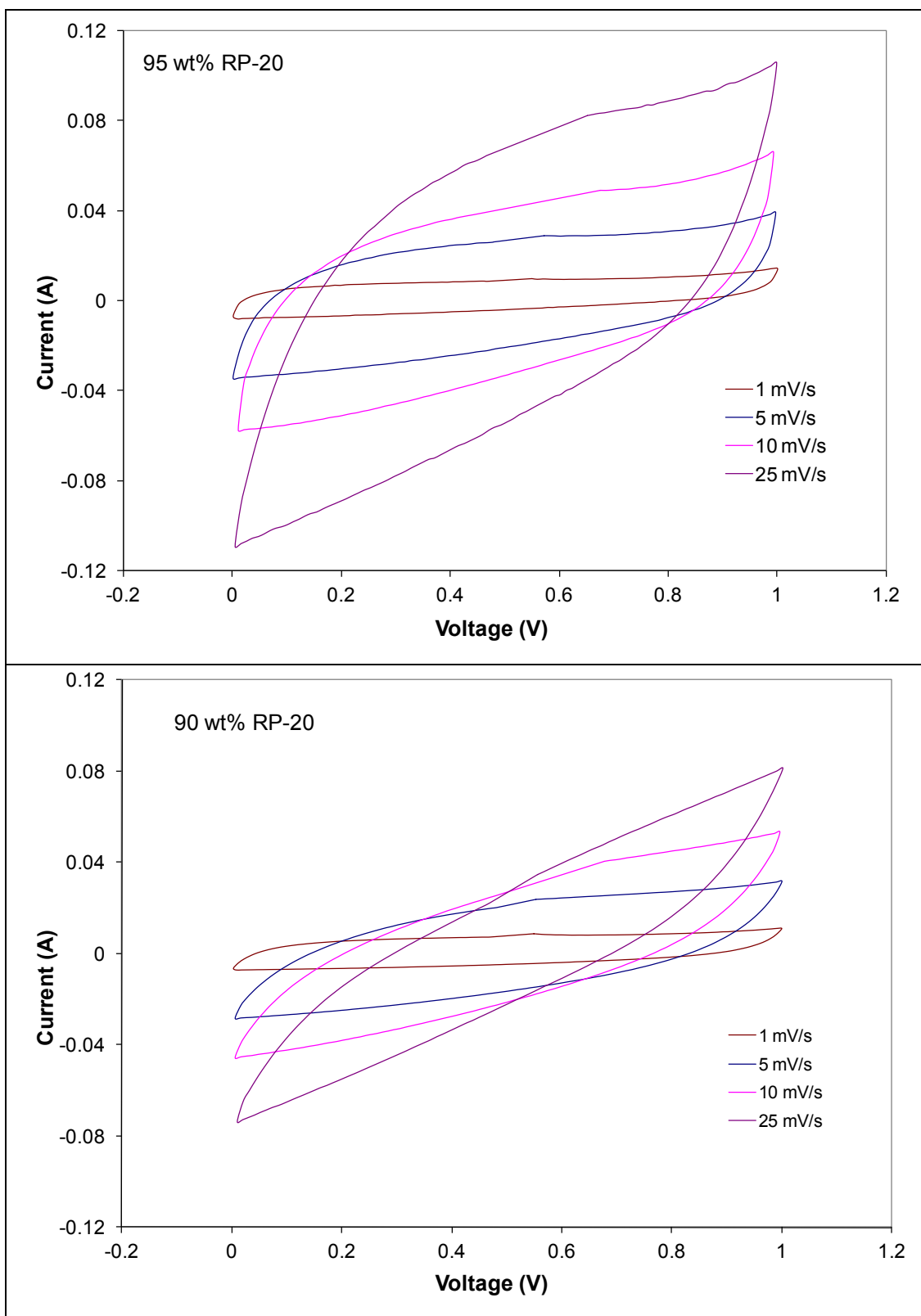


Figure 4.6. CV curves of RP-20 (top - 95 wt%, bottom - 90 wt%) at different scan rates.

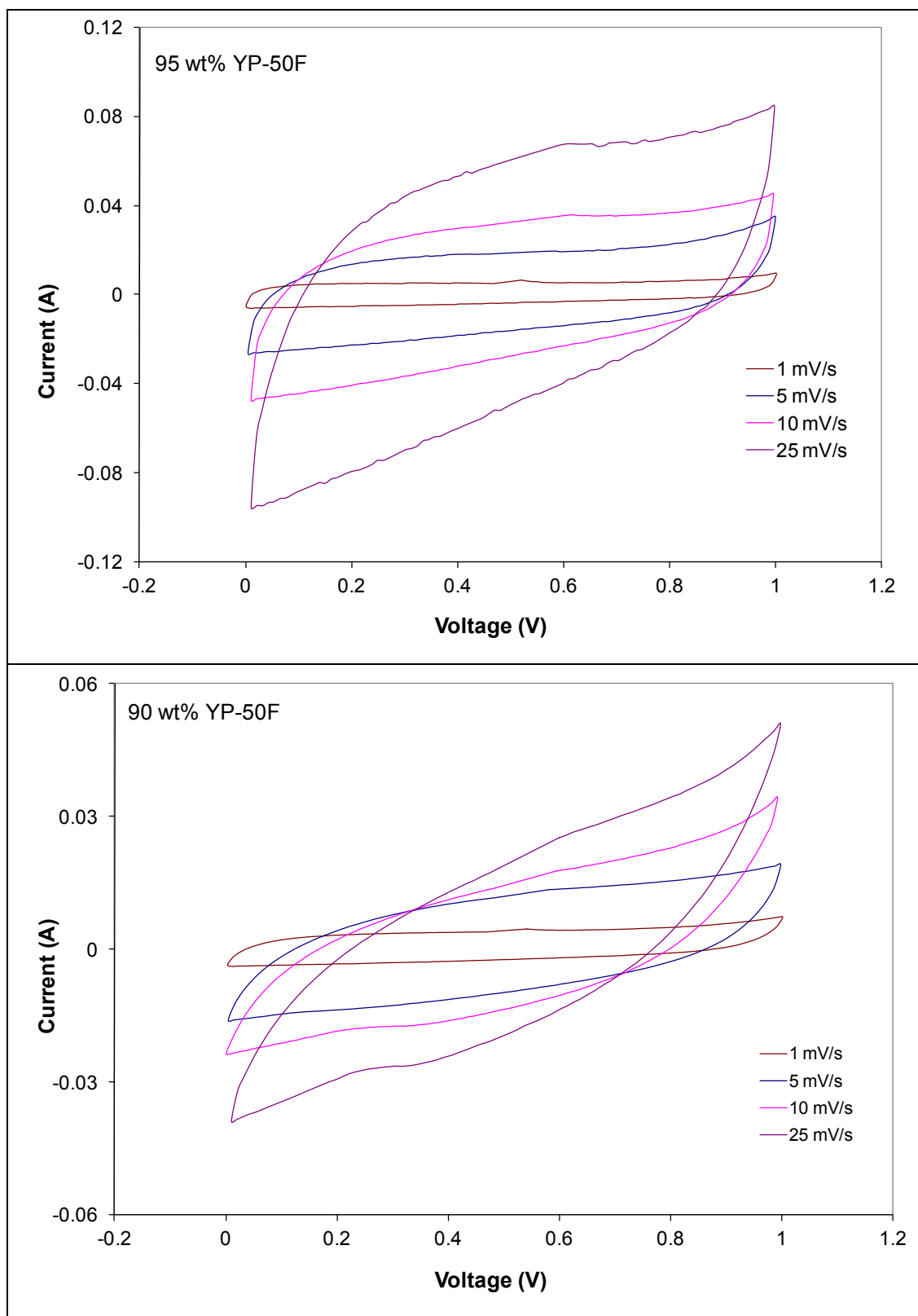


Figure 4.7. CV curves of YP-50F (top - 95 wt%, bottom - 90 wt%) at different scan rates.

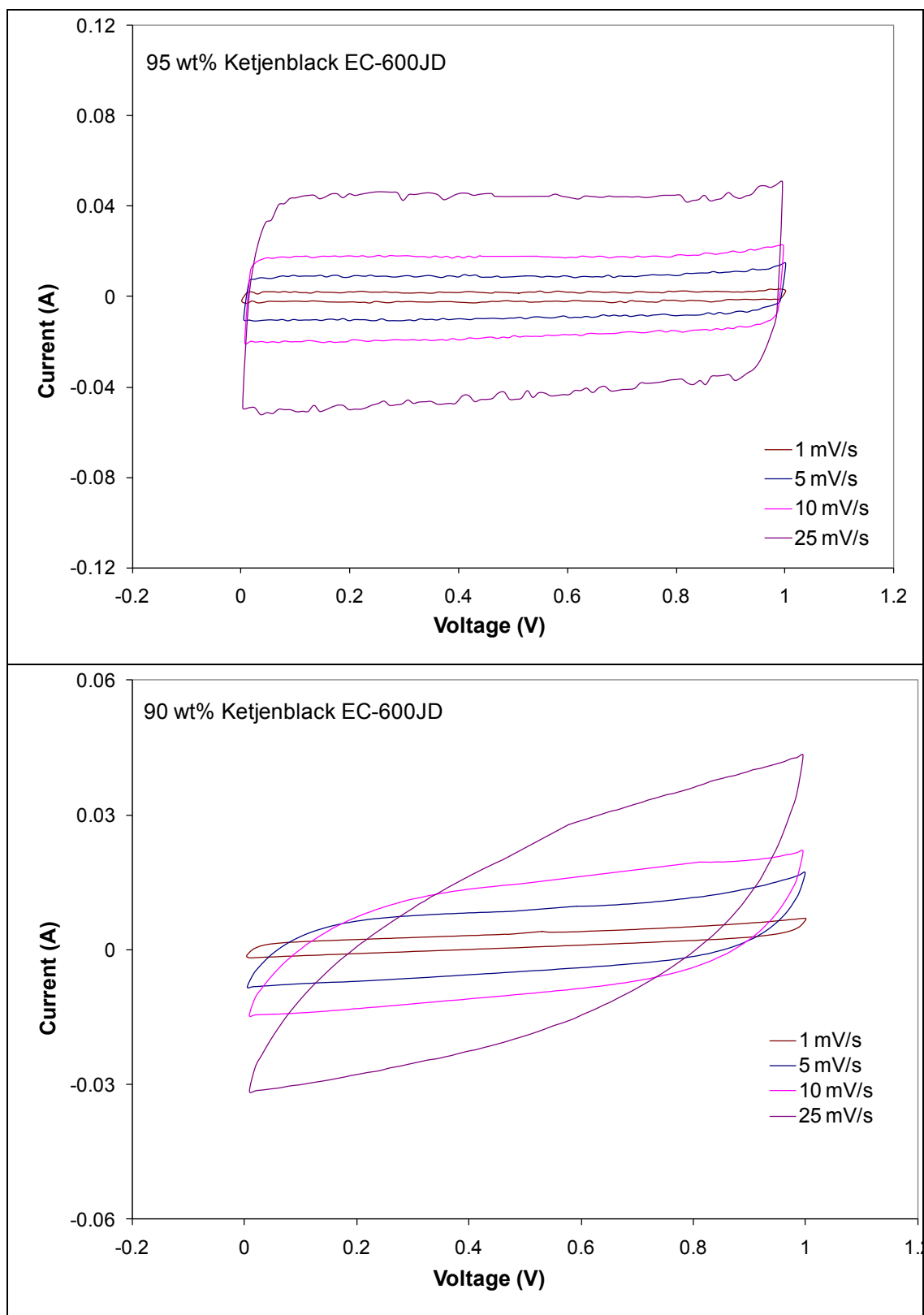


Figure 4.8. CV curves of Ketjenblack EC-600 JD (top - 95 wt%, bottom - 90 wt%) at different scan rates.

4.4.3 Galvanostatic Charge and Discharge

Charge and discharge of the AC capacitor cells were performed in the potential range between 0 and 1 V. The charge and discharge curves for all of the AC capacitor cells suggest a pure EDLC behavior. These results agree with those observed from the CV. An example of the charge and discharge behavior is shown in Figure 4.9. All the AC electrodes were also cycled at different current densities (5, 10, 20, and 50 mA/cm²) to determine the corresponding specific capacitance of a single electrode (Appendix C1). Figure 4.10 shows the specific capacitance of a single electrode at various discharge current densities. As indicated in Figure 4.10, 95 wt% RP-20 gave the highest specific capacitance (106 F/g) followed by 95 wt% YP-50F (98 F/g) at low current density. This is because RP-20 and YP-50F electrodes have high specific surface area, a microporous structure, and a limited amount of PTFE binder (5 wt%). However, the efficiency of the RP-20 electrodes (both 90 and 95 wt%) is lower (about 90%) compared to the others (above 98%). Ketjenblack electrodes had a modest change in specific capacitance with the change in current density. This is because they are mostly mesoporous, which makes them favorable for quick electrolyte ion diffusion.⁶⁴ In general, the electrochemical performance of these three ACs is in agreement with the results predicted by the XRD powder areas.

Each of the symmetric capacitors was cycled over 300 cycles to examine their stability. They were charged and discharged between 0 and 1 V at a current density of 20 mA/cm². The variation of the specific capacitance with cycle number is shown in Figure 4.11. Overall, the specific capacitance was maintained over the 300 cycles.

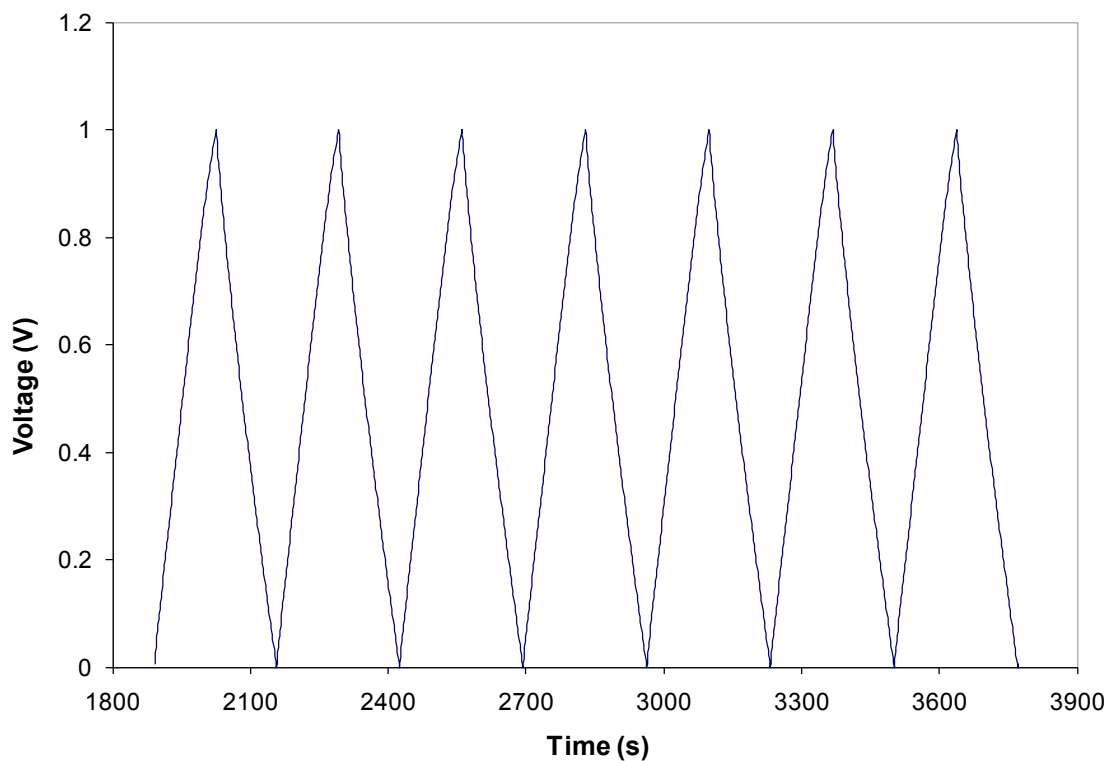


Figure 4.9. Charge and discharge curves of 95 wt% Ketjenblack EC-600JD symmetric capacitor.

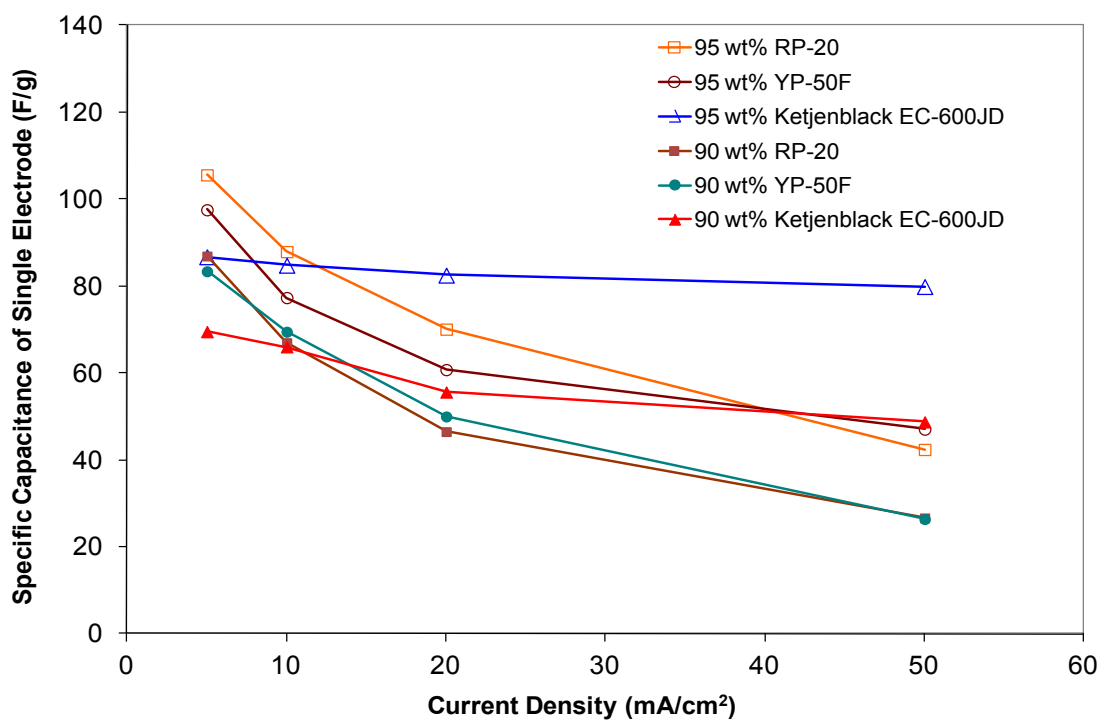


Figure 4.10. Specific capacitances of a single electrode at various discharge current densities.

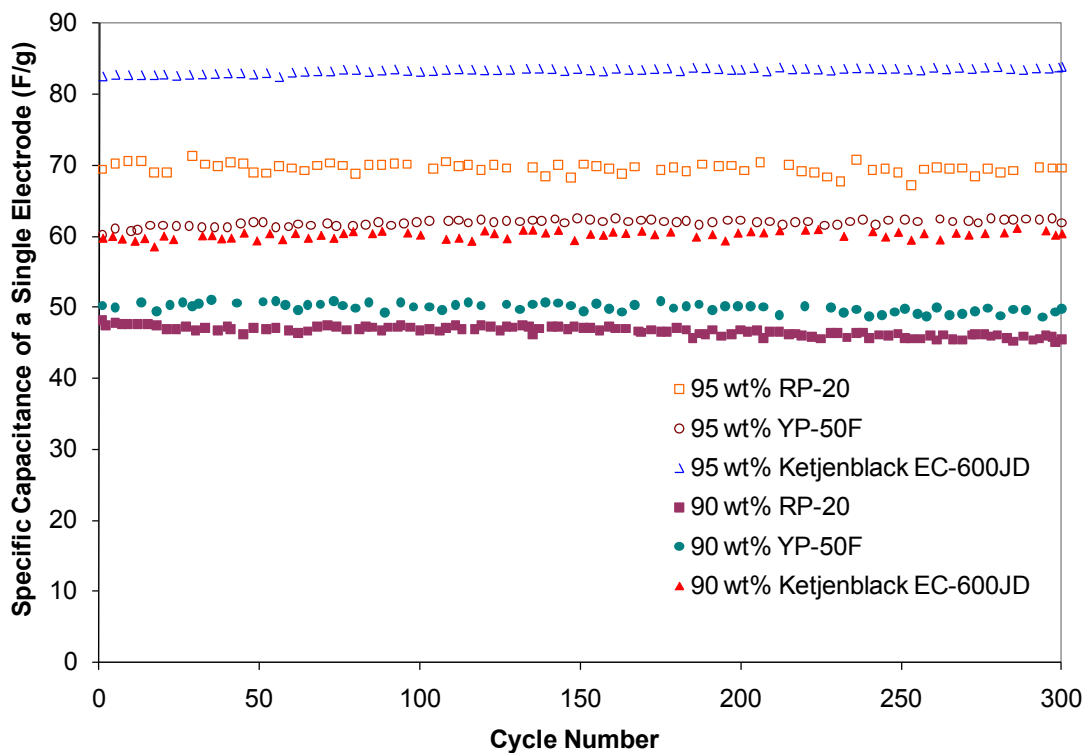


Figure 4.11. Specific capacitance of a single electrode as a function of cycle number for various AC symmetric capacitors cycled at 20 mA/cm².

4.5 Conclusions

RP-20, YP-50F and Ketjenblack EC-600JD were examined without further treatment for their suitability to serve as electrodes in symmetric capacitors. Their morphology and electrochemical performance were studied in symmetric aqueous capacitors. BET isotherms indicated the surface areas of the ACs were above 1300 m²/g. Surface area is one of the primary requirements for an AC to serve as an electrode in symmetric capacitors. Among the three ACs, the pore volume of Ketjenblack EC-600JD is much higher relative to RP-20 and YP-50F because of its mostly mesoporous structure. Each of the AC electrodes was also cycled at different current densities to determine the corresponding specific capacitance of a single electrode. At low current density, RP-20 gave the highest specific capacitance, followed by YP-50F as a result of the microporous structure, and as predicted by the powder XRD measurements. However, the lower efficiency for RP-20 makes YP-50F more attractive. At high current density, Ketjenblack

EC600-JD is more favorable. This is because the mesoporous structure of Ketjenblack EC600-JD gave rapid diffusion of electrolyte ions to the electrode surface. All three ACs can serve as electrodes in ECs, with the choice depending on the energy (low current density) or power (high current density) needs.

5.0

Optimization of the Performance of an Asymmetric Capacitor Based on a Nickel-Carbon Foam Positive Electrode

Wen Nee Yeo ¹, Tony N. Rogers ^{1,3}, Bahne C. Cornilsen ²

¹ Department of Chemical Engineering, Michigan Technological University, 1400 Townsend Drive, Houghton, MI 49931-1295

² Department of Chemistry, Michigan Technological University, 1400 Townsend Drive, Houghton, MI 49931-1295

³ To whom correspondence should be addressed: Telephone: 906-487-2210, Fax: 906-487-3213, Email: tnrogers@mtu.edu, Postal address: 1400 Townsend Drive, Houghton, MI 49931-1295

Manuscript in preparation

5.1 Abstract

An asymmetric capacitor consisting of a nickel-carbon foam (*i.e.*, a foam impregnated with nickel hydroxide) positive electrode and an AC negative electrode with different mass ratios of negative (-ve) to positive (+ve) active masses were fabricated to access conditions for optimum performance. The surface morphology and chemical structure of the positive electrode were studied through FE-SEM and XRD. The FE-SEM images showed that the carbon foam was loaded with uniform Ni(OH)_2 . The XRD results indicated that the positive electrode is a typical $\alpha\text{-Ni(OH)}_2$. Among the different mass ratios tested, the asymmetric capacitor with mass ratio of 3.71 gave the highest specific energy and specific power, 24.5 W.h/kg and 498 W/kg, respectively. In addition, the asymmetric capacitor exhibited stable cycle life when operated at 10 mA/cm² and between 1.4 and 0.4 V.

5.2 Introduction

ECs have drawn attention in recent years for use in various power and energy applications, such as hybrid vehicles, portable audio equipment, and memory back-up devices. The trend in ECs is toward a combination of a double layer electrode with a battery-type electrode.¹⁻⁴ These types of ECs are called asymmetric capacitors. The double layer electrode is usually AC since it has high surface area, good conductivity, and a relatively low cost.^{28,29} Typical battery-type electrodes can be $\text{PbO}_2/\text{PbSO}_4$, $\text{Ni(OH)}_2/\text{NiOOH}$ or LiMO_x (where M is a transition metal species). The most commonly studied battery-type electrode is Ni(OH)_2 .^{55,57,65,66}

Our previous study showed that a relatively high value of specific capacitance was obtained on a nickel-carbon foam electrode, where nickel hydroxide was impregnated on a carbon foam using electrochemical deposition (refer to Chapter 3). Carbon foam was used as a current collector for the active mass because of its electrical conductivity, pore size, and pore connectivity. The objective was to reduce the cost and weight of the ECs while maintaining or increasing its capacitance and gravimetric energy storage density. In this work, asymmetric capacitors consisting of a nickel-carbon foam electrode as the

battery-type electrode and AC as the double layer electrode were assembled with different mass ratios of negative to positive active mass in order to study the electrochemical performance.

5.3 Experimental Setup

5.3.1 Preparation of Nickel-Carbon Foam Positive Electrode

The preparation method is listed in Section 3.3.1 of Chapter 3. Since the amount of active material loaded into the carbon foam varied according to the desired mass ratio, the forming process varied accordingly. Six positive electrode loadings (full and partial deposition) have been prepared.

5.3.2 Preparation of Negative Electrode

The preparation method is listed in Section 4.3.1 of Chapter 4. The YP-50F carbon is used in this chapter to make the negative electrode. The composition of the electrode is 95 wt% YP-50F and 5 wt% PTFE binder.

5.3.3 Materials Characterization

The materials characterization on the positive electrode was the same procedure described in Section 3.3.2 of Chapter 3. Two samples (full and partial deposition) were prepared for the FE-SEM analysis and only the full deposition was analyzed using the powder XRD diffractometer.

5.3.4 Preparation of Asymmetric Capacitor

The preparation method is listed in Section 3.3.3.2 of Chapter 3. Two types of EC, for a total of seven cells (1 symmetric and 6 asymmetric), were fabricated. The first type of ECs (symmetric) was the EDLC, in which the positive and negative electrodes were the type of electrode described in Section 5.3.2. The second type of ECs was the asymmetric capacitor, in which the positive electrode is the electrode described in Section 5.3.1 and the negative electrode is the electrode described in Section 5.3.2. Six cells with active material mass ratios, defined as negative to positive active mass, from 0.80 to 9.98 were

fabricated. The assembled cells, active material mass ratios were controlled by adjusting the amount of $\text{Ni}(\text{OH})_2$ impregnated on the carbon foam current collector.

5.4 Results and Discussion

5.4.1 Materials Characteristics

The surface and cross-section morphology of the carbon foam positive electrode, fully and partially loaded with $\text{Ni}(\text{OH})_2$, were investigated by FE-SEM. Figure 5.1 shows the FE-SEM images of the surface morphology of the fully and partially deposited carbon foam positive electrode. The fully loaded electrode has a more uniform structure compared to the partially loaded electrode. Figure 5.2 shows the cross-section morphology to examine the extent of deposition in the inner pores of the carbon foam. The carbon foam with partial deposition was not completely covered with $\text{Ni}(\text{OH})_2$ as compared to the carbon foam with full deposition. It is also illustrated in the FE-SEM images that a thinner layer of $\text{Ni}(\text{OH})_2$ was formed in the carbon foam with partial deposition.

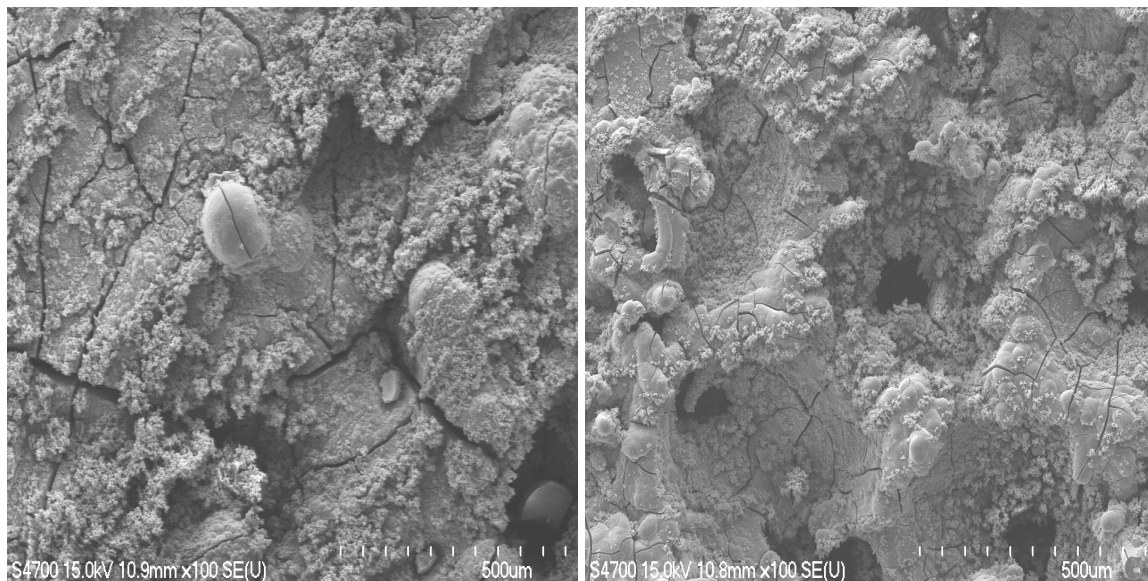


Figure 5.1. FE-SEM images of surface morphology of carbon foam impregnated with $\text{Ni}(\text{OH})_2$ taken at 100x magnification. The left photo was of the carbon foam with full deposition and the right photo was of the carbon foam with partial deposition (deposition time: 51 and 25 minutes, respectively).

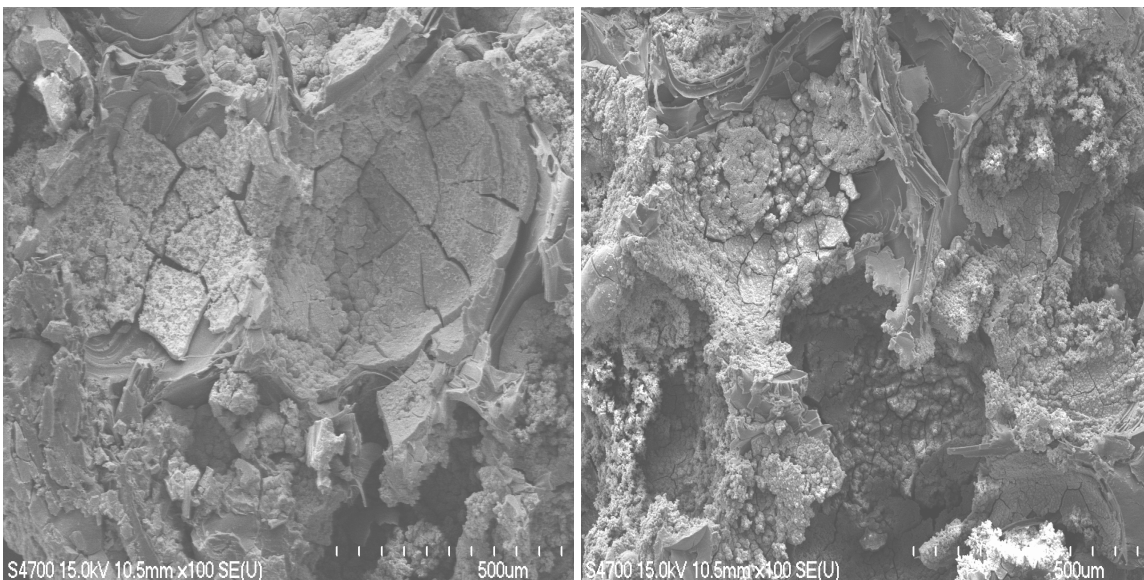


Figure 5.2. FE-SEM images of cross-section morphology of carbon foam (near the edge) impregnated with $\text{Ni}(\text{OH})_2$ at 100x magnification. The left photo was of the carbon foam with full deposition and the right photo was of the carbon foam with partial deposition.

The analysis of the XRD powder patterns of the positive electrode can be found in Section 3.4.2 of Chapter 3 and Appendix B2.

5.4.2 Electrochemical Characteristics

All seven cells were evaluated through galvanostatic charge and discharge processes. The purpose of the EDLC tests was for comparison. Asymmetric capacitors were tested between 0.4 V and 1.4 V, and the EDLC was tested between 0 V to 1 V. These cells were cycled at different current densities (5, 10, 20, and 50 mA/cm^2) to determine the corresponding specific cell capacitance. Figure 5.3 shows the specific capacitance as a function of current density for the seven cells. The specific capacitances of EDLC at 5, 10, 20, and 50 mA/cm^2 were 24, 19, 15, and 12 F/g, respectively. The minimum specific capacitances of the asymmetric capacitors at 5, 10, 20, and 50 mA/cm^2 were 64, 58, 48, and 34 F/g, respectively. The results indicated that the specific capacitance of the asymmetric capacitors is much higher compared to EDLC. Figure 5.4 shows the relationship between the specific energy and the mass ratio. The specific energy was calculated using equation 5.1, where C is the cell capacitance and V_2 and V_1 are the first and last voltages in the discharge process. Among the asymmetric capacitors tested, the

cell with the mass ratio of 3.71 gave the highest specific energy. This demonstrates that an asymmetric capacitor with a nickel-carbon foam positive electrode has a large specific energy and hence could be used in EC applications.

$$E = \frac{1}{2m} C(V_2^2 - V_1^2) \quad (5.1)$$

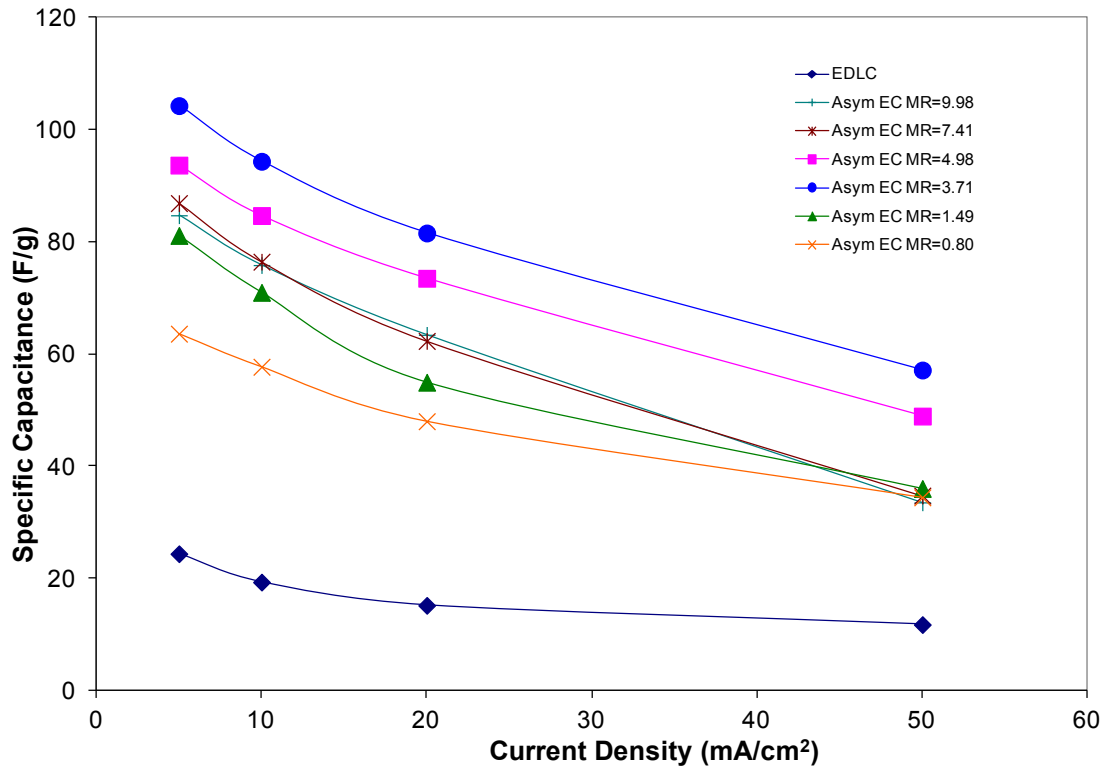


Figure 5.3. Specific capacitance as a function of discharge current density for an EDLC and six asymmetric capacitors with different mass ratios.

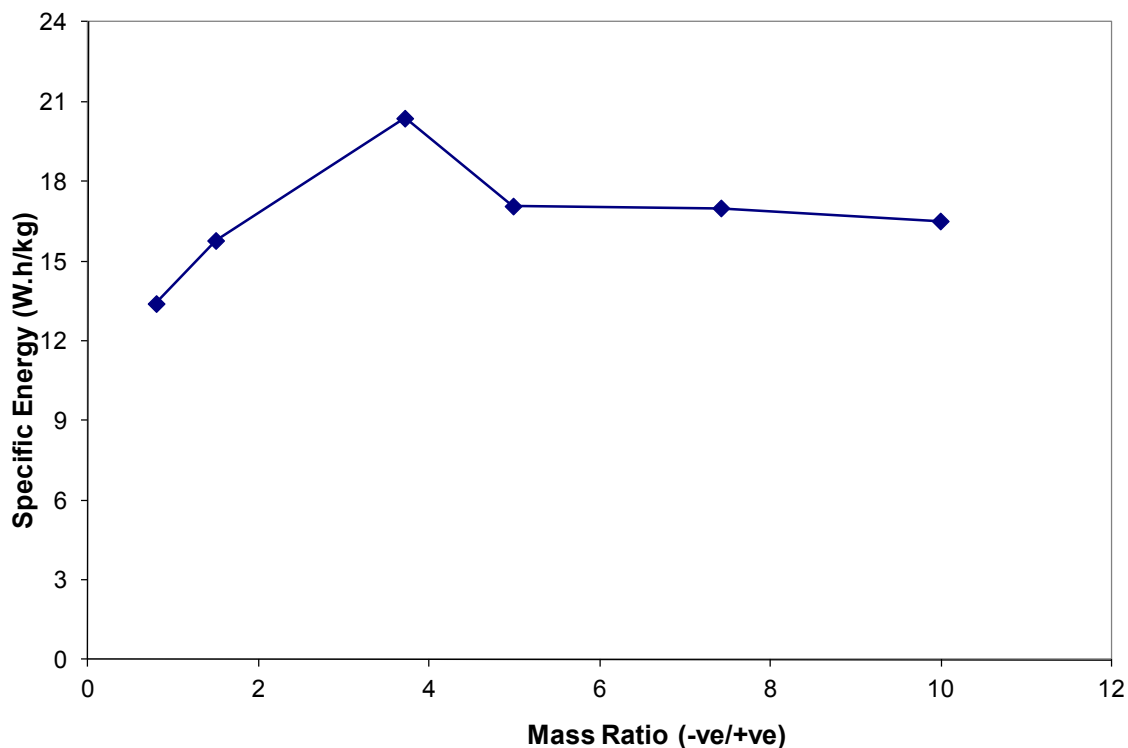


Figure 5.4. Specific energy as a function of mass ratio cycling at a current density of 10 mA/cm^2 .

A Ragone plot (Figure 5.5) relates the specific power to specific energy of the asymmetric capacitor at varying mass ratios. The specific power was calculated by dividing the specific energy by the discharge time. As seen in Figure 5.5, all the asymmetric capacitors followed the same general trend of a dramatic reduction in specific energy as specific power increased. The maximum specific energy of 24.5 W.h/kg and maximum specific power of 498 W/kg are achieved by the asymmetric capacitor with a mass ratio of 3.71.

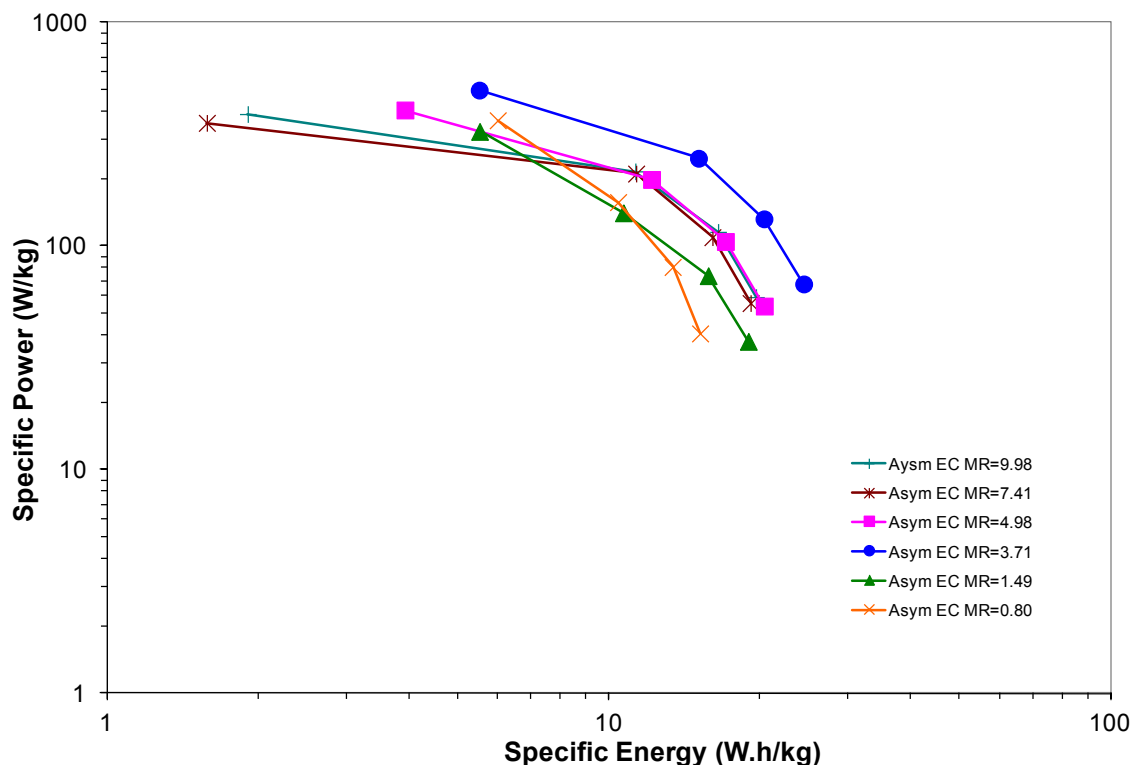


Figure 5.5. Ragone plot of asymmetric capacitors with various mass ratios at different current densities.

Among the seven cells, an asymmetric capacitor with a mass ratio of 0.80 was used to study stability of performance because it was the first assembled cell. It was observed through repeated charge and discharge processes for 10,000 cycles. The cell cycled at a current density of 10 mA/cm² and between 1.4 and 0.4 V. Figure 5.6 shows the specific capacitance and efficiency of the cell over 10,000 cycles. Efficiency is defined as the discharge capacitance over the charge capacitance. The cell maintained above 99% efficiency over the 10,000 cycles. At about cycle 8,900 as indicated in Figure 5.6, there was a sudden drop in the specific capacitance. A possible explanation is the change in the temperature in the laboratory, which increased and stayed between 90 and 100°F for about 6 days. After this period (at about cycle number 9,300), the cell's performance became stable again. The stability test demonstrated about a 33% decrease in the specific capacitance after 10,000 cycles compared to its initial value, probably due to deteriorating performance of the faradaic electrode (nickel-carbon foam electrode) and environmental changes in the laboratory.

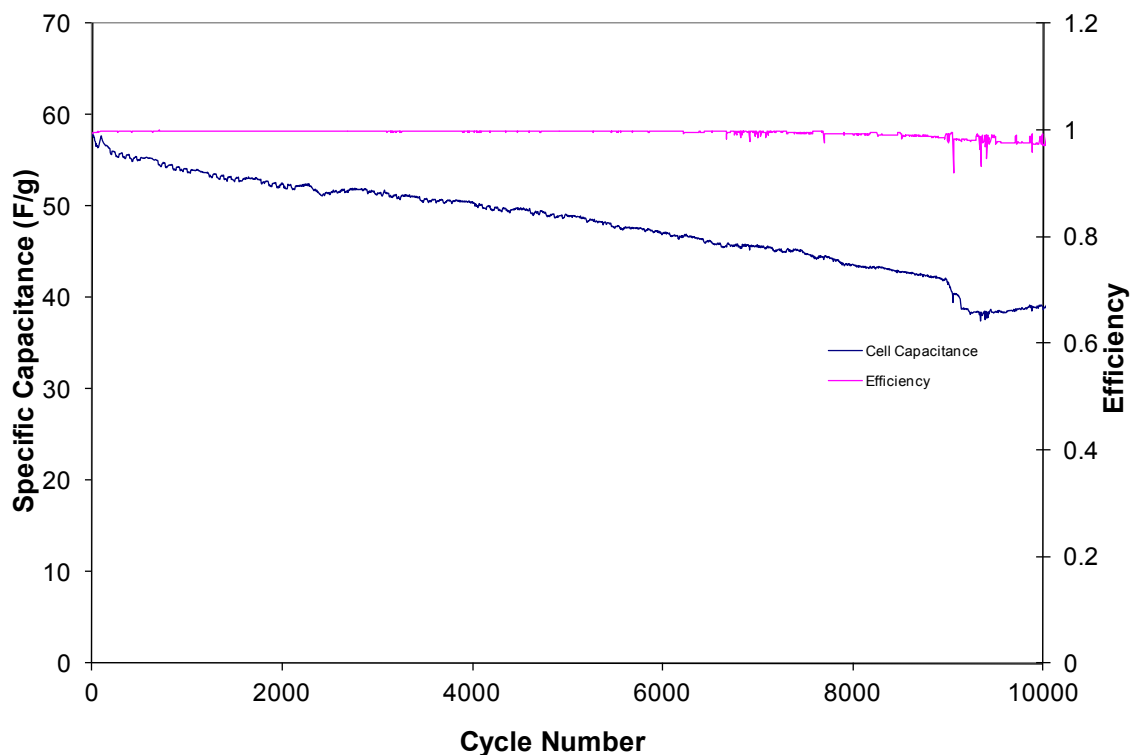


Figure 5.6. Specific capacitance and efficiency as a function of cycle number of an asymmetric capacitor with a mass ratio of 0.80 cycled at 10 mA/cm².

An asymmetric capacitor with a mass ratio of 3.71 was also analyzed through CV measurements. The CV of this asymmetric capacitor at different scan rates is presented in Figure 5.7. The CV behavior is similar to that seen in Figure 3.14. The CV curves have a smaller area (related to capacitance) at a high scan rate (*i.e.*, 25 mV/s) versus a low scan rate (*i.e.*, 5 mV/s). The reason for a larger area at a low scan rate is that the electrolyte ions can transport into the pores of the active materials more effectively.

5.5 Conclusions

Asymmetric capacitors with different mass ratios were fabricated to determine the optimum performance. FE-SEM and XRD were used to study the surface morphology and chemical structures of the positive electrodes. FE-SEM shows the fully-loaded electrode has a more uniform structure compared to the partially-loaded electrode. The XRD results indicated that the positive electrode is a typical α -Ni(OH)₂. All the asymmetric capacitors demonstrated good electrochemical performance, especially

asymmetric capacitor with mass ratio of 3.71. The specific energy and specific power achieved by this EC were 24.5 W.h/kg and 498 W/kg, respectively.

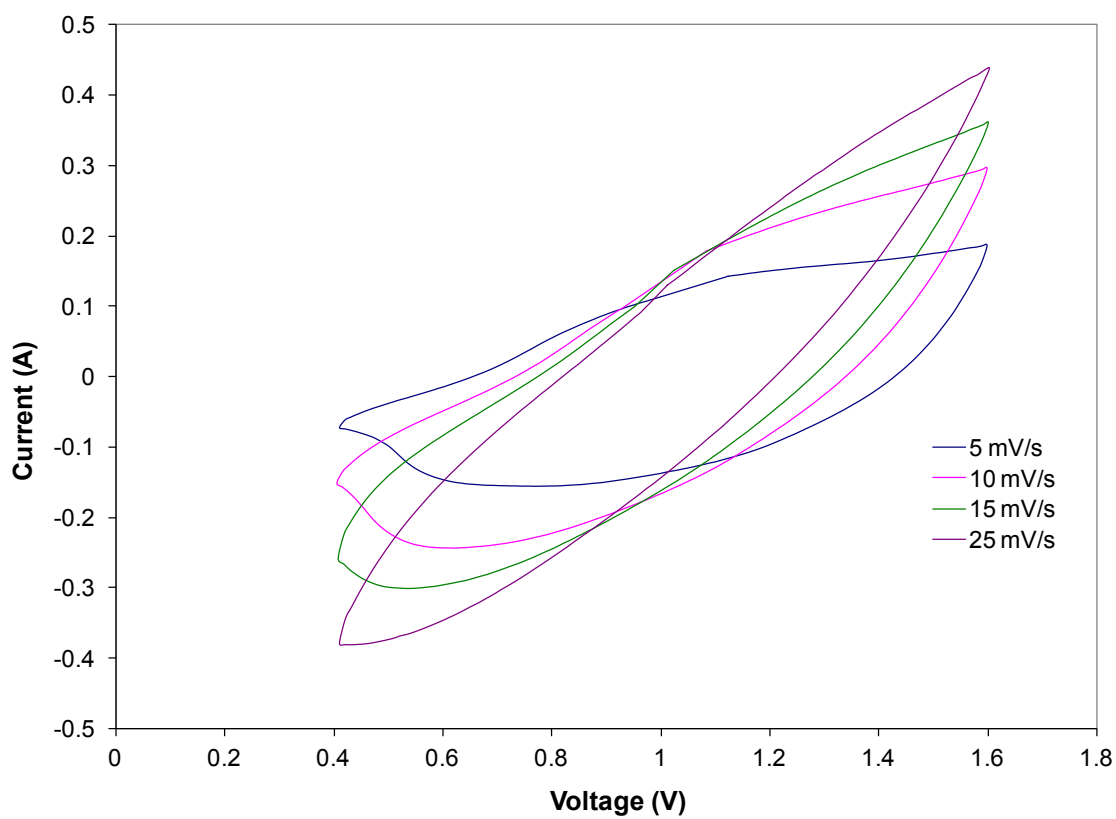


Figure 5.7. CV of an asymmetric capacitor with a mass ratio of 3.71.

6.0 Comparison of Asymmetric Capacitors with Various Carbon Materials as the Negative Electrodes

6.1 Objective

The main purpose of this chapter is to determine the effect of changing the negative electrode material (AC) on the performance of an asymmetric capacitor. As stated in chapter 4, Ketjenblack EC-600JD is a candidate AC to serve as the negative electrode in the asymmetric capacitor based on its morphology and electrochemical performance. Therefore, asymmetric capacitors with Ketjenblack EC-600JD as the negative electrode were evaluated for electrochemical performance and compared to asymmetric capacitors with YP-50F as the negative electrode.

6.2 Experimental Setup

The experimental setup was the same as described in Section 5.3 of Chapter 5. The only difference is the negative electrode, which is made of 95 wt% Ketjenblack EC-600JD and a 5 wt% PTFE binder.

6.3 Results and Discussion

Three asymmetric capacitors and an EDLC were assembled and evaluated using galvanostatic charge and discharge processes. The initial active material mass ratios for three asymmetric capacitors were 0.39, 4.66, and 6.50. Due to a technical fault during the deposition for the third cell, the mass ratio became 12.87. The purpose of the EDLC was for comparison. Asymmetric capacitors were tested between 0.4 V and 1.4 V, and the EDLC was tested between 0 V to 1 V. These cells were cycled at different current densities (5, 10, 20, and 50 mA/cm²) to determine the corresponding specific cell capacitance. Figure 6.1 shows the specific capacitance as a function of current density for the four cells. As demonstrated in Figure 6.1, these cells had a similar performance trend as seen in Figure 5.3, but with lower specific capacitances. This result was expected since

the specific capacitance of a Ketjenblack EC-600JD electrode is lower compared to that of a YP-50F electrode, namely 87 versus 98 F/g at 5 mA/cm² (refer to Figure 4.10).

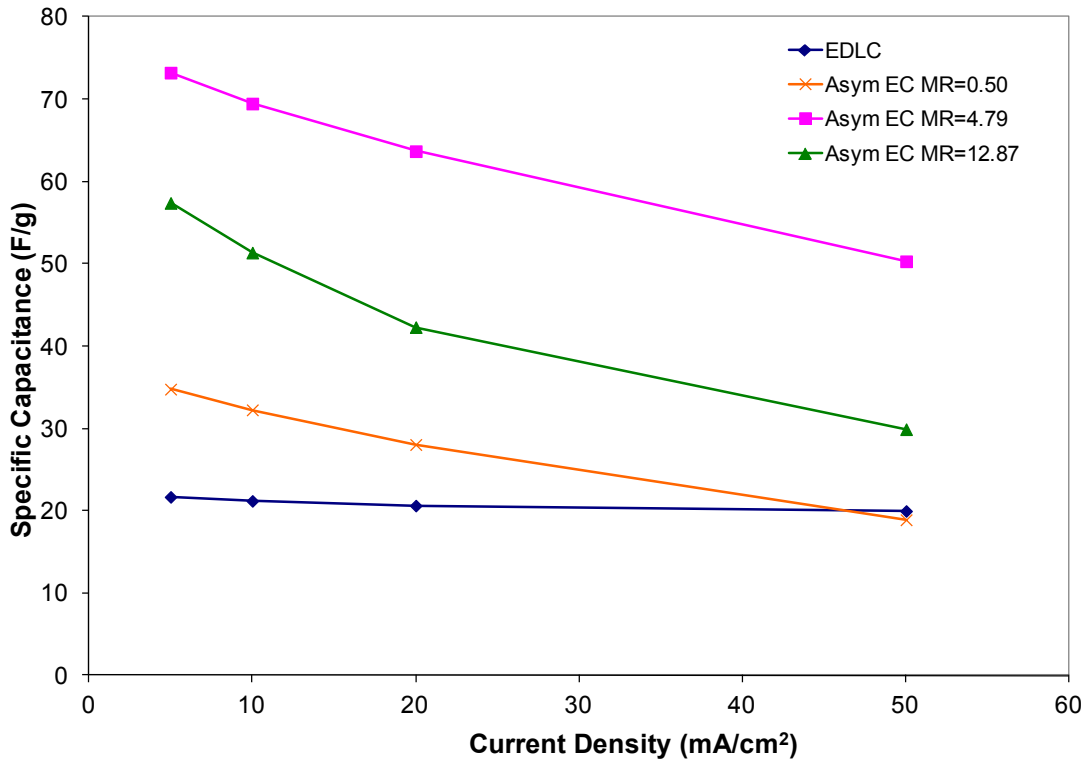


Figure 6.1. Specific capacitance as a function of discharge current density for an EDLC and asymmetric capacitors with different mass ratios.

6.4 Conclusions

From the cell experiments, regardless of which material is used for the negative electrode, a similar trend in the electrochemical performance is observed when changing the active material mass ratio. Experiments also verify that the specific capacitance of asymmetric capacitors is limited by the negative electrode. It is recommended to use the methodology in Chapter 5 to determine the optimum mass ratio when Ketjenblack EC-600JD serves as the negative electrode. It is also recommend replicating the cell with a mass ratio of 12.87 to verify the data presented in Figure 6.1.

7.0 Pouch Cell Design and Testing

7.1 Objectives

Constructing an operational pouch cell was essential for demonstrating cell durability. It is also for establishing potential commercial applications.

7.2 Experimental Setup

The pouch cell was constructed using a fabrication method similar to that used for a PFA cell. Initially, a symmetric cell was assembled with the intention of later constructing an asymmetric cell. The electrodes used within the symmetric pouch cell were composed of 95 wt% Ketjenblack EC-600JD and 5 wt% PTFE binder. Molded into a coin shape, each electrode had a diameter of approximately 1.90 cm (3/4 in) and a thickness of 0.6 mm. The electrodes were stacked and separated by two layers of separator. Both the electrodes and the separators were soaked in KOH prior to the assembly of the pouch cell. A nickel-mesh current collector was placed on the back of each electrode. Additionally, nickel foil was connected to each current collector to act as terminals. The electrodes, separators, current collectors, and foil were then aligned and this stack was placed into a vacuum pouch.

The vacuum pouch used in this research was a 4" x 6" 3 mil poly-nylon vacuum pouch, which is a three-layer blend of nylon, polyethylene, and linear low density resins (manufacturer by Elkay Plastics, product code: 30NV0406) . The function of the nylon (outer layer) is to make the pouch rigid and the polyethylene (inner layer) provides resistance to the KOH and the ability to hold a vacuum. Proper sealing is important to ensure low internal resistance of the cell. Therefore, the vacuum pouch was cut in half, and square pieces cut from the top were placed over the nickel foil to provide a surface that could be heat-sealed by the Minipack Cyclone 30 vacuum sealer. The bottom half of the bag was used to hold the electrode stack. To further ensure that the elements in the electrode stack were held in contact with each other, the pouch cell was placed between two PTFE plates. Figure 7.1 shows the actual cell.

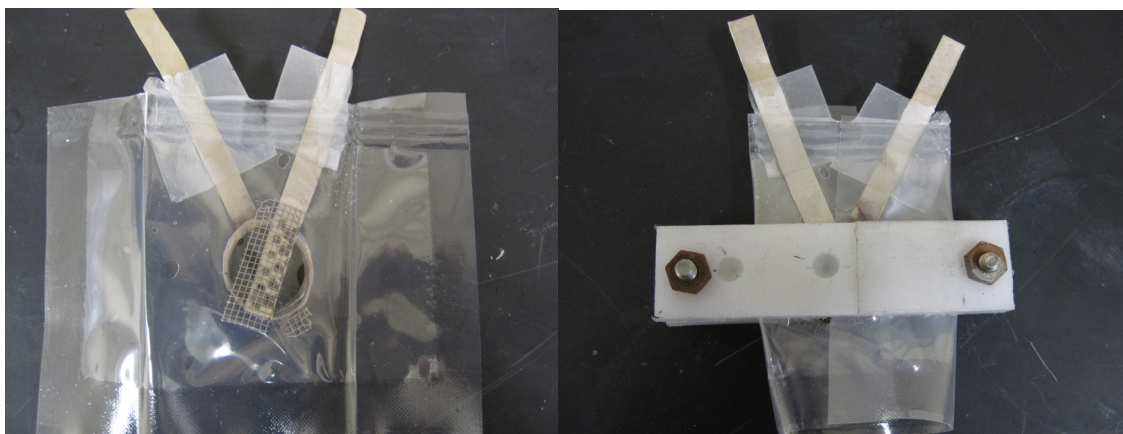


Figure 7.1. Symmetric pouch cell based on Ketjenblack EC-600JD electrodes. Left photo is the completed cell and right photo is the completed cell compressed between two PTFE plates.

7.3 Results and Discussion

Galvanostatic charge and discharge measurements have been used to evaluate the performance of the symmetric pouch cell. Figure 7.2 shows the charge and discharge behaviors of the symmetric pouch cell. It can be noticed from the figure that the voltage profile varies linearly with time, which demonstrates a pure electric double layer capacitor. In addition, there is no significant internal resistance observed. Figure 7.3 shows the specific capacitance of a single electrode versus cycle number at 5 mA/cm^2 . The results indicated that the performance of the cell was maintained for about 1000 cycles and began to decrease after that. The specific capacitance of a single electrode at 5 mA/cm^2 obtained from the pouch cell was 86 F/g , which is the same obtained from the PFA cell in Chapter 4 (87 F/g).

7.4 Conclusions

The next step is to find a better way to maintain the vacuum within the cell in order to prolong the cycle life. The cell had 3 parallel, independent heat seals by the Minipack Cyclone 30 vacuum sealer, but pressure built up inside the cell over time, either from air leakage or electrode off gassing. A better vacuum sealer might be needed to solve the problem. After solving the sealing problem, an asymmetric cell with the optimum mass ratio should be constructed and evaluated for electrochemical performance. The results obtained should then be compared with the earlier results obtained from the PFA cell in

Chapter 5. A pouch cell with at least 50,000 cycles and an efficiency of more than 95% is needed to prove the durability of the nickel-carbon foam asymmetric capacitor.

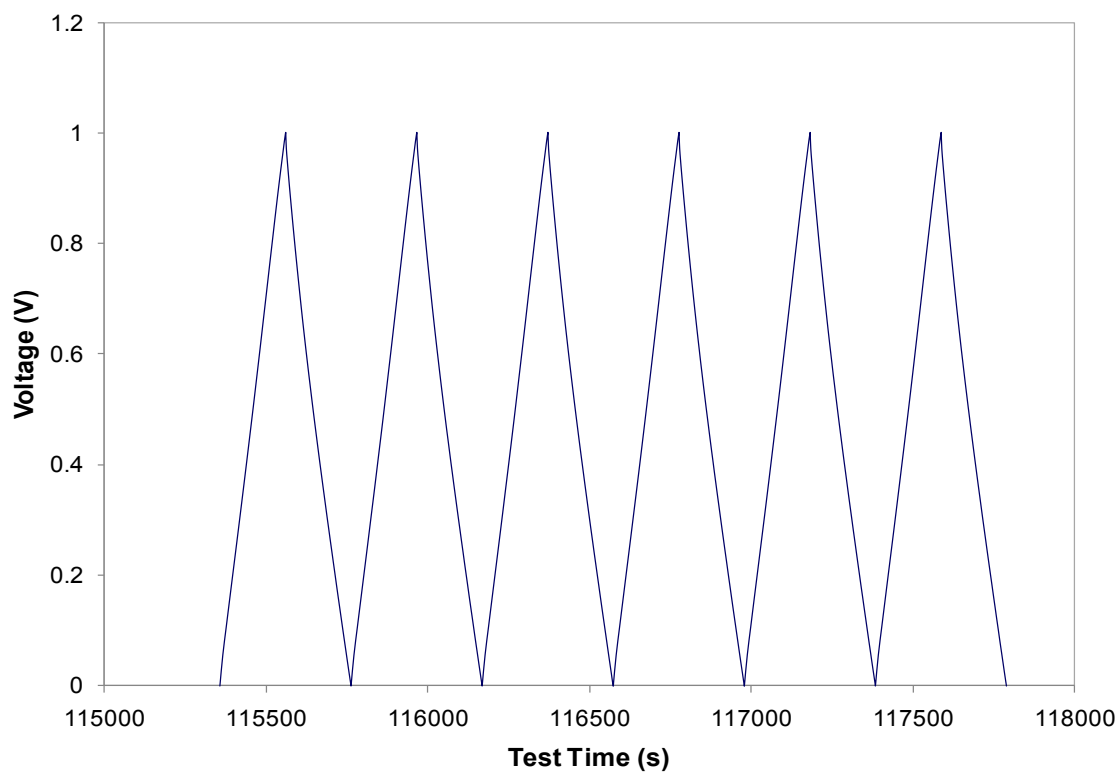


Figure 7.2. Charge and discharge behavior of the 95 wt% Ketjenblack EC-600JD symmetric capacitor (pouch cell) at 5 mA/cm².

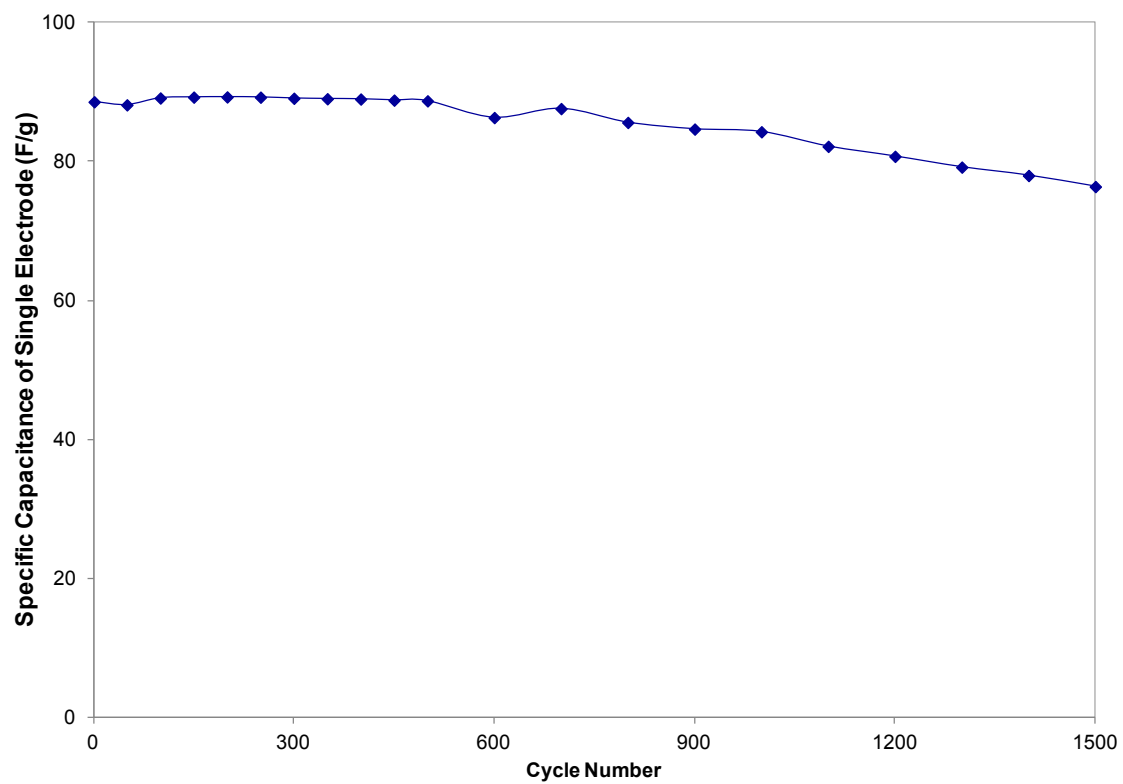


Figure 7.3. Specific capacitance of single electrode versus cycle number. The pouch cell was cycled at 5 mA/cm².

8.0 Conclusions and Future Work

8.1 Conclusions

ECs have gained popularity in the market in recent years due to the trend for high power and long cycle life energy storage devices. Asymmetric capacitors are of particular interest because they have higher specific power compared to batteries and higher specific energy compared to conventional capacitors. During this research, asymmetric capacitors using a nickel-carbon foam positive electrode and an AC electrode were fabricated and tested. The morphology of these electrodes was studied through FE-SEM, BET, porosity measurements, and powder XRD. Below summarizes how the findings of this research to satisfy the objectives stated in chapter 1:

(iv) *To determine the specific capacitance and the material characteristics of the nickel-carbon foam electrode.*

- a. Specific capacitance of the nickel-carbon foam electrode at 5 mA/cm^2 was 2641 F/g , which is higher than the reported value (2080 F/g) of a 7.5% Al-substituted $\alpha\text{-Ni(OH)}_2$ electrode.
- b. FE-SEM indicated uniform particle shape and a loose packed structure, allowing the electrolyte ions to access the Ni(OH)_2 .
- c. The XRD powder pattern of the nickel-carbon foam electrode is a $\alpha\text{-Ni(OH)}_2$ with dimensions of $a = 3.091 \text{ \AA}$ and $c = 24.184 \text{ \AA}$ for a hexagonal cell.

(v) *To examine different carbon-based materials to serve as the negative electrode in an asymmetric capacitor through the study of an EDLC and variation of the carbon-based material morphology.*

- RP-20, YP-50F, and Ketjenblack EC-600JD were tested in a symmetric cell configuration to determine their suitability to serve as the negative electrode in the asymmetric configuration. YP-50F was chosen because of its overall performance.
- The three ACs have high surface areas, mesopores, and micropores. The majority of pores for RP-20 and YP-50F are micropores, whereas Ketjenblack

EC-600JD has mostly mesopores as indicated by N₂ adsorption/desorption. The surface area and pore structure are important factors that affect the performance of the AC capacitors.

- The XRD powder patterns of the three ACs imply that these ACs are amorphous carbons, with Ketjenblack EC-600JD having somewhat more graphitic order than the others.
- The XRD analyses of the ACs agree with the trend in electrochemical performance: RP-20 has the highest specific capacitance, followed by YP-50F and Ketjenblack EC-600JD.

(vi) *To determine the optimum mass ratio for maximum specific energy through the study of electrochemical performance of asymmetric capacitors assembled with different mass ratios.*

- a. The specific cell capacitance of an asymmetric capacitor is limited by the specific capacitance of the negative electrode.
- b. An optimum specific energy of 24.5W.h/kg and specific power of 498 W/kg were obtained through cell tests at a mass ratio of 3.71.

8.2 Future Work

This research has demonstrated that a nickel-carbon foam electrode is capable of serving as the positive electrode in an asymmetric capacitor. Further testing and improvements are needed to achieve higher specific capacitance and hence, higher specific energy and specific power. These improvements fall into three categories:

(i) *Negative electrode*

- Apply chemical treatment to activate the ACs to increase the surface area and/or pore volume to further improve the specific capacitance of the cell.
- Include graphite powders in the negative electrode formulation to further improve the conductivity of the electrode, and evaluate whether the new formulation improves the electrochemical performance of symmetric and asymmetric cells.

- Alter the method of making the negative electrodes, such as using a film applicator or a paint brush to better control the uniformity of the thin film electrode. A consistent quality of electrode is needed, especially for large batch production.

(ii) Cell design

- Determine the cycle life of an asymmetric capacitor with the optimum mass ratio of 3.71.
- Reduce the thickness of POCOfoam[®] so that full Ni(OH)₂ deposition can be performed in high mass ratio cells in order to minimize the change in the specific cell capacitance over extended cycling.
- Build a prototype cell (pouch cell) based on the conclusions drawn from the PFA cell tests to confirm the performance of the asymmetric capacitor with nickel-carbon foam electrodes that are commercially feasible.
- Assemble several cells in series to increase the operational voltage to 3 V and hence, increase the stored energy.

(iii) Current collector choice

- Replace POCOfoam[®] with KFOAM[™] (L1250) from Koppers Inc. as the current collector of the positive electrode and evaluate the electrode's electrochemical performance as well as its morphology. KFOAM[™] has better mechanical strength when machined to thin electrodes (less than 1 mm).

References

1. Becker HI; General Electric Company, assignee. Low Voltage Electrolytic Capacitor. U.S patent US 2,800,616. 1957 July 23.
2. Rightmire RA; Standard Oil Company, assignee. Electrical Energy Storage Apparatus. U.S patent US 3,288,641. 1966 Nov. 29.
3. Brodd RJ, Bullock KR, Leising RA, Middaugh RL, Miller JR, Takeuchi E. Batteries, 1977 to 2002. *Journal of the Electrochemical Society* 2004;151(3):K1-11.
4. Pell WG, Conway BE. Peculiarities and Requirements of Asymmetric Capacitor Devices based on Combination of Capacitor and Battery-Type Electrodes. *Journal of Power Sources* 2004;136:334-345.
5. Ultracapacitors for Off-Grid Solar Energy Applications [Internet]. [updated November 8th, 2009, cited November 9th, 2009]. Available from: http://www.solrayo.com/SolRayo/Off-Grid_Solar_Energy_Applications_files/Ultracapacitors%20for%20Off-Grid%20Solar%20Applications.pdf
6. Bhatia AS. Nickel Hydroxide Impregnated Carbon Foam Electrodes for Rechargeable Nickel Batteries [M.S Thesis]. Houghton: Michigan Technological University; 2003.
7. Duffy NW, Baldsing W, Pandolfo AG. The Nickel-Carbon Asymmetric Supercapacitor - Performance, Energy Density and Electrode Mass Ratios. *Electrochimica Acta* 2008;54:535 - 539.
8. Barnard R, Randell CF, Tye FL. Studies Concerning the Ageing of alpha and beta-Ni(OH)₂ in Relation to Nickel-Cadmium Cells. *Power Sources* 1981;8:401-425.
9. Loyselle PL, Karjala PJ, Cornilsen BC. A Point Defect Model for Nickel Electrode Structures. In: J. Robert Selman HCM, editor. *Electrochemical and Thermal Modeling of Battery, Fuel Cell and Photoenergy Conversion Systems*. Pennington, NJ: J. Selman and H. C. Maru, Eds., The Electrochemical Society Proceedings Series; 1986. p 114.

10. Munoz-Rojas D, Leriche J-B, Delacourt C, Poizot P, Palacin MR, Tarascon J-M. Development and Implementation of a High Temperature Electrochemical Cell for Lithium Batteries. *Electrochemistry Communications* 2007;9:708-712.
11. Conway BE. *Electrochemical Supercapacitors - Scientific Fundamentals and Technological Applications*. New York: Kluwer Academic / Plenum; 1999.
12. Brodd RJ, Bullock KR, Leising RA, Midaugh RL, Miller JR, Takeuchi E. Batteries, 1977 to 2002. *Journal of the Electrochemical Society* 2004;151(3):K1-K11.
13. Kotz R, Carlen M. Principles and Applications of Electrochemical Capacitors. *Electrochimica Acta* 2000;45:2483-2498.
14. Double layer (interfacial) [Internet]. Wikipedia, The Free Encyclopedia[updated Aug 31, 2011, cited Sept 22, 2011]. Available from: [http://en.wikipedia.org/wiki/Double_layer_\(interfacial\)](http://en.wikipedia.org/wiki/Double_layer_(interfacial))
15. Capacitance [Internet]. Wikipedia, The Free Encyclopedia[updated Oct 19, 2011, cited Oct 30, 2011]. Available from: <http://en.wikipedia.org/wiki/Capacitance>
16. Miller JR, Simon P. Fundamentals of Electrochemical Capacitor Design and Operation. *The Electrochemical Society's Interface* 2008:31-32.
17. Trasatti S, Kurzweil P. Electrochemical Supercapacitors as Versatile Energy Stores. *Platinum Metals Review* 1994;38(2):46-55.
18. Razoumov S, Klementov A, Litvinenko S, Beliakov A; Joint Stock Company "Elton", Moscow, assignee. Asymmetric Electrochemical Capacitor and Method of Making. US patent US 6,222,723. 2001 Apr. 24.
19. Beliakov AI, Brintsev AM. Development and Applications of Combined Capacitors: Double Electric Layer - Pseudocapacity. 1997 Dec 8-11; Deerfield Beach, FL.
20. Volfkovich YM, Shmatko PA. High Energy Density Supercapacitor. 1998 Dec 7-9; Deerfield Beach, FL.
21. Belyakov AI. Asymmetric Electrochemical Supercapacitors with Aqueous Electrolytes. 3rd European Symposium on Supercapacitors and Applications (ESSCAP) Roma, Italy 2008.

22. Klementov AD, Varakin IV, Litvinenko S, Starodubtsev N, Stepanov A. New Ultracapacitors Developed by JSC "ESMA" for Various Applications. 1998 Dec 7-9; Deerfield Beach, FL.
23. Electric Battery [Internet]. Vaunt Design Group[updated February 02, 2009, cited February 15, 2009]. Available from:
<http://www.ideafinder.com/history/inventions/battery.htm>
24. Bode H, Dehmelt K, White J. Zur kenntnis der nickelhydroxidelektrode—I. Über das nickel (II)-hydroxidhydrat. *Electrochimica Acta* 1966;11(8):1079-1087.
25. Cornilsen BC, Karjala PJ, Loyselle PL. Structural Models for Nickel Electrode Active Mass. *Journal of Power Sources* 1988;22:351-357.
26. Cornilsen BC, Shan X, Loyselle PL. Structural Comparison of Nickel Electrodes and Precursor Phases. *Journal of Power Sources* 1990;29:453.
27. Srinivasan V, Cornilsen BC, Weidner JW. A Nonstoichiometric Structural Model to Characterize Changes in the Nickel Hydroxide Electrode during Cycling *Journal of Solid State Electrochemistry* 2005;9:61-76.
28. Taberna P-L, Chevallier G, Simon P, Plee D, Aubert T. Activated Carbon-Carbon Nanotube Composite Porous Film for Supercapacitor Applications. *Materials Research Bulletin* 2006;41:478-484.
29. Babel K, Jurewicz K. KOH Activated Carbon Fabrics as Supercapacitor Material. *Journal of Physics and Chemistry of Solids* 2004;65:275-280.
30. Pandolfo AG, Hollenkamp AF. Carbon Properties and Their Role in Supercapacitors. *Journal of Power Sources* 2006;157:11-27.
31. Frackowiak E. Carbon Materials for Supercapacitor Application. *Physical Chemistry Chemical Physics* 2006;9:1774 - 1785.
32. Salitra G, Soffer A, Eliad L, Cohen Y, Aurbach D. Carbon Electrodes for Double-Layer Capacitors I. Relations between Ions and Pore Dimensions. *Journal of the Electrochemical Society* 2000;147(7):2486 - 2493.
33. Eliad L, Salitra G, Soffer A, Aurbach D. Ion Sieving Effects in the Electrical Double Layer of Porous Carbon Electrodes: Estimating Effective Ion Size in

- Electrolytic Solutions. *The Journal of Physical Chemistry B* 2001;105(29):6880 - 6887.
34. Qu DY, Shi H. Studies of Activated Carbons Used in Double- Layer Capacitors. *Journal of Power Sources* 1998;74(1):99-107.
 35. Wang KP, Teng HS. The Performance of Electric Double Layer Capacitors using Particular Porous Carbons Derived from PAN Fiber and Phenol-Formaldehyde Resin. *Carbon* 2006;44(15):3218-3225.
 36. Jurewicz K, Babel K, Ziolkowski A, Wachowska H, Kozlowski M. Ammoxidation of Brown Coals for Supercapacitors. *Fuel Processing Technology* 2002;77-78:191-198.
 37. Jurewicz K, Babel K, Ziolkowski A, Wachowska H. Ammoxidation of Active Carbons for Improvement of Supercapacitor Characteristics. *Electrochimica Acta* 2003;48(11):1491-1498.
 38. Frackowiak E, Lota G, Machnikowski J, Vix-Guterl C, Beguin F. Optimisation of Supercapacitors using Carbons with Controlled Nanotexture and Nitrogen Content. *Electrochimica Acta* 2006;51(11):2209-2214.
 39. Li C, Reuss RH; Motorola Inc., Schaumburg Ill, assignee. Electrochemical Capacitor with Solid Electrolyte patent US 5,986,878. 1999 Nov 16
 40. Yoshida A, Nishida K, Nonaka S, Nomoto S, Ikeda M, Ikuta S. Japan patent 9-266143. 1997.
 41. Zheng JP, Jow TR. The Effect of Salt Concentration in Electrolytes on the Maximum Energy Storage for Double Layer Capacitors. *Journal of the Electrochemical Society* 1997;144(7):2417-2420.
 42. Lipka SM, Miller JR, Xiao TD, Dai J; U.S Nanocorp, Inc., assignee. Asymmetric Electrochemical Supercapacitor and Method of Manufacture Thereof patent US 7,576,971 B2. 2009 Aug. 18.
 43. Yeo WN. Electrochemical Applications of Carbon Foam Electrodes [M.S Thesis]. Houghton: Michigan Technological University; 2003.

44. Zhao D, Zhou W, Li H. Effects of Deposition Potential and Anneal Temperature on the Hexagonal Nanoporous Nickel Hydroxide Films. *Chemistry of Materials* 2007;19:3882-3891.
45. Yuan A, Cheng S, Zhang J, Cao C. Effects of Metallic Cobalt Addition on the Performance of Pasted Nickel Electrodes. *Journal of Power Sources* 1999;77(2):178-182.
46. Watanabe K-i, Koseki M, Kumagai N. Effect of Cobalt Addition to Nickel Hydroxide as a Positive Material for Rechargeable Alkaline Batteries. *Journal of Power Sources* 1996;58(1):23-28.
47. Oshitani M, Yufu H, K.Takashima, Tsuji S, Matsumaru Y. Development of a Pasted Nickel Electrode with High Active Material Utilization. *Journal of the Electrochemical Society* 1989;136(6):1590-1593.
48. Oshitani M, Takayama T, Takashima K, Tsuji S. A Study on the Swelling of a Sintered Nickel Hydroxide Electrode. *Journal of Applied Electrochemistry* 1986;16:403-412.
49. Armstrong RD, Briggs GWD, Charles EA. Some Effects of the Addition of Cobalt to the Nickel Hydroxide Electrode. *Journal of Applied Electrochemistry* 1988;18:215-219.
50. Chye MB. Development and Characterization of a Rechargeable Carbon Foam Electrode Containing Nickel Oxyhydroxide Active Mass [PhD Dissertation]. Houghton Michigan Technological University; 2011.
51. Morgan DR. Thermal, Electrical, and Structural Analysis of Graphite Foam [M.S Thesis]: University of North Texas; 2001.
52. Database of Zeolite Structures [Internet]. [updated September 22, 2011, cited September 30, 2011]. Available from: <http://www.iza-structure.org/databases/>
53. Lim HS, Smithrick JJ. Advantages of 26% KOH Electrolyte Over Conventional 31% KOH Electrolyte for Nickel-hydrogen Cells. *Proceedings of the 28th International Energy Conversion Engineering Conference. Volume 1. Atlanta, GA*1993. p 151-156.

54. Loyselle PL, Shan X, Cornilsen BC. Raman Spectral Observation of a 'New Phase' Observed in Nickel Electrodes Cycled to Failure. *Journal of Power Sources* 1991;36:279-284.
55. Zhao D-D, Bao S-J, Zhou W-J, Li H-L. Preparation of Hexagonal Nanoporous Nickel Hydroxide Film and Its Application for Electrochemical Capacitor. *Electrochemistry Communications* 2007;9:869-874.
56. Seiger HN. *Electrochemistry: A Consistent Theoretical Treatment*. Lincoln: Writers Club Press; 2001.
57. Lang J-W, Kong L-B, Liu M, Luo Y-C, Kang L. Asymmetric Supercapacitors Based on Stabilized Alpha-Ni(OH)₂ and Activated Carbon. *Journal of Solid State Electrochemistry* 2010;14:1533-1539.
58. Li J, Wang X, Huang Q, Gamboa S, Sebastian PJ. A New Type of MnO₂.xH₂O/CRF Composite Electrode for Supercapacitors. *Journal of Power Sources* 2006;160:1501-1505.
59. Lipka SM, Kunadian V, Chen R, Swartz C. Activated Carbon Spheres Prepared from Hydrothermal Synthesis of Biomass Waste. 2011 June 6-12; Mainz, Germany.
60. Barrett EP, Joyner LG, Halenda PP. The Determination of Pore Volume and Area Distributions in Porous Substances. I. Computations from Nitrogen Isotherms. *Journal of The American Chemical Society* 1951;73:373-380.
61. Lowell S, Shields JE, Thomas MA, Thommes M. *Characterization of Porous Solids and Powders: Surface Area, Pore Size, and Density*. Netherlands: Springer; 2006.
62. Tamai H, Kouzu M, Morita M, Yasuda H. Highly Mesoporous Carbon Electrodes for Electric Double-Layer Capacitors. *Electrochemical and Solid-State Letters* 2003;6(10):A214-A217.
63. Qu D. Studies of the Activated Carbons Used in Double-Layer Supercapacitors. *Journal of Power Sources* 2002;109:403-411.

64. Xia K, Gao Q, Jiang J, Hu J. Hierarchical Porous Carbons with Controlled Micropores and Mesopores for Supercapacitor Electrode Materials. *Carbon* 2008;46:1718-1726.
65. Park JH, Kim S, Park OO, Ko JM. Improved Asymmetric Electrochemical Capacitor using Zn-Co Co-Doped Ni(OH)₂ Positive Electrode Material. *Applied Physics A* 2006;82:593-597.
66. Huang Q, Wang X, Li J, Dai C, Gamboa S, Sebastian PJ. Nickel Hydroxide/Activated Carbon Composite Electrodes for Electrochemical Capacitors. *Journal of Power Sources* 2007;164(425-429).

Appendix A Experimental Setup and Procedures

Appendix A1 Experimental Apparatus

The major experimental apparatus used in the research are:

- (a) Arbin 8 channel MSTAT electrochemical testing system: to perform deposition on the positive electrodes, CV, and galvanostatic charge and discharge measurements.
- (b) Temperature bath: to maintain the temperature during the deposition.
- (c) Miromeritics ASAP 2020 Accelerated Surface Area and Porosimetry Analyzer: to measure the surface area and pore size of the electrodes.
- (d) Hitachi S-4700 FE-SEM: to study the morphology carbon foam (as-received) and nickel-carbon foam positive electrodes.
- (e) Scintag XDS2000 Powder Diffractometer: to observe any changes in the structure of the nickel hydroxide active mass after deposition and after charge and discharge; and the XRD patterns for the ACs.

Appendix A2 Experimental Procedures

Deposition solution preparation

- (a) Measure the amount of $\text{Ni}(\text{NO}_3)_2$ and $\text{Co}(\text{NO}_3)_2$. For 1L of 1.8 M $\text{Ni}(\text{NO}_3)_2$ and 0.26 M $\text{Co}(\text{NO}_3)_2$ solution, measure 523.46 g and 74.78 g of $\text{Ni}(\text{NO}_3)_2$ and $\text{Co}(\text{NO}_3)_2$ respectively, to produce a mole ratio of $\text{Co/Ni} = 0.143$.
- (b) Measure 475 mL of 95 % EtOH and mix with 525 mL of deionized water, for 45 vol% EtOH solution.
- (c) Place the chemicals from (a) into a volumetric flask and add the solution from (b) to the mark on the volumetric flask.

Electrolyte solution preparation (26 wt% KOH)

- (a) Measure 305 g of KOH pellets (85 % ACS Reagent) and keep in a closed container.
- (b) Measure 695 g of deionized water and heat it on a hot plate to remove any O₂.
- (c) Slowly add the KOH pellets into the warm water.

Positive electrode preparation and handling

- (a) Cut the carbon foam using the low speed saw to a dimension of 25 x 25 x 1.5 mm and use a cutter to punch the carbon foam into a circular shape ($d = \frac{3}{4}$ in).
- (b) Wash the carbon foam with 50/50 EtOH/deionized water in a sonicator for 30 minutes and dry under vacuum for an hour.

Deposition on the carbon foam electrode

- (a) Carefully attach the working (carbon foam) and the counter (nickel plates) electrodes in a (Nalgene®) 250 ml translucent polypropylene jar that contains the deposition solution.
- (b) Heat the cell assembly in a constant temperature bath up to 70 °C.
- (c) Begin the pre-deposition step by connecting the Green and Red electrode leads to the working electrode (carbon foam) and White and Black electrode leads to the counter electrode (nickel plate).
- (d) Operate the MSTAT using MIST Pro software. All depositions are done at a constant current. The current applied for each deposition is based on the current density used, multiplied by the projected area of one side of the working electrode.
- (e) Perform the deposition step after the pre-deposition step is completed. Connect the Green and Red electrode leads to the counter electrode (nickel plate) and White and Black electrode leads to the working electrode (carbon foam).
- (f) Operate the MSTAT using MIST Pro software as before.
- (g) After the deposition is complete, remove the cell from the bath and wash the electrodes with deionized water to remove the excess deposition solution.
- (h) Dispose the deposition solution in the chemical disposal canister and write an entry in the waste chemical logbook.

Formation of the nickel-carbon foam electrode

- (a) Clean the counter electrode (nickel plate) from the deposition process with deionized water or with dilute nitric acid.
- (b) Clean the working electrode (nickel-carbon foam electrode) with deionized water to remove any nickel (II) nitrate solution on the surface.
- (c) Place the electrodes in a (Nalgene®) 250 ml translucent polypropylene jar that contains the electrolyte solution. Insert the Hg/HgO reference electrode as well. The cell is called the flooded cell.
- (d) Connect to the MSTAT by connecting the Red and White electrode lead to the working electrode (carbon foam), the Black electrode lead to the counter electrode (nickel plate), and the Green electrode lead to the reference electrode.
- (e) Operate the MSTAT using the MIST Pro software.

Negative electrode preparation

- (a) Measure the carbon black powder and PTFE according to the formulation.
- (b) Mix and grind together in a mortar for about an hour or until the PTFE is well dispersed in the carbon black powder.
- (c) Heat the mixture at 120 °C in an oven for an hour, followed by 20 minutes of grinding in the mortar.
- (d) Repeat step (c) twice.
- (e) Press the mixture using a rod to form dough with the help of isopropyl alcohol.
- (f) Roll the dough to the desired thickness (0.6 mm) and air dry for a few hours to evaporate the isopropyl alcohol.
- (g) Punch out the electrode in a coin shape with a diameter of $\frac{3}{4}$ inch and heat at 80 °C in an oven for an hour.
- (h) Soak the electrodes in electrolyte (KOH) to allow electrolyte uptake within the pores of the electrode network.

Assemble the sealed cell

- (a) Place a layer of nickel mesh on one plunger, then the nickel-carbon foam electrode.

- (b) Place two layers of pre-soaked separators on top of the nickel-carbon foam electrode followed by the negative electrode, and a plunger.
- (c) Connect to the MSTAT by connecting the Red and White electrode leads to the positive electrode, and the Black and Green electrode leads to the negative electrode.
- (d) Operate the MSTAT using the MIST Pro software.

Appendix B Electrode Morphology and Chemical Structure

Appendix B1 Experimental Apparatus

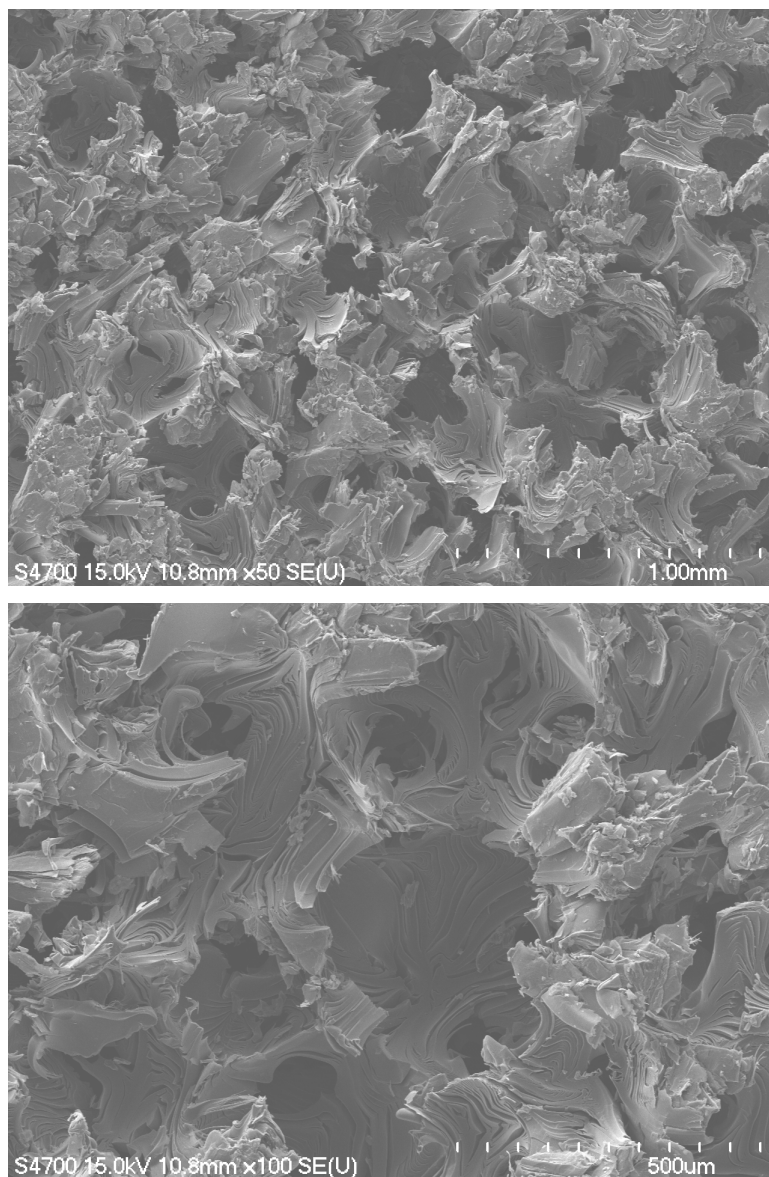


Figure B.1. FE-SEM images of surface morphology of carbon foam at 50x (upper photo) and 100x (lower photo) magnifications.

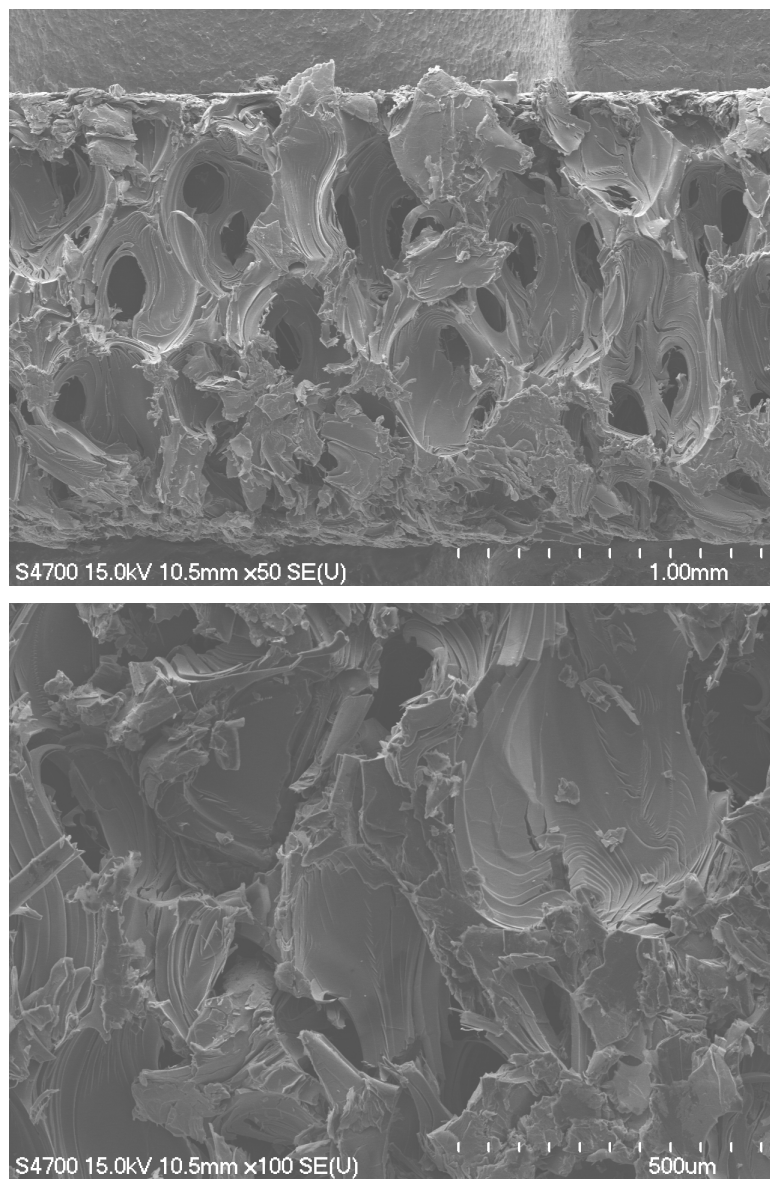


Figure B.2. FE-SEM images of cross-section morphology of carbon foam at 50x (upper photo) and 100x (lower photo) magnifications.

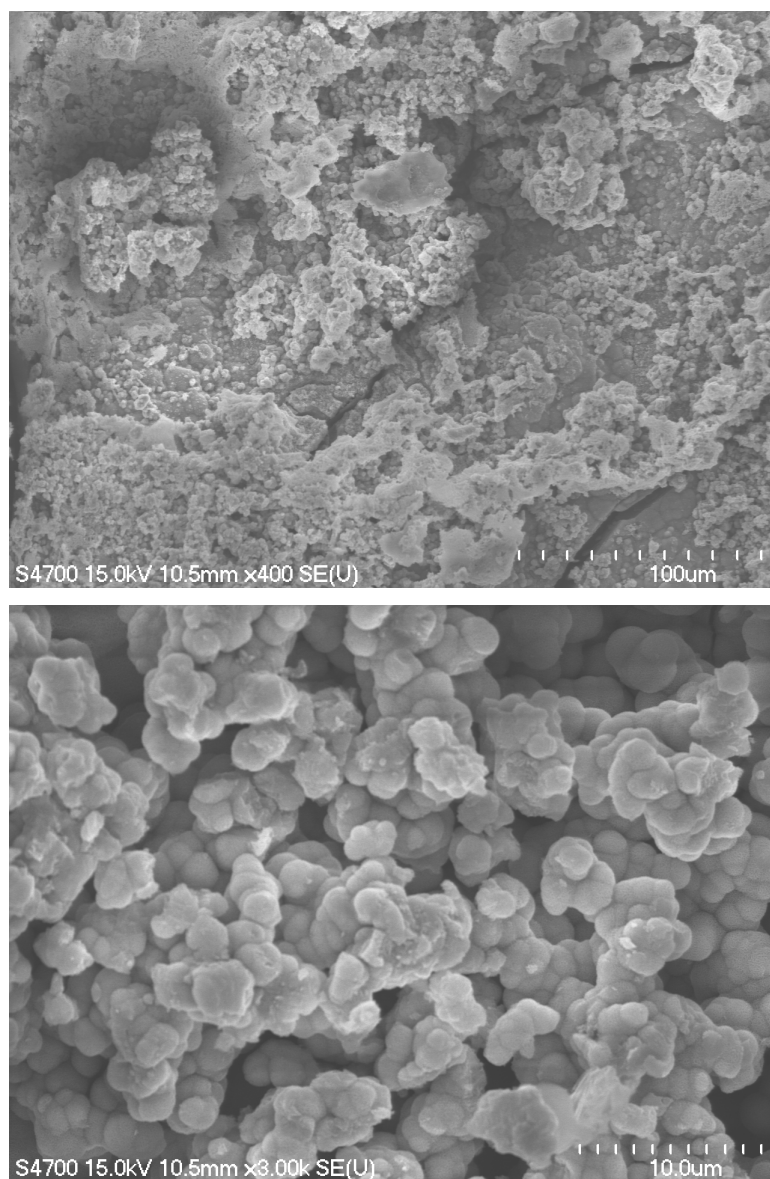


Figure B.3. FE-SEM images of surface morphology of carbon foam impregnated with Ni(OH)_2 (full deposition) taken at 400x (upper photo) and 3,000x (lower photo) magnifications.

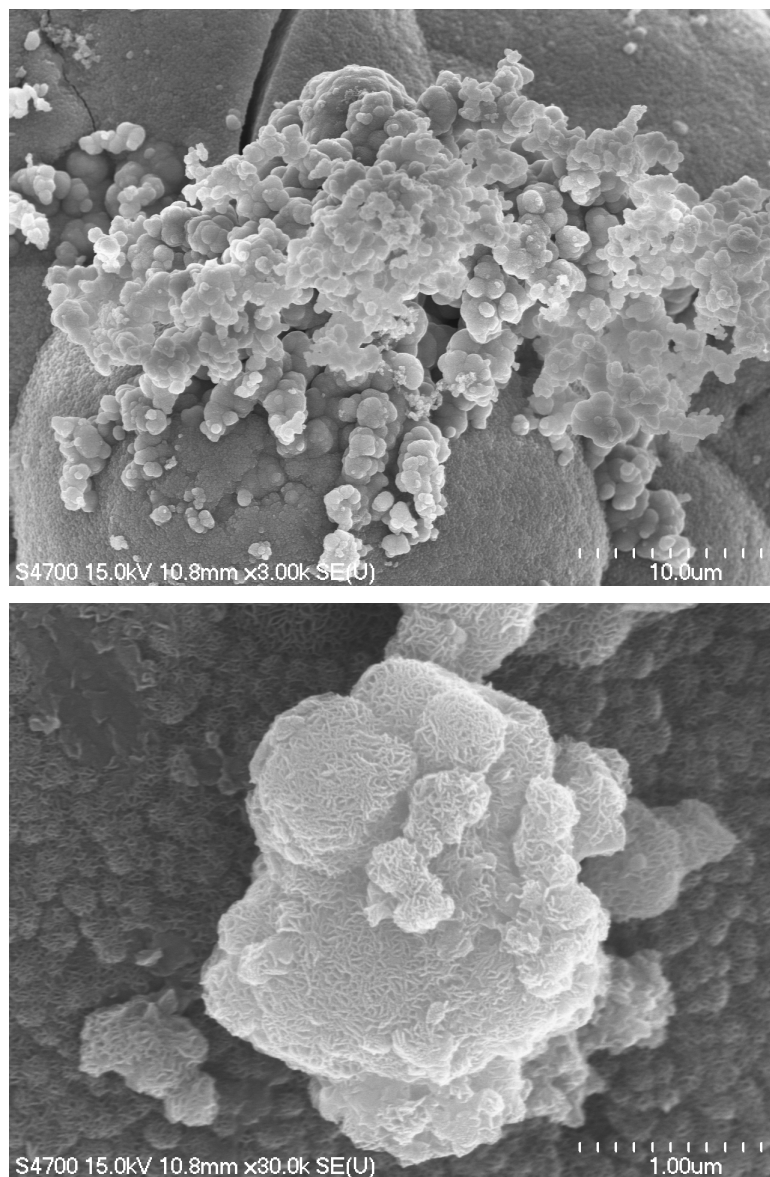


Figure B.4. FE-SEM images of the Ni(OH)₂ (full deposition) at 3,000x (upper photo) and 30,000x (lower photo) magnifications.

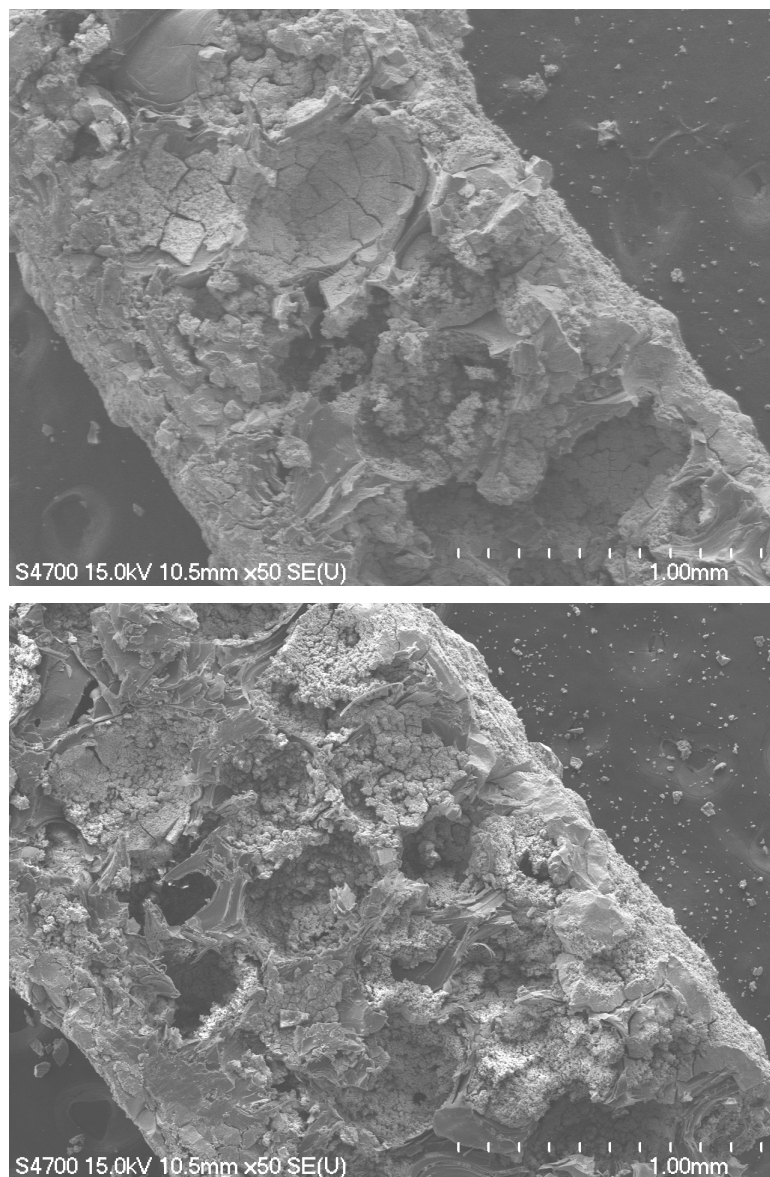


Figure B.5. FE-SEM images of cross-section morphology of carbon foam impregnated with $\text{Ni}(\text{OH})_2$ (full deposition) taken at 50x magnifications. The upper photo was taken near the edge of the foam and the bottom photo was taken near the center of the foam.

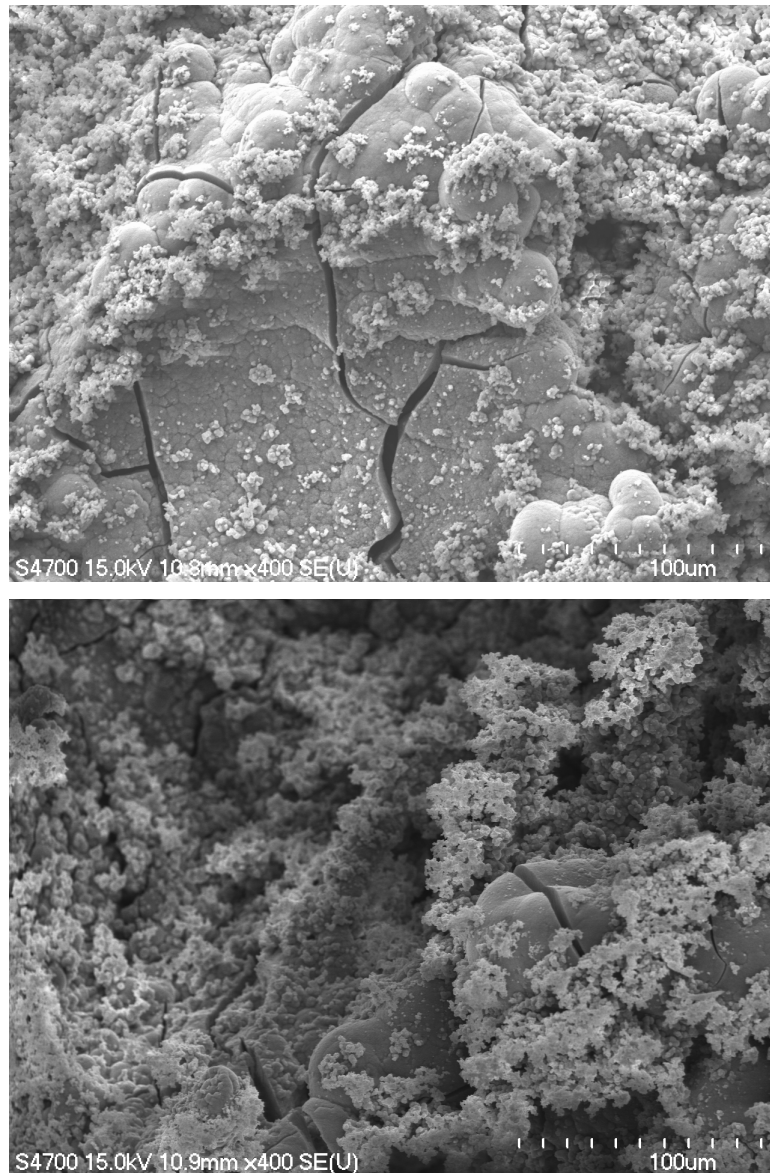


Figure B.6. FE-SEM images of surface morphology of carbon foam, both partial deposition, taken at 400x magnification.

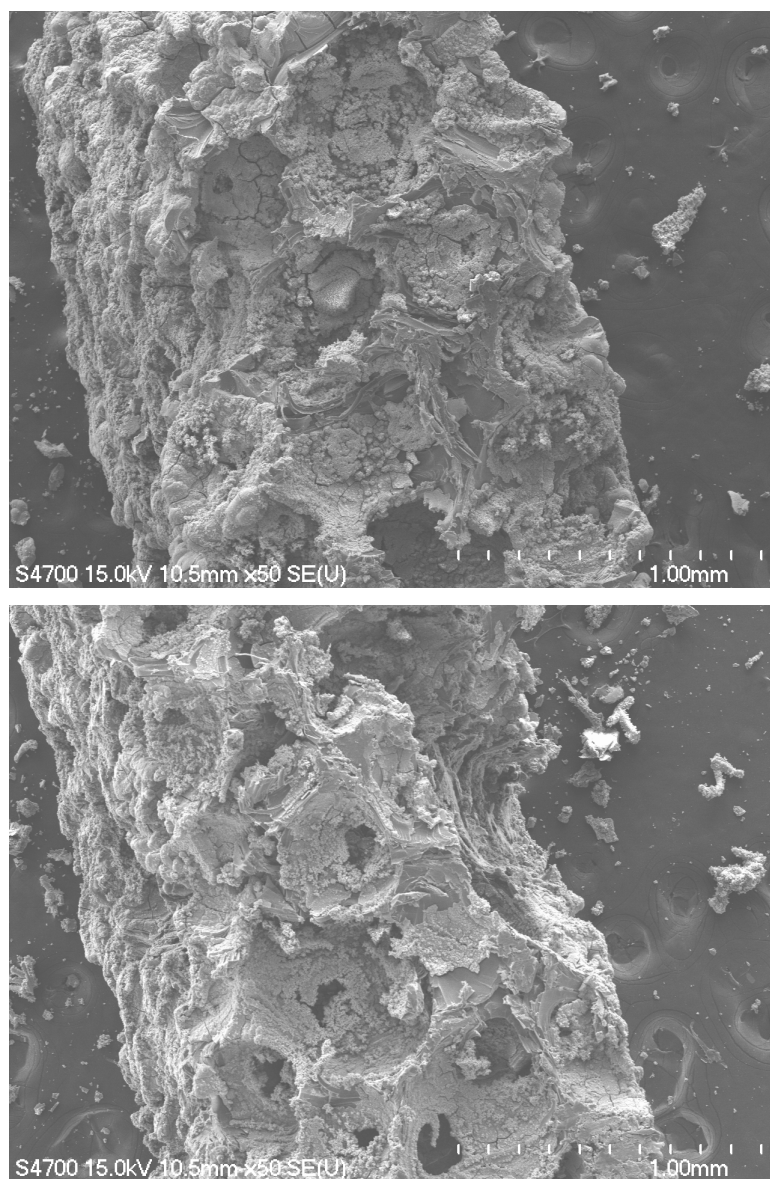


Figure B.7. FE-SEM images of cross-section morphology of carbon foam with partial deposition taken at 50x magnifications. The upper photo was taken near the edge of the foam and the bottom photo was taken near the center of the foam.

Appendix B2 XRD Powder Patterns

Information on space group, atomic coordinates, and set parameters to calculate the XRD patterns.

(a) Carbon foam (POCOfoam[®])

Space Group: P6₃/mmc (No. 194) System: Hexagonal

a = 2.461 Å c = 6.705 Å

Atomic coordinates: C1 = (0, 0, 0.25), C2 = (1/3, 2/3, 0.25)

Step size: 0.03°

FWHM = 0.3 at 26.5° 2-theta, 0.6 at 44.0° 2-Theta

Population parameter = B(iso) = 1 for all atoms

(b) α-Ni(OH)₂

Space Group: R $\bar{3}$ m (No. 166) System: Rhombohedral

a = 8.256 Å

α = 21.574°

Atomic coordinates: Ni = (0, 0, 0), O1 = (0.377, 0.377, 0.377), O2 = (1/2, 1/2, 1/2)

Step size: 0.03°

FWHM = 3 at 11.0° 2-theta, 6 at 22.0° 2-Theta

Population parameter*: Ni = 1, O1 = 1, O2 = 0.667

B(iso)*: Ni = 0.714, O1 = 0.763, O2 = 0.763

*Karjala PJ. Structural Studies of Nickel Electrode Model Compounds [M.S Thesis]. Houghton: Michigan Technological University; 1987.

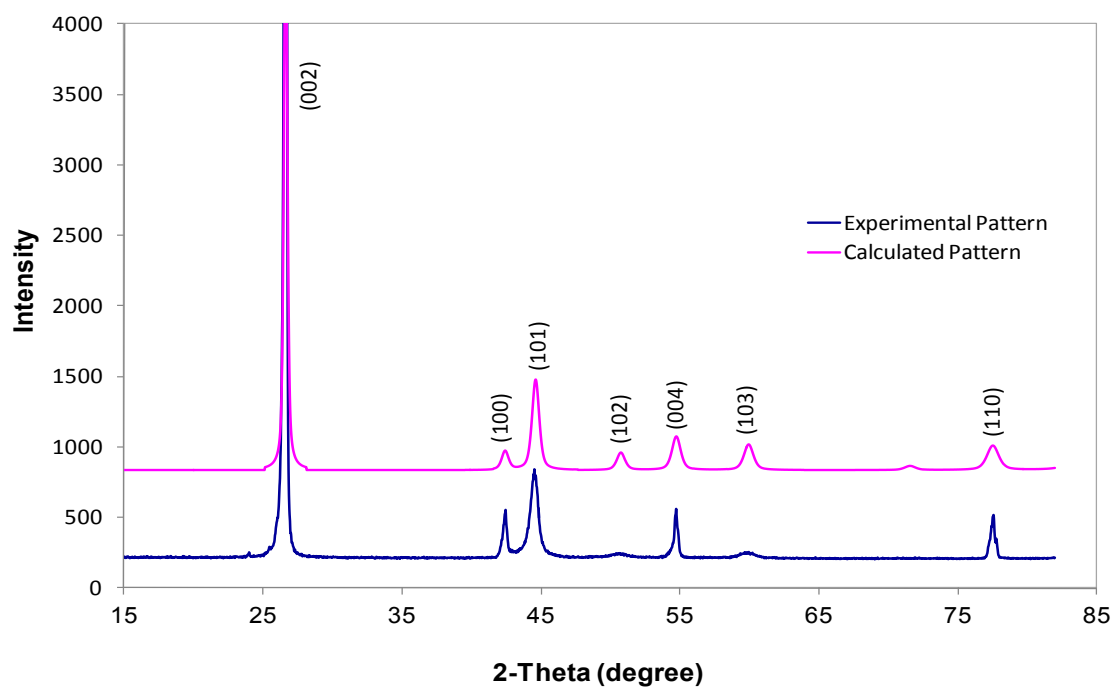


Figure B.8. Comparison of experimental and calculated XRD patterns of POCOfoam®.

Table B.1.
Comparison of experimental and calculated hkl and relative intensity of POCOfoam®.

h	k	l	Experimental			Calculated		
			2-Theta	d	I(rel)	2-Theta	d	I(rel)
0	0	2	26.64	3.34	100.00	26.57	3.35	100.00
1	0	0	42.45	2.13	4.06	42.37	2.13	4.13
1	0	1	44.54	2.03	6.17	44.57	2.03	13.56
1	0	2	50.68	1.80	1.81	50.72	1.80	4.13
0	0	4	54.73	1.68	4.11	54.71	1.68	5.35
1	0	3	59.87	1.54	1.79	59.92	1.54	3.28
1	1	0	77.55	1.23	3.80	77.51	1.23	3.46

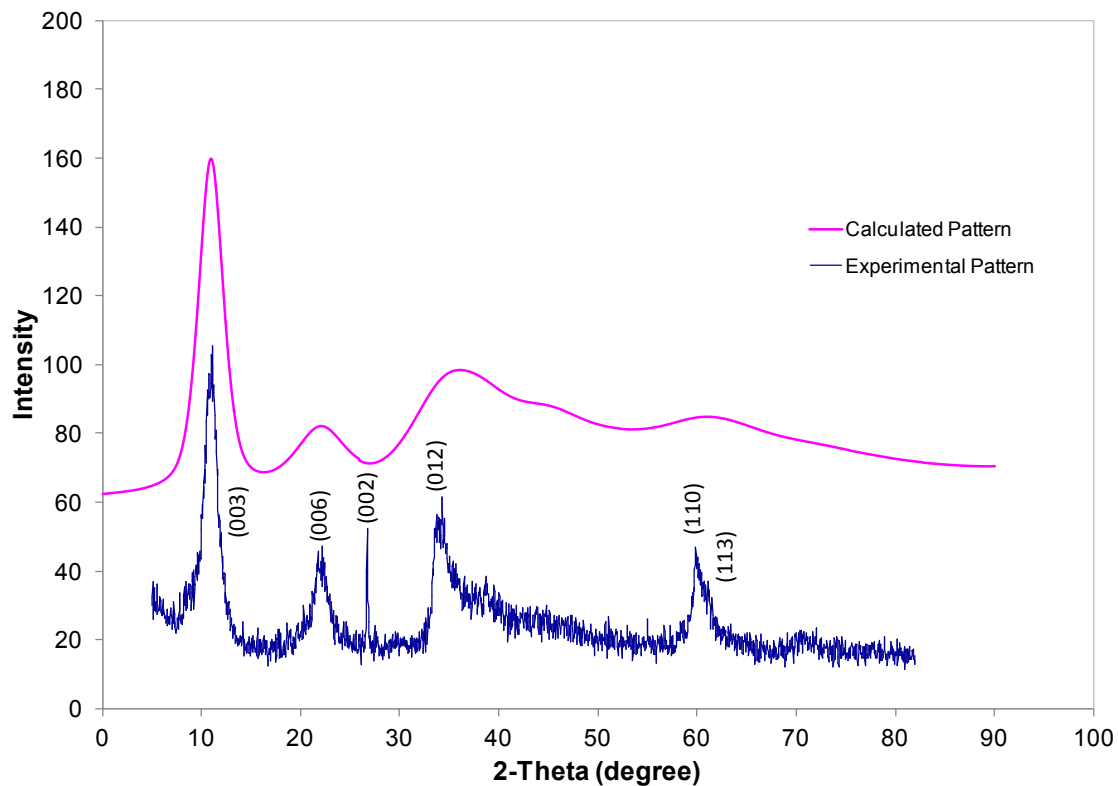


Figure B.9. Comparison of experimental and calculated XRD patterns of α -Ni(OH)₂. The diffraction peak indexed at (002) of the experimental pattern belongs to the carbon foam.

Table B.2.
Comparison of experimental and calculated hkl and relative intensity of α -Ni(OH)₂.

h	k	l	Experimental			Calculated		
			2-Theta	d	I(rel)	2-Theta	d	I(rel)
0	0	3	10.97	8.06	100.00	10.97	8.06	100.00
0	0	6	22.03	4.01	47.50	22.04	4.03	18.05
0	1	2	34.10	2.63	56.25	34.29	2.61	17.70
1	1	0	59.80	1.55	41.25	59.80	1.55	5.04
1	1	3	61.12	1.52	30.42	61.01	1.52	5.47

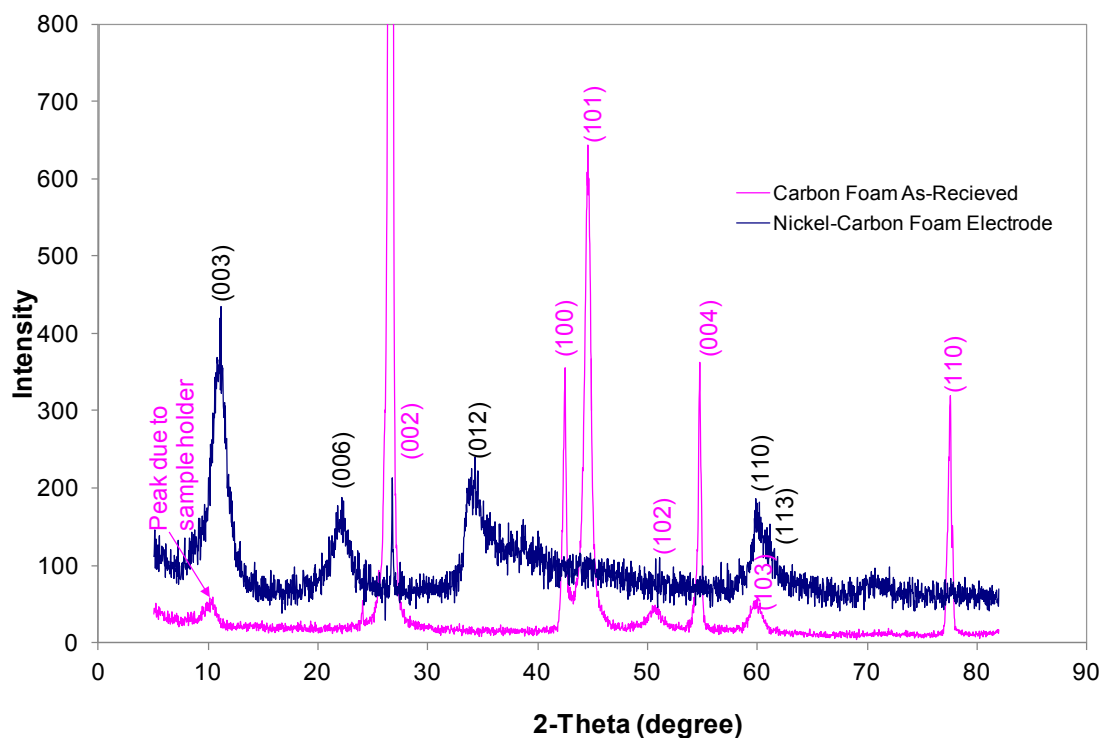


Figure B.10. Comparison of XRD patterns of carbon foam and nickel-carbon foam electrode.

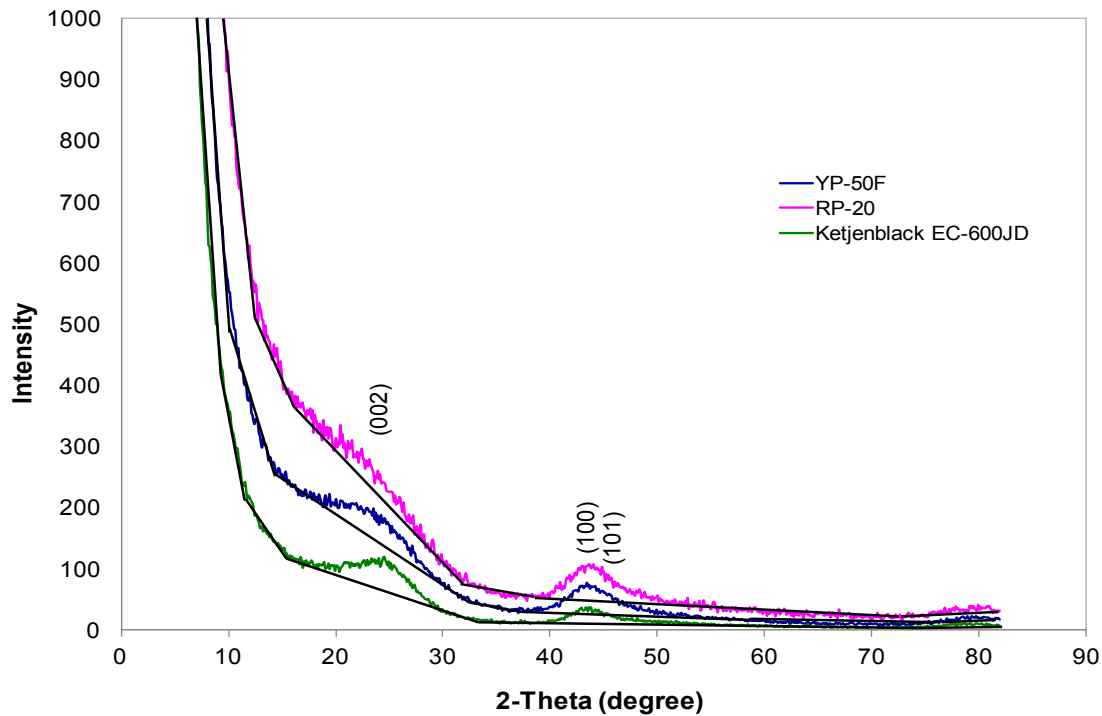


Figure B.11. Comparison of XRD patterns of YP-50F, RP-20, and Ketjenblack EC-600JD, straight lines show how background being subtracted.

Appendix B3 BET and Porosimetry

Experiment Conditions:

The N₂ adsorption/desorption data were collected in the relative pressure range (P/P_0) of $0.01 < P/P_0 < 1$, where P_0 is the vapor pressure of the adsorbing gas (N₂) at the testing temperature of 77.35 K. Specific surface areas were calculated from N₂ adsorption data in the P/P_0 range between 0.1 and 0.3 via BET method. The micropores areas were estimated by t-plot method. This method modeled the multi-layer adsorption mathematically. The thickness, t , of an adsorbate layer increases with increasing P/P_0 . The volume adsorbed is plotted versus the statistical thickness based on STSA thickness curve for carbon black materials suggested in the ASTM standard D-6556-01 for each P/P_0 from 0 to 0.75. Data were also collected to analyze the pore size distribution by BJH method with Faas correction. BJH method is a modification of Kelvin equation. Kelvin equation determined the pore size based on adsorption porosimetry. All the data were analyzed via ASAP 2020 by Micromeritics.

Table B.3.
Summary table of pore characteristics of ACs on all trials.

Acs	BET (m ² /g)	Micropore Area (m ² /g)	Mesopore Area (m ² /g)	Single Point Pore Volume 10 ⁻⁶ m ³ /g	BJH Adsorption Average Pore Diameter (nm)	BJH Desorption Average Pore Diameter (nm)
RP-20	1520	N/A	N/A	0.76	3.32	N/A
	1333	1139	194	0.69	3.76	3.46
	1240	1041	199	0.67	2.95	13.2
YP-50F (YP-17)	1331	N/A	N/A	0.69	3.80	N/A
	1314	1085	229	0.68	3.82	3.48
Ketjenblack EC-600JD	1184	N/A	N/A	2.08	7.76	N/A
	1192	N/A	N/A	2.06	7.60	N/A
	1422	44	1378	2.42	8.74	7.69

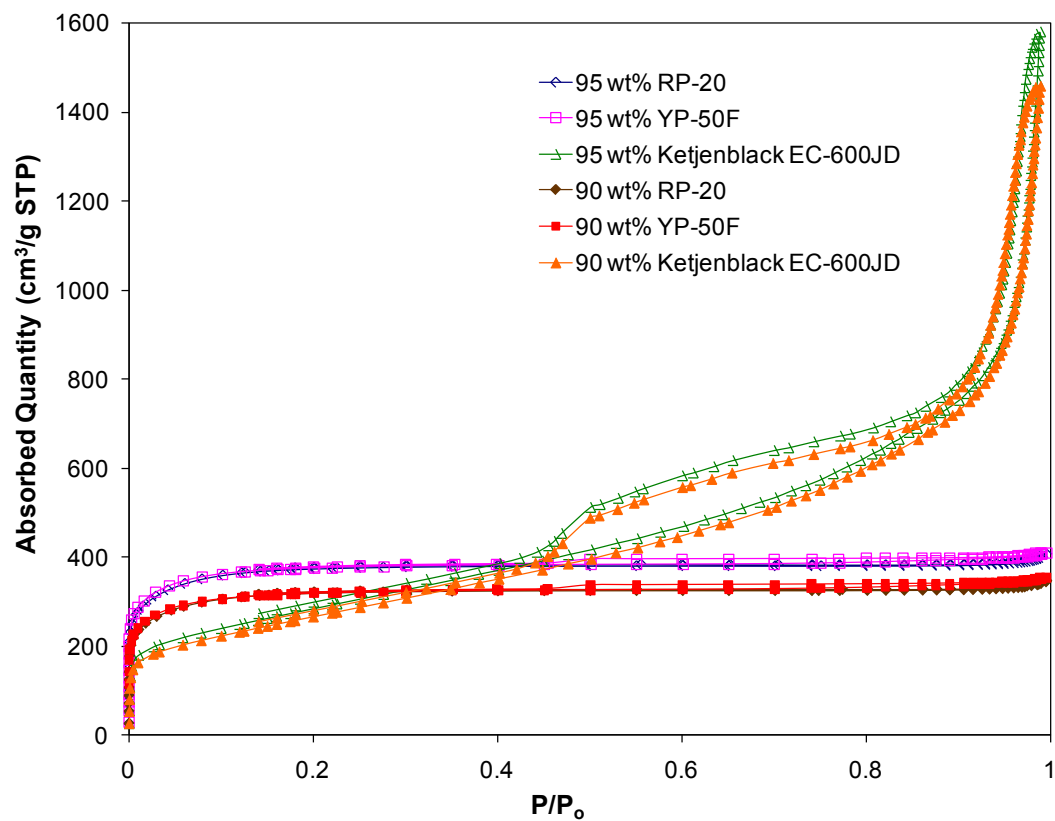


Figure B.12. N₂ adsorption/desorption isotherms of electrodes.

Table B.4.
Summary table of pore characteristics of electrodes on all trials.

Electrodes	BET (m ² /g)	Micropore Area (m ² /g)	Mesopore Area (m ² /g)	Single Point Pore Volume 10 ⁻⁶ m ³ /g	BJH Adsorption Average Pore Diameter (nm)	BJH Desorption Average Pore Diameter (nm)
Commercial Electrode *	1132	N/A	N/A	N/A	N/A	N/A
	1201	N/A	N/A	0.58	3.55	N/A
	1043	802	241	0.61	4.12	4.09
	1049	792	257	0.60	3.96	3.73
95 wt% RP-20	1091	899	192	0.58	2.91	61.48
	1093	892	201	0.61	3.91	3.75
	1086	850	236	0.60	3.58	4.01
95 wt% YP-50F	1036	885	151	0.56	3.61	3.19
	1096	862	234	0.63	3.98	3.51
95 wt% Ketjenblack EC-600JD	797	25	772	1.59	9.95	8.72
	1029	30	999	1.99	9.71	8.52
	1153	49	1104	2.19	9.75	8.49
90 wt% RP-20	1028	819	209	0.56	3.36	15.97
	933	711	222	0.52	3.66	3.70
	880	685	195	0.48	4.02	4.54
90 wt% YP-50F	910	741	169	0.51	3.91	3.52
	932	718	214	0.54	4.07	3.67
90 wt% Ketjenblack EC-600JD	591	5	586	1.21	9.44	8.20
	967	10	957	1.92	9.26	8.15
	874	16	858	1.77	9.57	8.35

* Electrodes donated by JME Capacitor Inc.

Appendix C Electrochemical Performance of Electrochemical Capacitors

Appendix C1 Symmetric Capacitors

The explanation for why the specific capacitance of a single electrode is 4 times that of the specific cell capacitance for a symmetric capacitor.

$$\frac{1}{C_{cell}} = \frac{1}{C_+} + \frac{1}{C_-} \quad \text{where } C_+ = C_-$$
$$C_{cell} = \frac{1}{2} C_+ \quad (C.1)$$

$$\text{Let } \bar{C} = \frac{C}{m} \quad \text{where } m = \text{mass of single electrode}$$

$$\therefore C_{cell} = 2m\bar{C}_{cell} \text{ and } C_+ = m\bar{C}_+$$

Substituting the two above equations into equation C.1, gives

$$2m\bar{C}_{cell} = \frac{1}{2} m\bar{C}_+$$
$$\bar{C}_{cell} = \frac{1}{4} \bar{C}_+$$

Table C.1.
Summary of all symmetric capacitors.

Electrode	Current Density (mA/cm ²)	Specific Cell Capacitance (F/g)	Average Specific Capacitance of Single Electrode (F/g)	Efficiency
Commercial Electrode*	5	52.50	209.98	98.0%
	10	46.86	187.44	97.4%
	20	41.13	164.53	98.1%
	50	27.70	110.78	99.8%
95 wt% RP-20, Batch 1	5	22.80	91.22	95.9%
	10	17.29	69.15	98.4%
	20	10.89	43.54	97.6%
	50	7.30	29.20	95.6%
95 wt% RP-20, Batch 2	5	26.40	105.58	84.9%
	10	21.98	87.92	91.8%
	20	17.52	70.08	95.7%
	50	10.60	42.40	91.6%
95 wt% YP-50F	5	24.39	97.55	99.0%
	10	19.33	77.34	99.3%
	20	15.19	60.76	99.9%
	50	11.77	47.07	100.0%
95 wt% Ketjenblack EC-600JD	5	21.68	86.73	98.6%
	10	21.20	84.78	99.5%
	20	20.63	82.50	99.9%
	50	19.97	79.88	99.8%
90 wt% RP-20	5	21.73	86.91	94.3%
	10	16.74	66.98	97.6%
	20	11.62	46.50	98.2%
	50	6.66	26.64	87.4%
90 wt% YP-50F	5	20.85	83.39	97.2%
	10	17.37	69.49	99.0%
	20	12.50	49.99	99.7%
	50	6.60	26.39	97.5%
90 wt% Ketjenblack EC-600JD	5	17.39	69.50	99.0%
	10	16.59	66.02	99.4%
	20	13.91	55.61	98.5%
	50	12.18	48.74	99.6%

* Electrodes donated by JME Capacitor Inc.

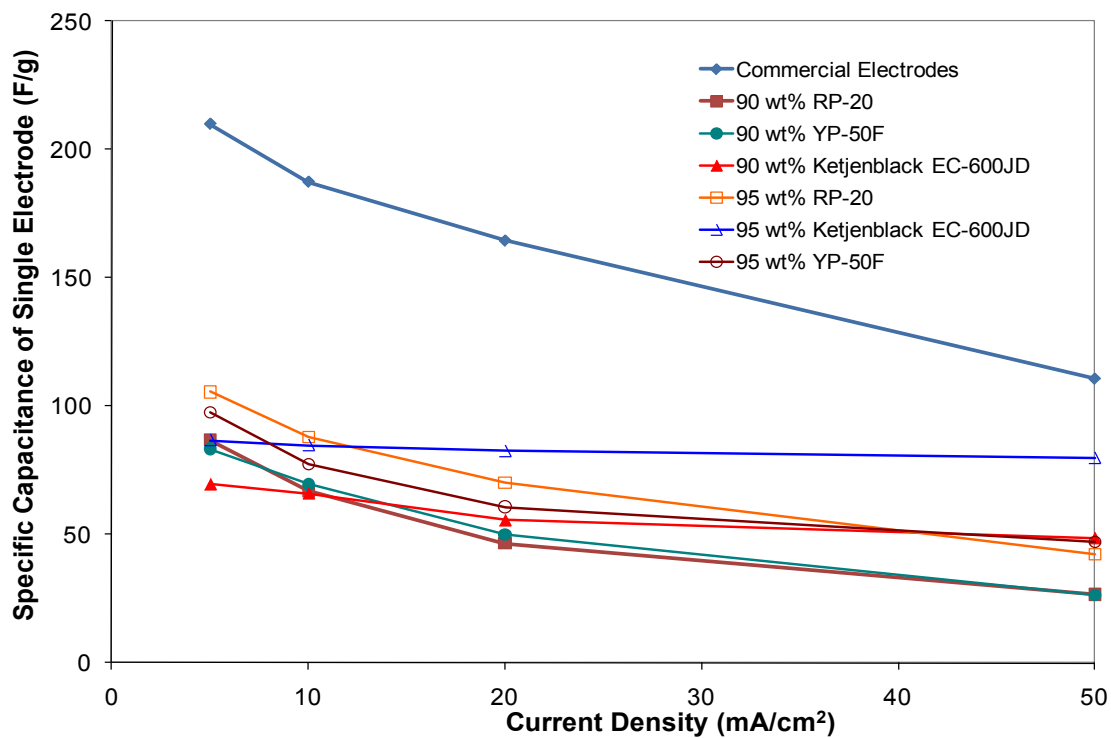


Figure C.1. Specific capacitance of single electrode as a function of current density.

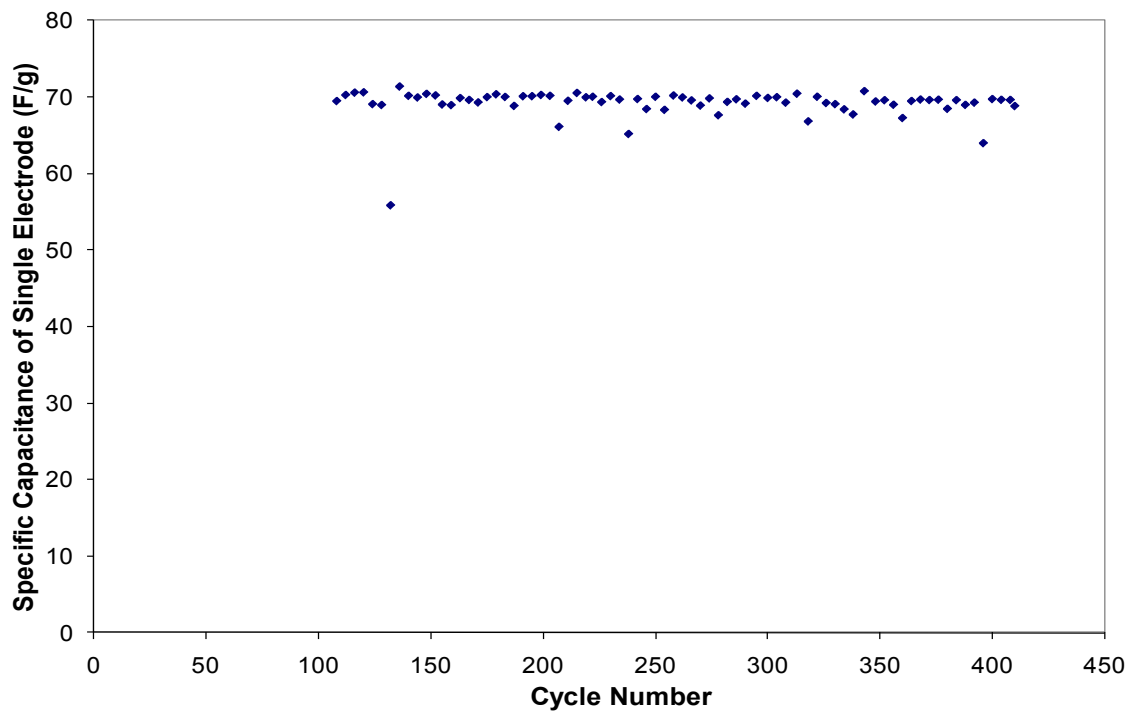


Figure C.2. Specific capacitance of single electrode as a function of cycle number for symmetric capacitor made of 95 wt% RP-20 electrodes cycled at 20 mA/cm².

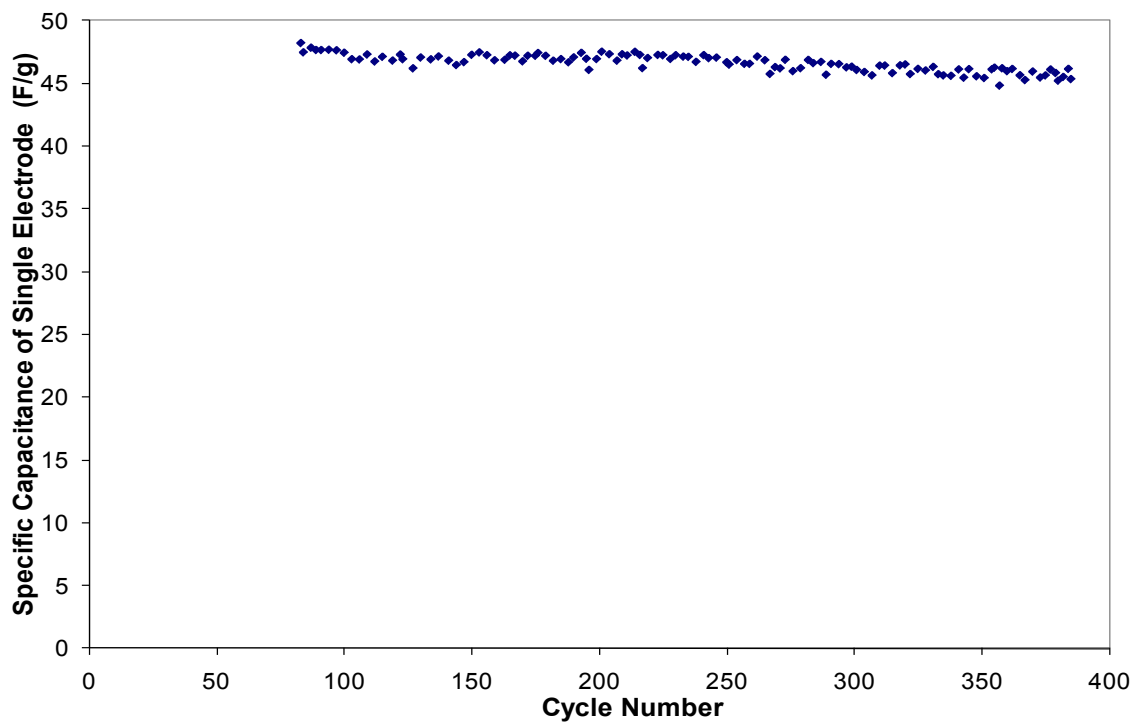


Figure C.3. Specific capacitance of single electrode as a function of cycle number for symmetric capacitor made of 90 wt% RP-20 electrodes cycled at 20 mA/cm².

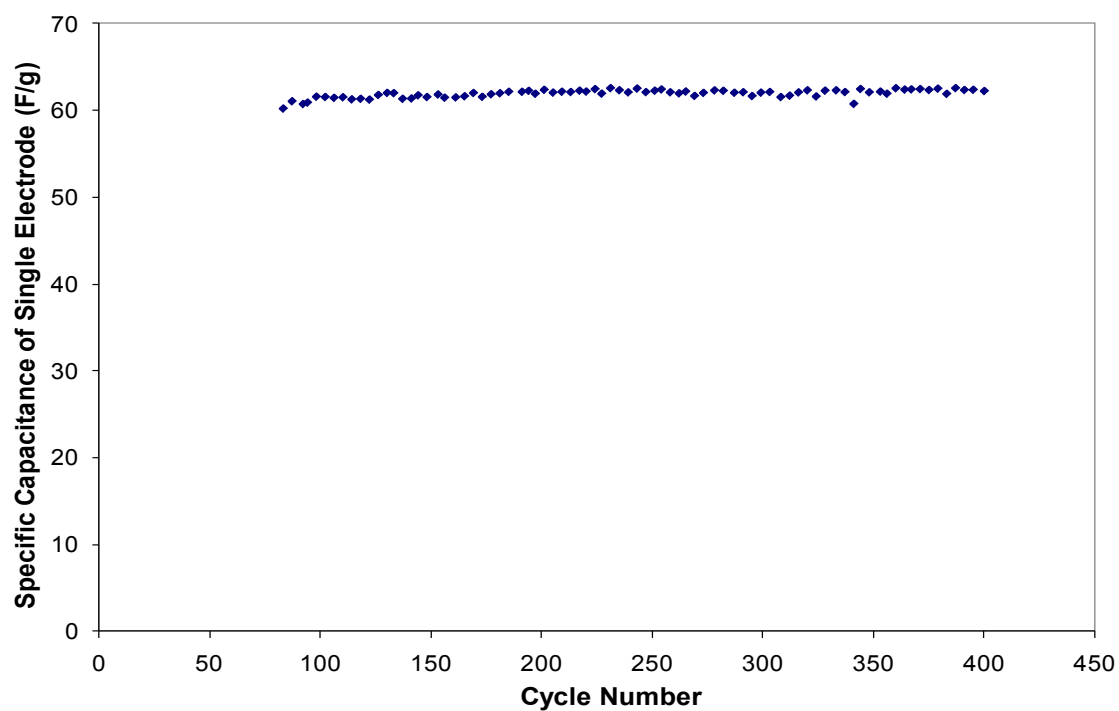


Figure C.4. Specific capacitance of single electrode as a function of cycle number for symmetric capacitor made of 95 wt% YP-50F electrodes cycled at 20 mA/cm².

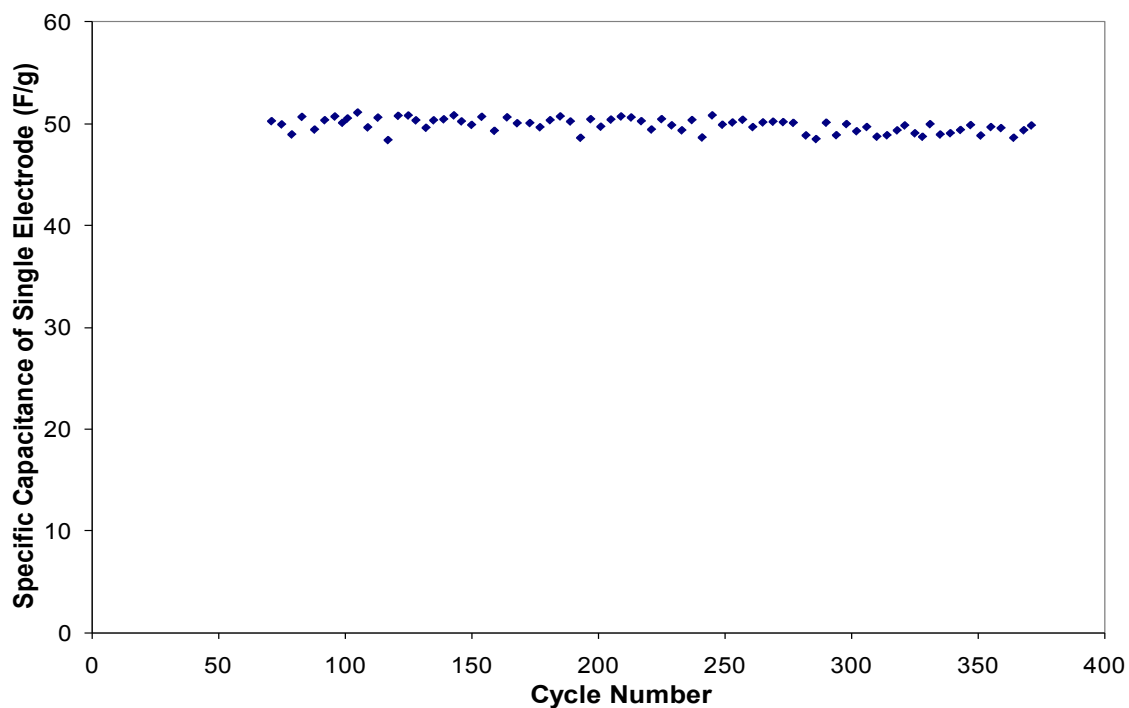


Figure C.5. Specific capacitance of single electrode as a function of cycle number for symmetric capacitor made of 90 wt% YP-50F electrodes cycled at 20 mA/cm².

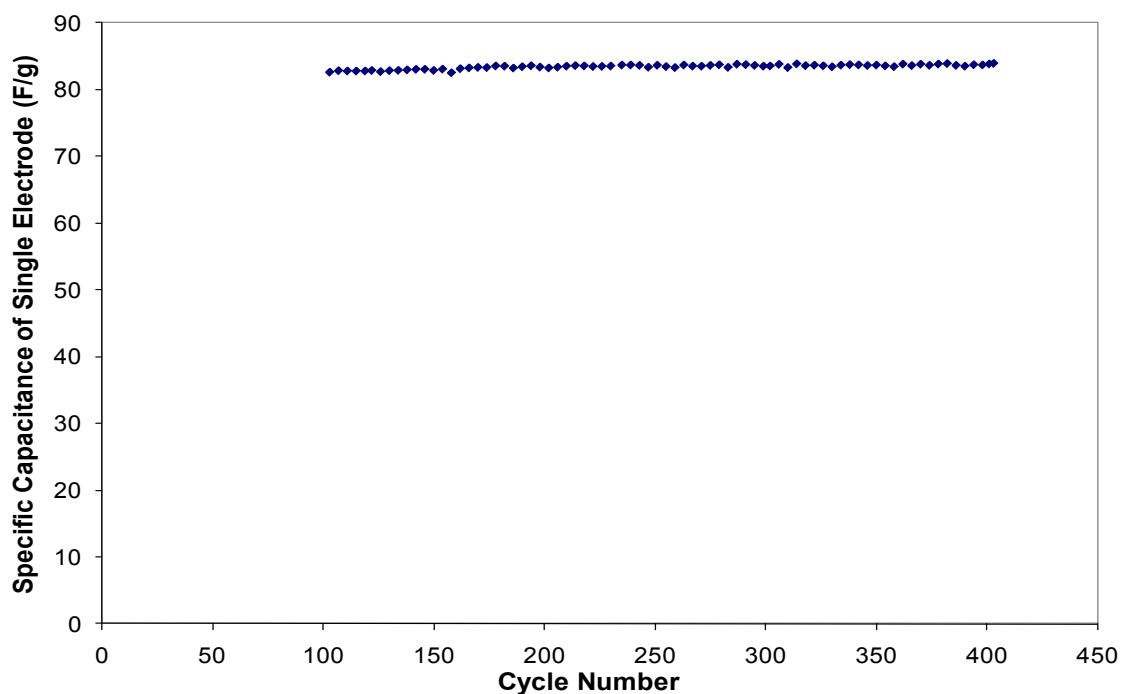


Figure C.6. Specific capacitance of single electrode as a function of cycle number for symmetric capacitor made of 95 wt% Ketjenblack EC-600JD electrodes cycled at 20 mA/cm².

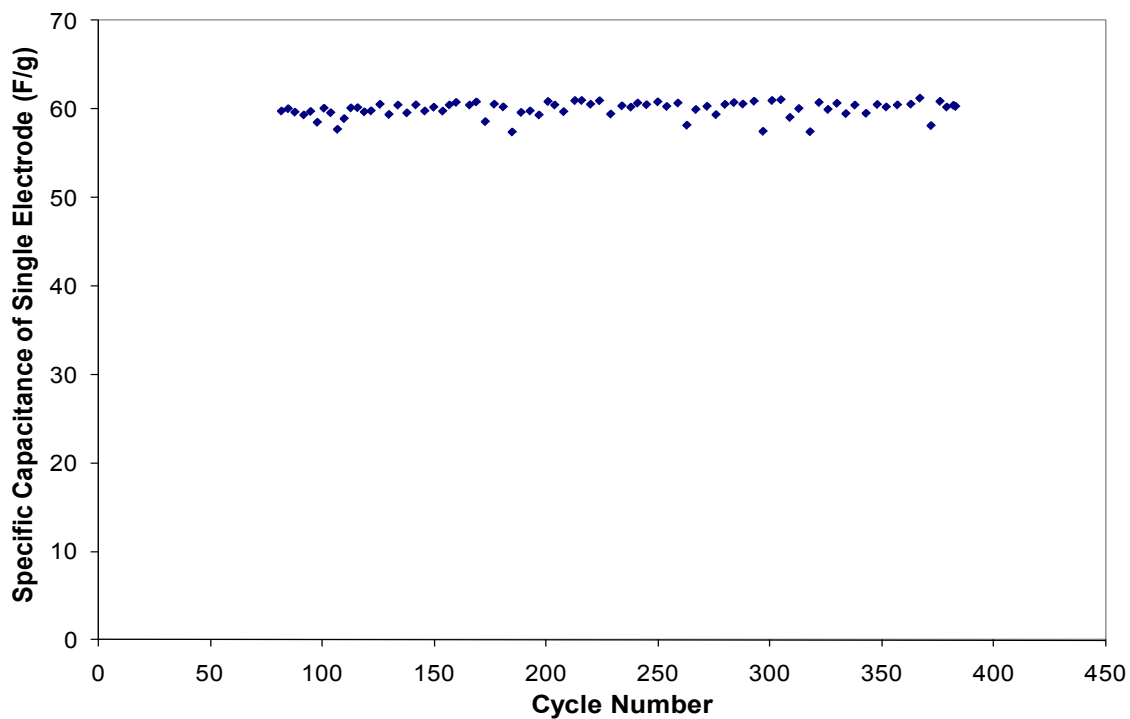


Figure C.7. Specific capacitance of single electrode as a function of cycle number for symmetric capacitor made of 90 wt% Ketjenblack EC-600JD electrodes cycled at 20 mA/cm².

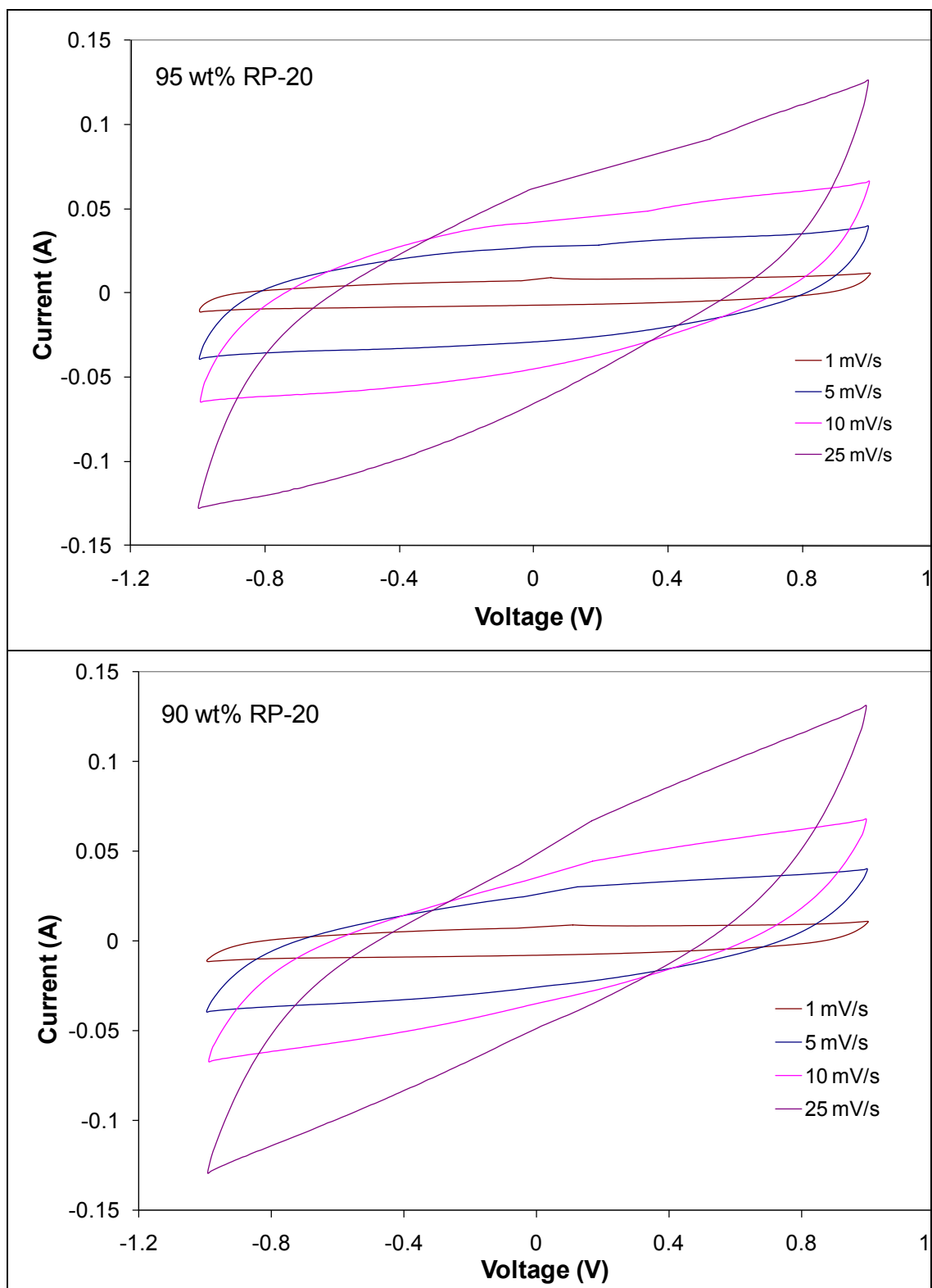


Figure C.8. CV curves of RP-20 (top – 95 wt%, bottom – 90 wt%) at different scan rates and the voltage window range between -1 to 1 V.

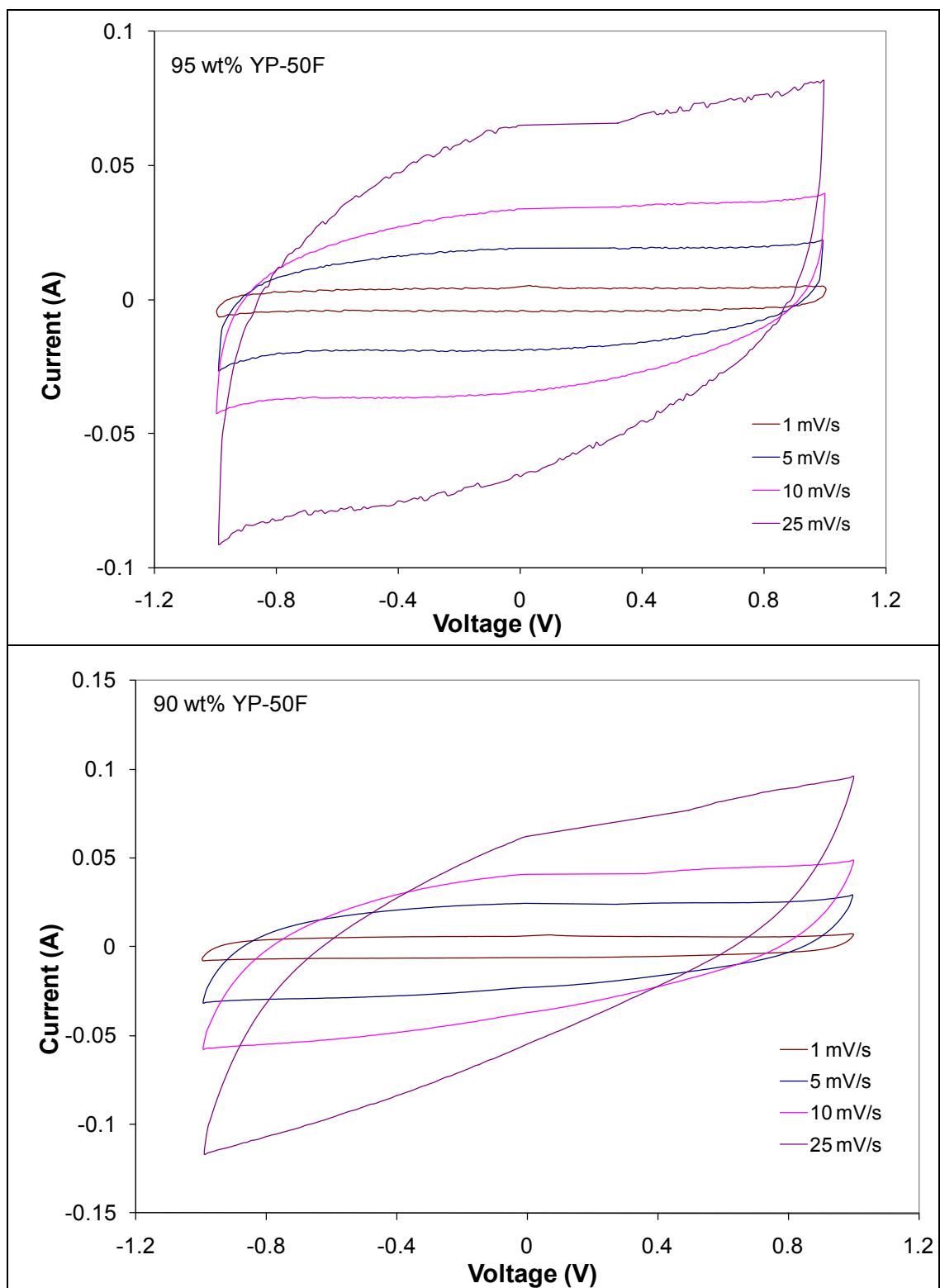


Figure C.9. CV curves of YP-50F (top – 95 wt%, bottom – 90 wt%) at different scan rates and the voltage window range between -1 to 1 V.

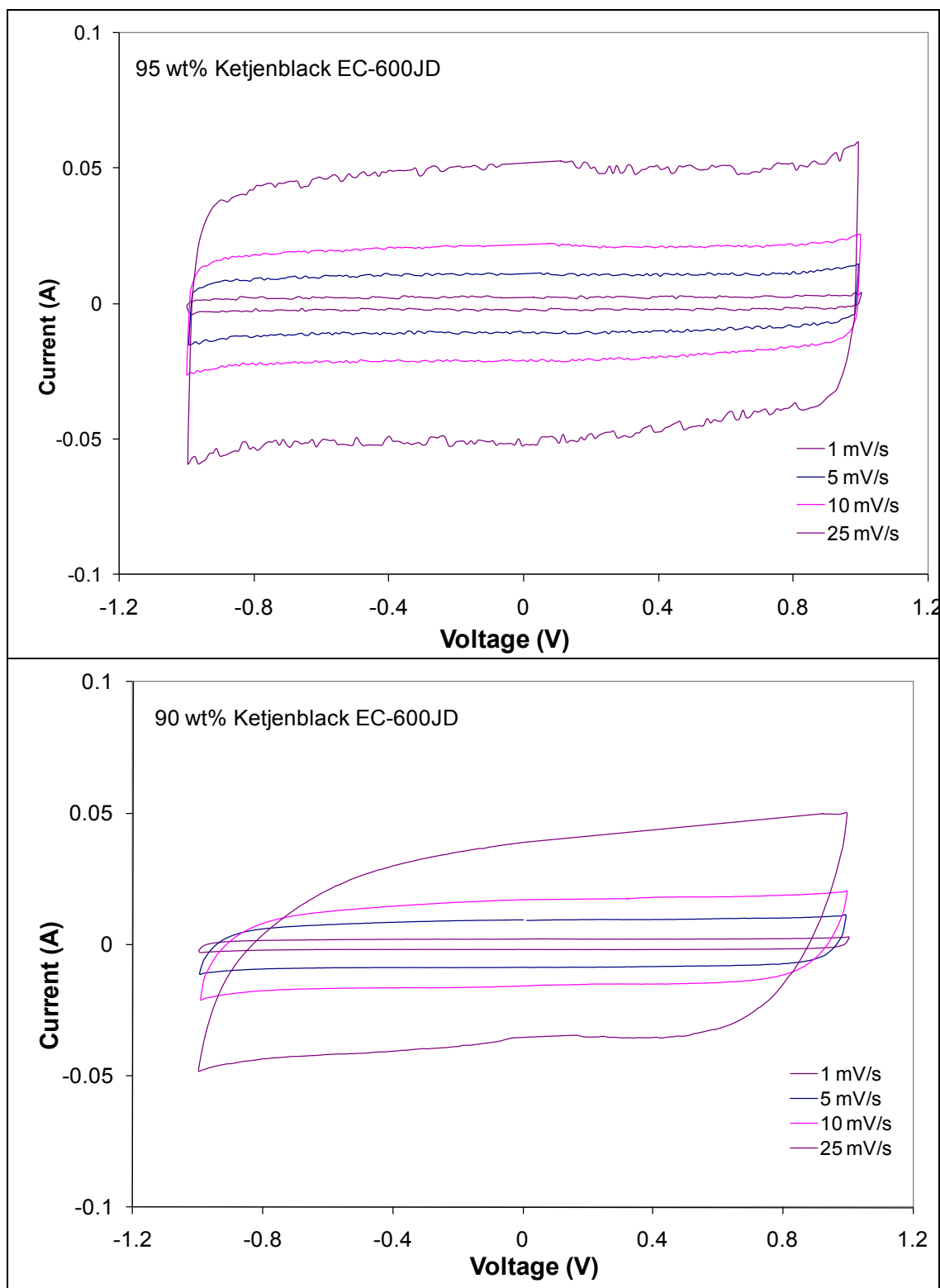


Figure C.10. CV curves of Ketjenblack EC-600JD (top – 95 wt%, bottom – 90 wt%) at different scan rates and the voltage window range between -1 to 1 V.

Appendix C2 Asymmetric Capacitors

Sample calculation to determine the capacity needed for the deposition in order to prepared a positive electrode with a known active mass, 0.0553 g.

Faraday's Law of Electrolysis:

$$m = \frac{Q}{F} \frac{M}{z} \quad (C.2)$$

where m = active mass (g)

Q = the total electric charge passed through the substance (C)

F = Faraday constant, 96485 C/mol

M = molar mass of the $\text{Ni}(\text{OH})_2$, 92.708 g/mol

z = electrons transferred per ion, 1.6 for electrochemical deposition

The deposition efficiency is 37.5% according to Seiger. Therefore, equation C.2 becomes

$$\begin{aligned} Q &= \frac{m \times F \times z}{M \times 0.375} \\ &= \frac{0.0553 \text{ g} \times 96485 \frac{\text{C}}{\text{mol}} \times 1.6}{92.708 \frac{\text{g}}{\text{mol}} \times 0.375} \\ &= 245.56 \text{ C} \end{aligned}$$

Then convert Q to capacity in the following way:

$$\text{Capacity} = 245.56 \text{ C} \times \frac{h}{3600s} = 0.0682 \text{ Ah}$$

Table C.2.
Summary table of all asymmetric capacitors (nickel-carbon foam/95 wt% YP-50F) with different mass ratios.

Cell #/ Mass Ratio (-ve/+ve)*	Current Density (mA/cm ²)	Cell Capacitance** (F)	Specific Capacitance (F/g)	Specific Energy (W.h/kg)	Specific Power (W/kg)	Efficiency
SW 89	5	16.83	93.64	20.41	53.90	91.39%
4.98	10	15.22	84.65	17.07	104.80	95.26%
4.66	20	13.21	73.48	12.17	198.54	97.12%
	50	8.79	48.92	3.92	405.90	98.34%
SW 90	5	16.65	92.61	20.17	51.65	91.05%
4.99	10	15.19	84.50	17.14	100.09	94.70%
4.66	20	13.23	73.60	12.17	188.70	97.08%
	50	8.86	49.26	3.93	397.08	97.97%
SW 91***	5	17.29	76.93	17.54	53.44	85.99%
1.54	10	16.02	71.30	14.85	103.60	92.88%
1.54	20	13.83	61.57	10.47	193.51	95.82%
	50	7.93	35.31	2.73	382.43	96.03%
SW 92	5	19.35	63.60	15.20	40.67	98.25%
0.80	10	17.55	57.71	13.40	80.61	99.51%
0.84	20	14.60	48.00	10.43	157.20	99.79%
	50	10.48	34.44	6.01	365.02	99.77%
SW 93	5	24.88	81.11	18.97	37.48	98.84%
1.49	10	21.77	70.97	15.78	73.70	99.47%
1.54	20	16.85	54.95	10.69	140.79	99.51%
	50	11.05	36.02	5.53	325.53	98.37%
SW 94***	5	19.87	90.56	18.31	48.05	98.91%
6.80	10	18.31	83.45	14.34	92.84	99.41%
6.50	20	15.31	69.76	10.97	157.75	99.70%
	50	8.03	36.60	1.75	292.33	99.79%
SW 98	5	23.01	101.45	23.38	67.66	97.92%
3.73	10	20.80	91.74	19.28	132.57	99.10%
3.30	20	17.98	79.30	14.05	246.78	99.57%
	50	11.68	51.53	5.23	497.31	99.90%
SW 100	5	15.66	76.06	17.49	58.93	95.73%
10.01	10	13.61	66.11	14.82	113.26	98.49%
8.00	20	11.44	55.57	8.82	194.54	99.32%
	50	6.91	33.54	1.91	379.23	99.02%
SW 102	5	17.44	84.70	19.65	59.11	97.95%
9.98	10	15.62	75.82	16.51	115.67	98.62%
8.00	20	13.06	63.40	11.29	215.77	99.40%
	50	6.91	33.54	1.91	389.23	99.04%
SW 103	5	19.58	86.87	20.16	55.58	97.97%
7.41	10	17.23	76.43	17.00	109.55	98.84%
6.50	20	14.04	62.31	12.44	210.86	99.52%
	50	7.83	34.76	1.74	355.50	99.15%
SW 104	5	24.14	104.24	24.45	67.68	98.77%
3.71	10	21.84	94.32	20.38	132.31	99.52%
3.30	20	18.88	81.54	15.09	246.89	99.43%
	50	13.23	57.13	5.52	498.05	99.91%

* the first mass ratio indicates the measured mass ratio based on 0.2 C-rate discharge capacity of positive electrode, where as the second mass ratio indicates the target mass ratio

** difference in cell capacitance may due to thickness and diameter of the electrodes, where as

*** relatively low efficiency compared to other cells

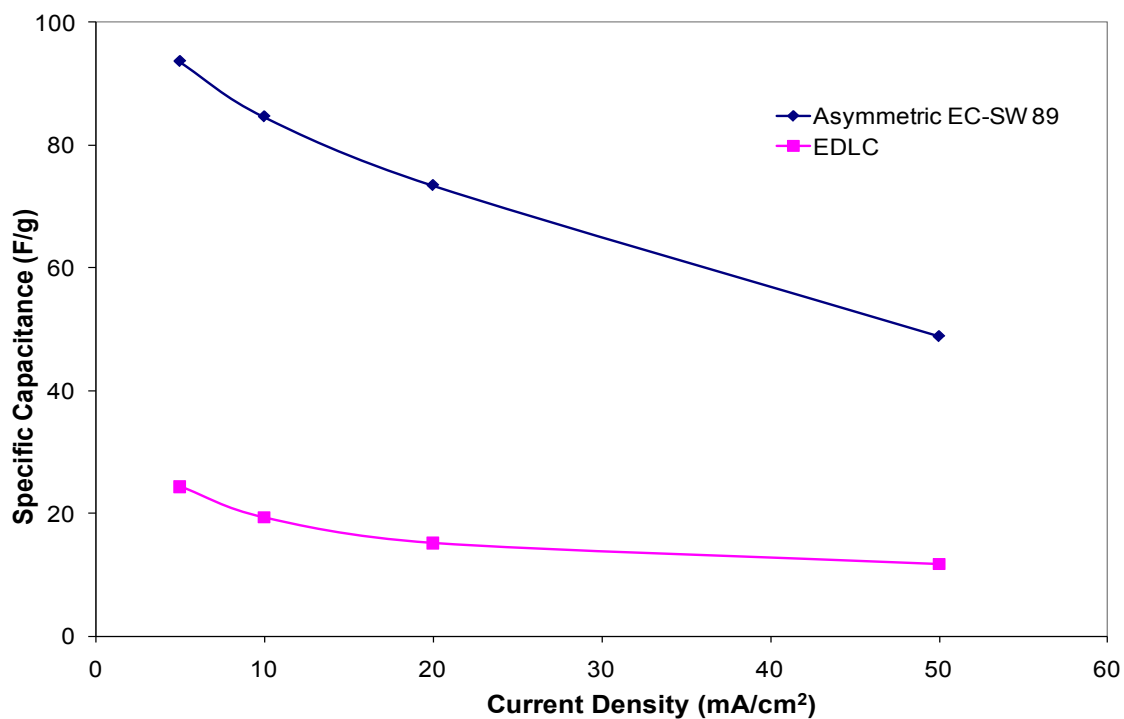


Figure C.11. Specific capacitance as a function of discharge current density of SW 89 and EDLC (95 wt% YP-50F electrodes).

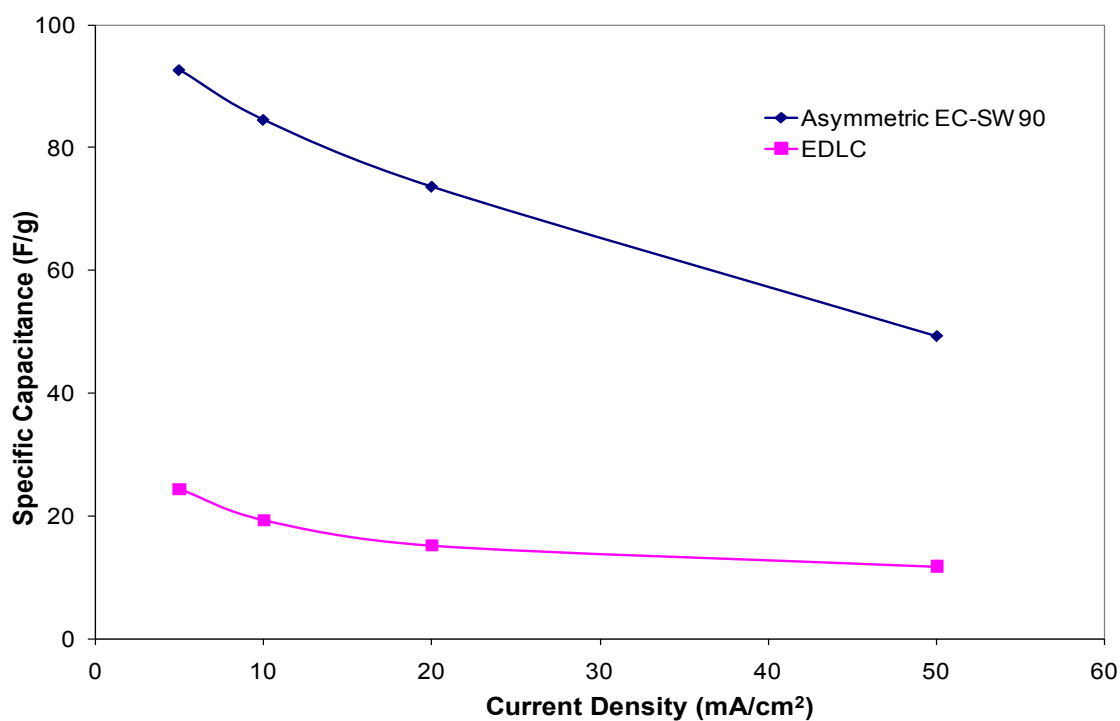


Figure C.12. Specific capacitance as a function of discharge current density of SW 90 and EDLC (95 wt% YP-50F electrodes).

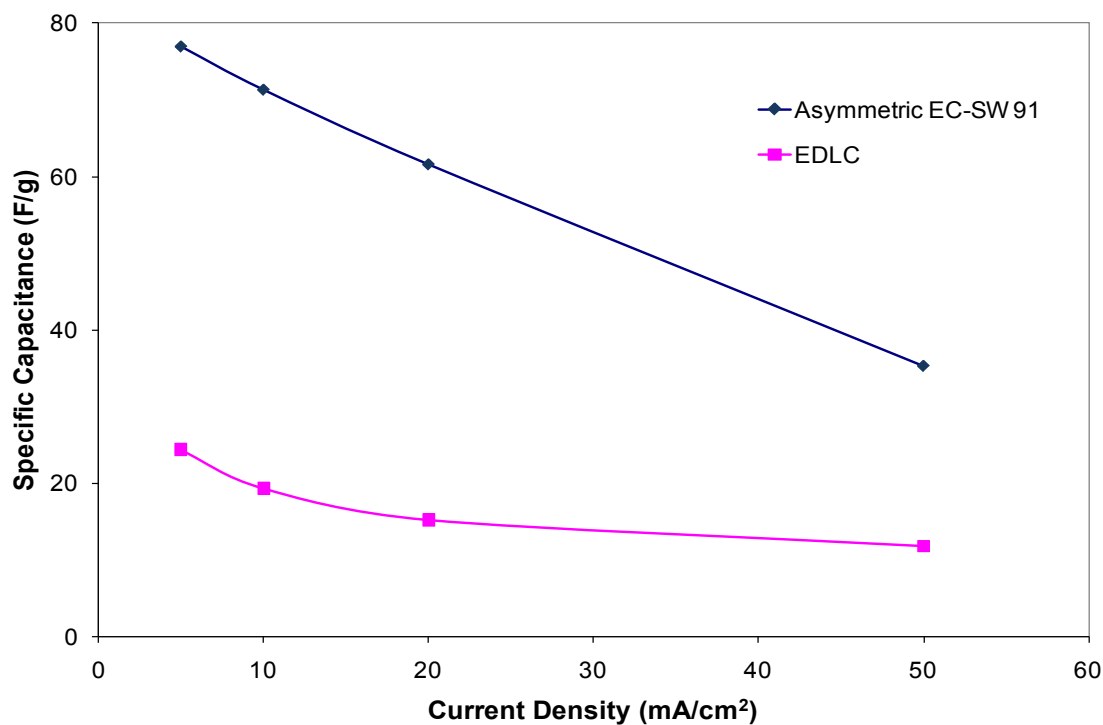


Figure C.13. Specific capacitance as a function of discharge current density of SW 91 and EDLC (95 wt% YP-50F electrodes).

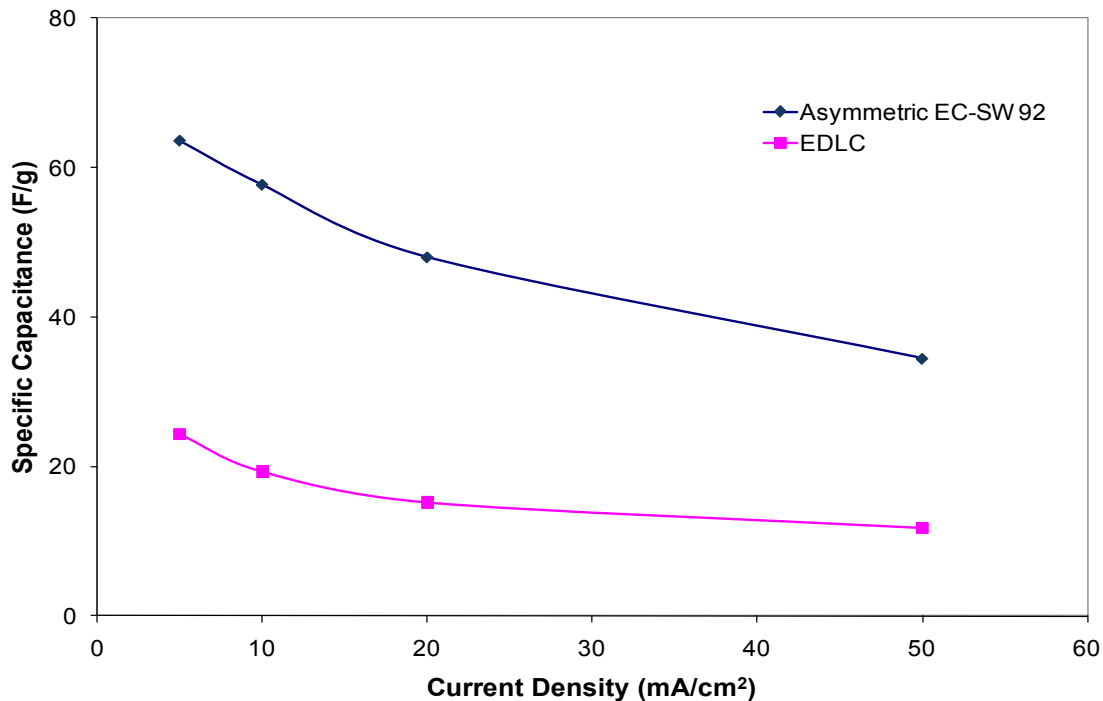


Figure C.14. Specific capacitance as a function of discharge current density of SW 92 and EDLC (95 wt% YP-50F electrodes).

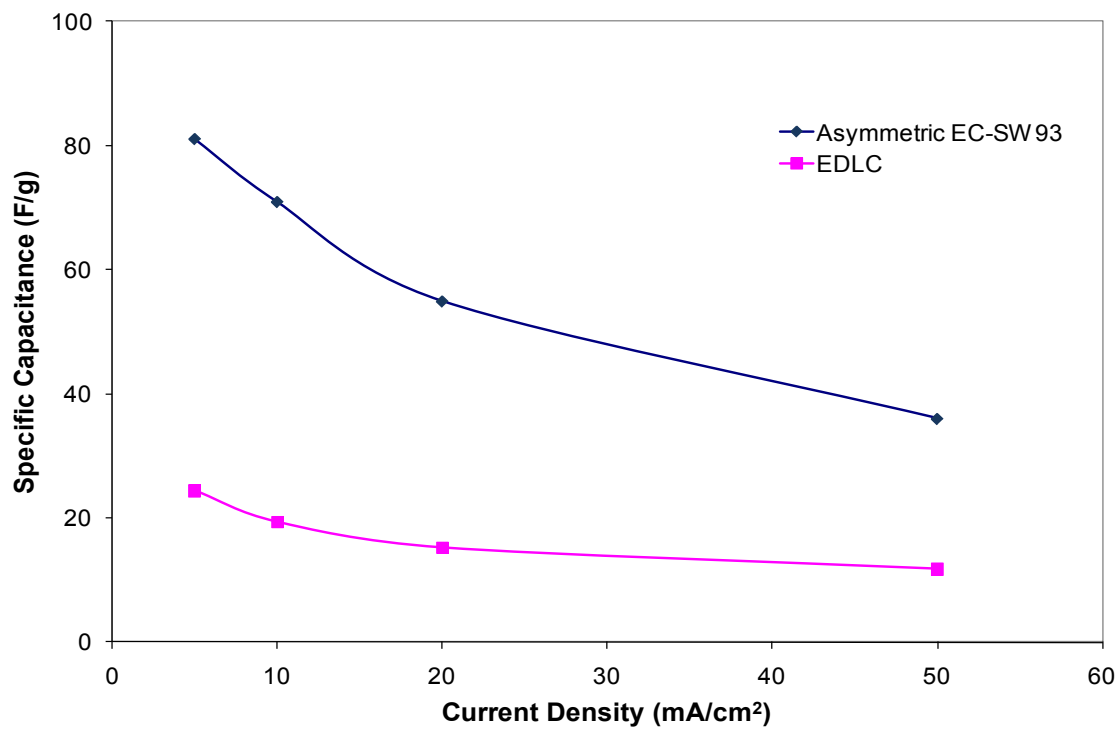


Figure C.15. Specific capacitance as a function of discharge current density of SW 93 and EDLC (95 wt% YP-50F electrodes).

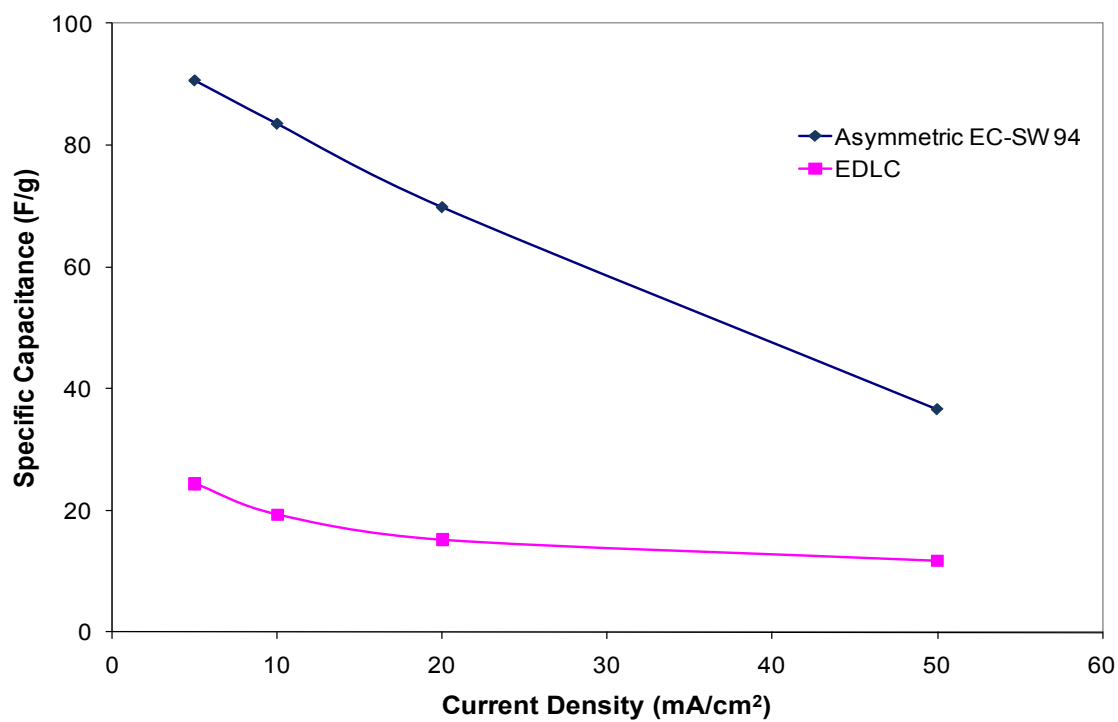


Figure C.16. Specific capacitance as a function of discharge current density of SW 94 and EDLC (95 wt% YP-50F electrodes).

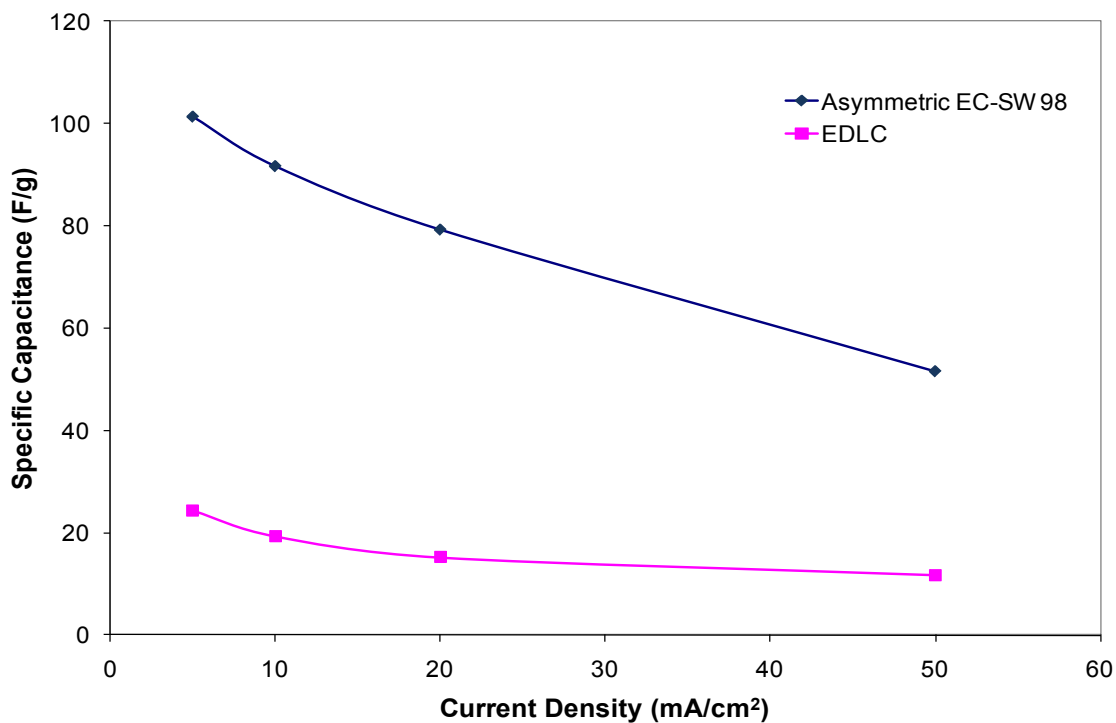


Figure C.17. Specific capacitance as a function of discharge current density of SW 98 and EDLC (95 wt% YP-50F electrodes).

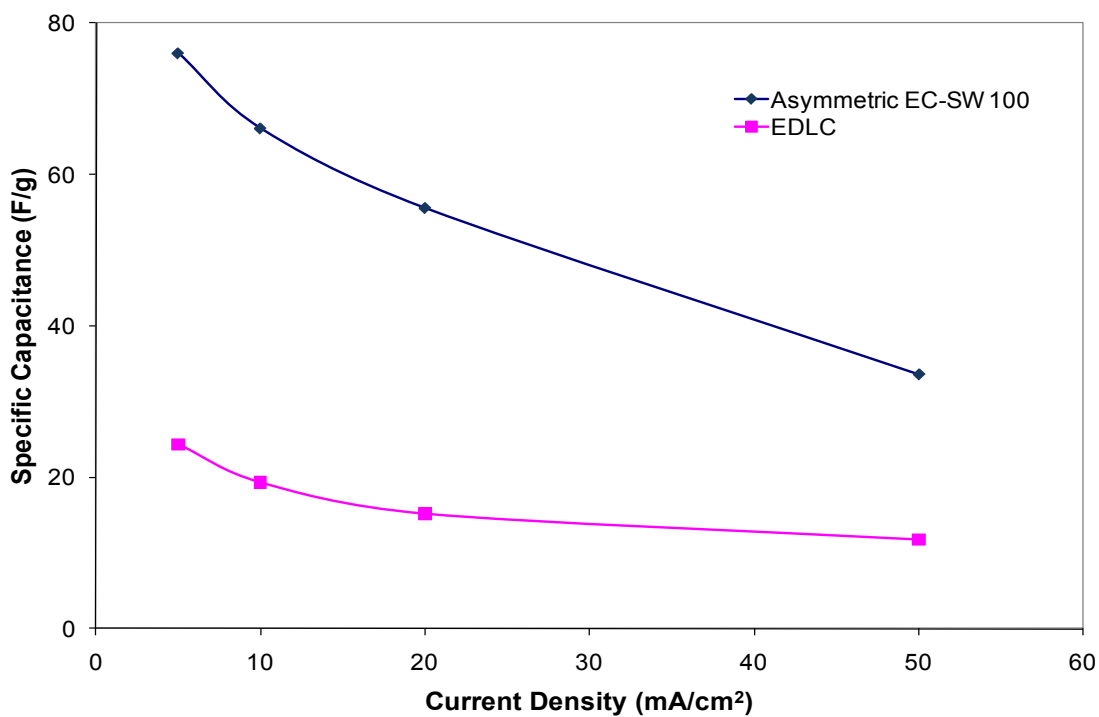


Figure C.18. Specific capacitance as a function of discharge current density of SW 100 and EDLC (95 wt% YP-50F electrodes).

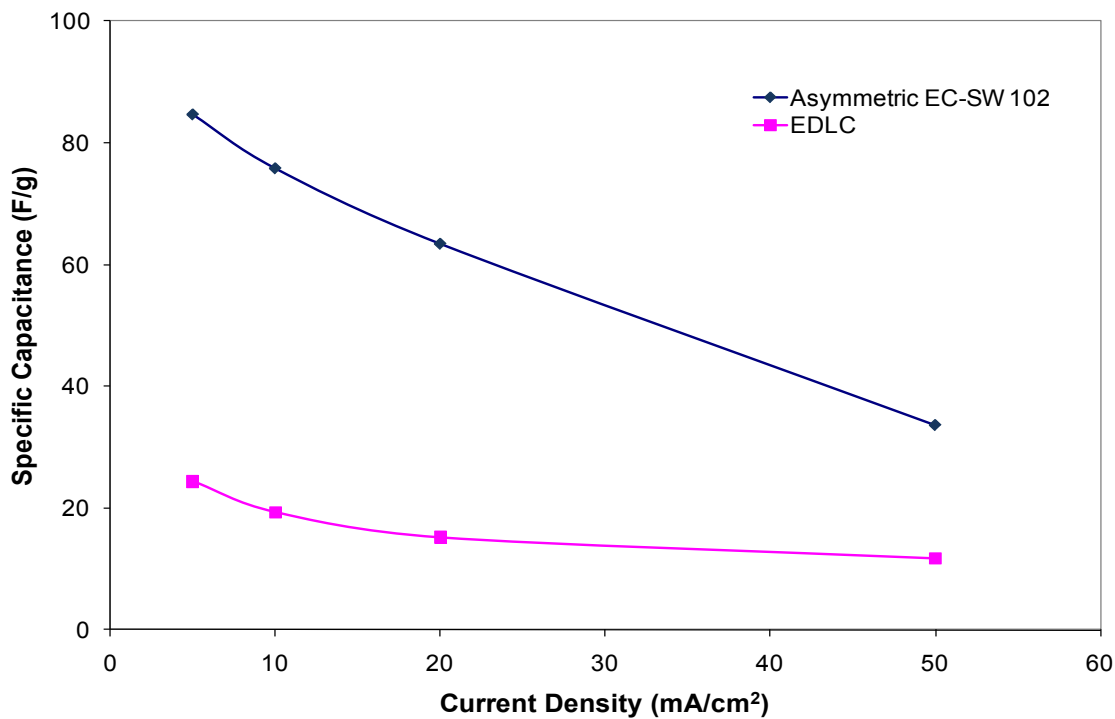


Figure C.19. Specific capacitance as a function of discharge current density of SW 102 and EDLC (95 wt% YP-50F electrodes).

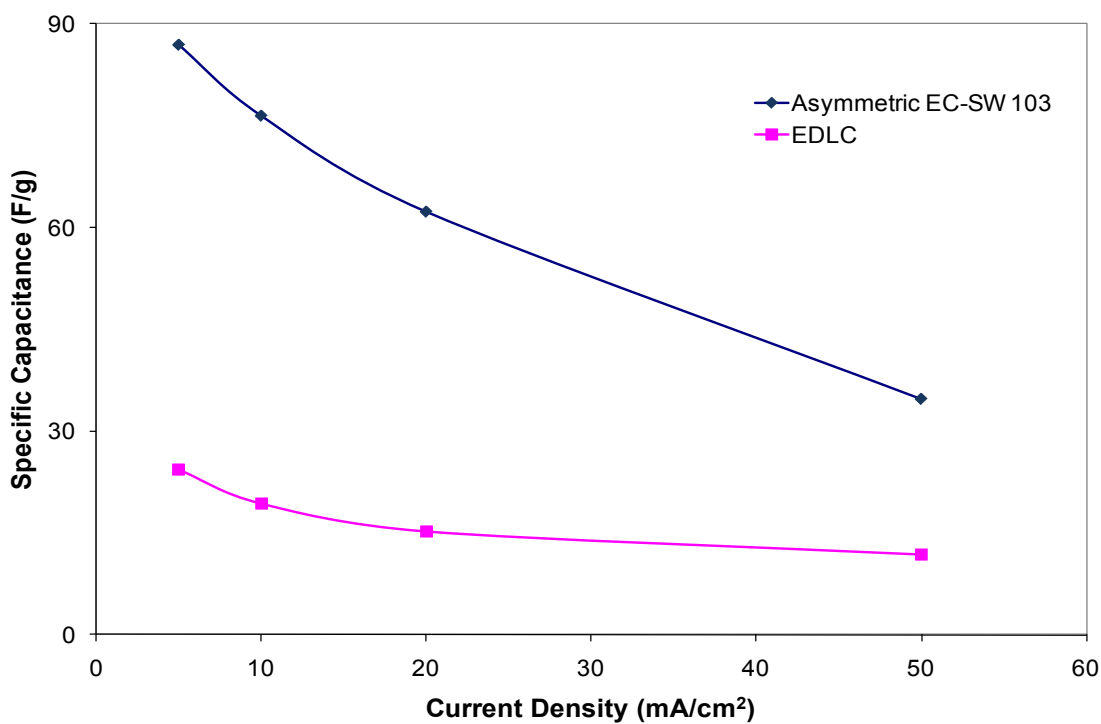


Figure C.20. Specific capacitance as a function of discharge current density of SW 103 and EDLC (95 wt% YP-50F electrodes).

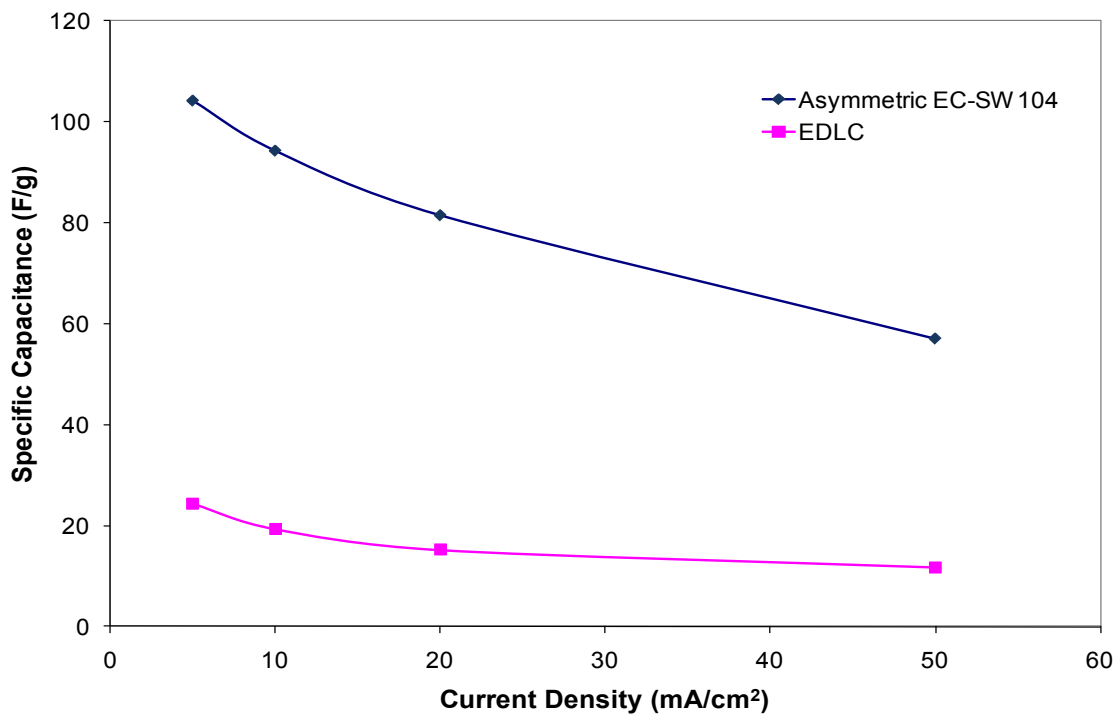


Figure C.21. Specific capacitance as a function of discharge current density of SW 104 and EDLC (95 wt% YP-50F electrodes).

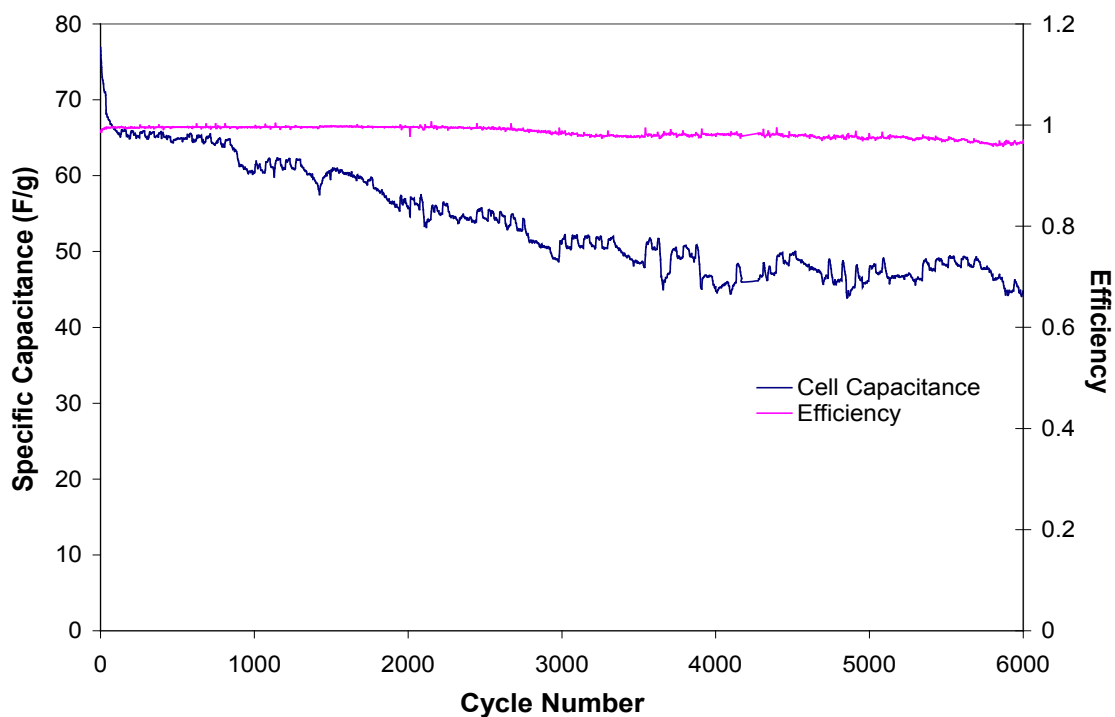


Figure C.22. Specific capacitance and efficiency as a function of cycle number of SW 93 (mass ratio of 1.49) cycled at 10 mA/cm²

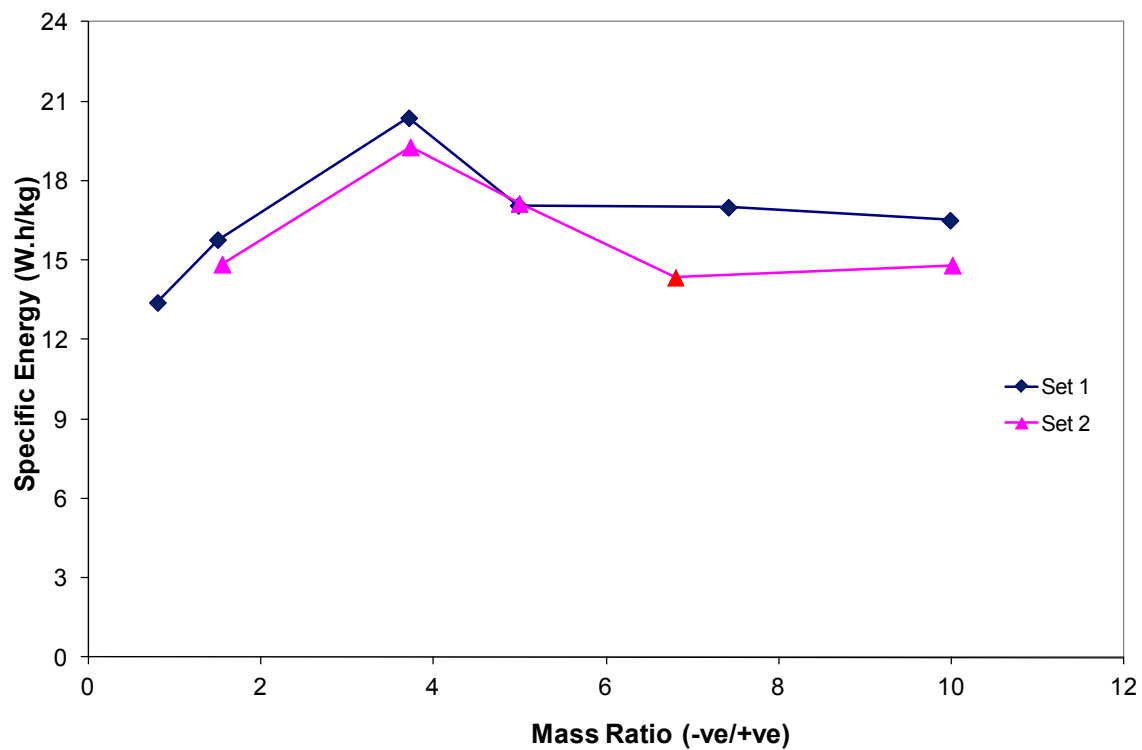


Figure C.23. Specific energy as a function of mass ratio of all the asymmetric cells cycling at a current density of 10 mA/cm^2 . The red color point has a lower value was due to the cell was having a lower efficiency (~86%).

Table C.3.
Average values of every 1,000 cycles cycled at 10 mA/cm².

Average values after x cycles #s	Cell #	Mass Ratio (-ve/+ve)	Specific Capacitance (F/g)	Specific Energy (W.h/kg)	Specific Power (W/kg)	Efficiency
1,000	SW 92	0.80	55.33	12.61	80.47	99.76%
	SW 93	1.49	65.45	13.67	73.19	99.54%
	SW 91	1.54	66.90	13.90	104.15	86.24%
	SW 89	4.98	74.95	16.63	134.75	98.62%
2,000	SW 92	0.80	54.21	12.36	80.41	99.76%
	SW 93	1.49	62.48	12.93	73.02	99.60%
	SW 89	4.98	68.81	15.52	135.18	98.95%
3,000	SW 92	0.80	53.41	12.18	80.36	99.76%
	SW 93	1.49	59.62	12.25	72.94	99.48%
4,000	SW 92	0.80	52.77	12.02	80.33	99.74%
	SW 93	1.49	57.18	11.68	72.80	99.12%
5,000	SW 92	0.80	52.13	11.87	80.30	99.74%
	SW 93	1.49	55.37	11.24	72.66	98.90%
6,000	SW 92	0.80	51.44	11.70	80.28	99.73%
	SW 93	1.49	54.03	10.92	72.55	98.59%
7,000	SW 92	0.80	50.69	11.52	80.25	99.72%
	SW 93	1.49	52.07	10.43	72.31	98.35%
8,000	SW 92	0.80	49.95	11.33	80.22	99.69%
	SW 93	1.49	50.29	9.96	72.02	98.19%
9,000	SW 92	0.80	49.17	11.12	80.16	99.62%
	SW 93	1.49	49.47	9.75	71.84	98.16%
10,000	SW 92	0.80	48.40	10.89	79.98	99.50%
	SW 93	1.49	49.10	9.64	71.74	98.14%

Table C.4.
Summary table of all asymmetric capacitors (nickel-carbon foam/95 wt% Ketjenblack EC-600JD) with different mass ratios.

Cell #/ Mass Ratio (-ve/+ve)*	Current Density (mA/cm ²)	Cell Capacitance** (F)	Specific Capacitance (F/g)	Specific Energy (W.h/kg)	Specific Power (W/kg)	Efficiency
SW 96	5	6.20	73.22	16.23	135.49	96.97%
4.79	10	5.89	69.47	13.22	258.09	98.51%
4.66	20	5.40	63.68	8.72	465.73	99.30%
	50	4.26	50.30	2.49	886.77	99.20%
SW 101	5	8.83	34.77	8.55	46.31	99.05%
0.50	10	8.19	32.26	7.67	91.98	99.25%
0.39	20	7.12	28.05	6.14	178.53	99.67%
	50	4.80	18.91	3.17	405.81	99.73%
SW 105***	5	4.97	57.40	12.99	136.75	98.62%
12.87	10	4.44	51.36	10.67	265.25	99.15%
6.50	20	3.66	42.31	7.21	495.52	98.77%
	50	2.59	29.91	3.05	1044.21	99.24%

* the first mass ratio indicates the measured mass ratio based on 0.2 C-rate discharge capacity of positive electrode, where as the second mass ratio indicates the target mass ratio

** difference in cell capacitance may due to thickness and diameter of the electrodes

*** technical fault during the deposition process-the position of the electrode shifted

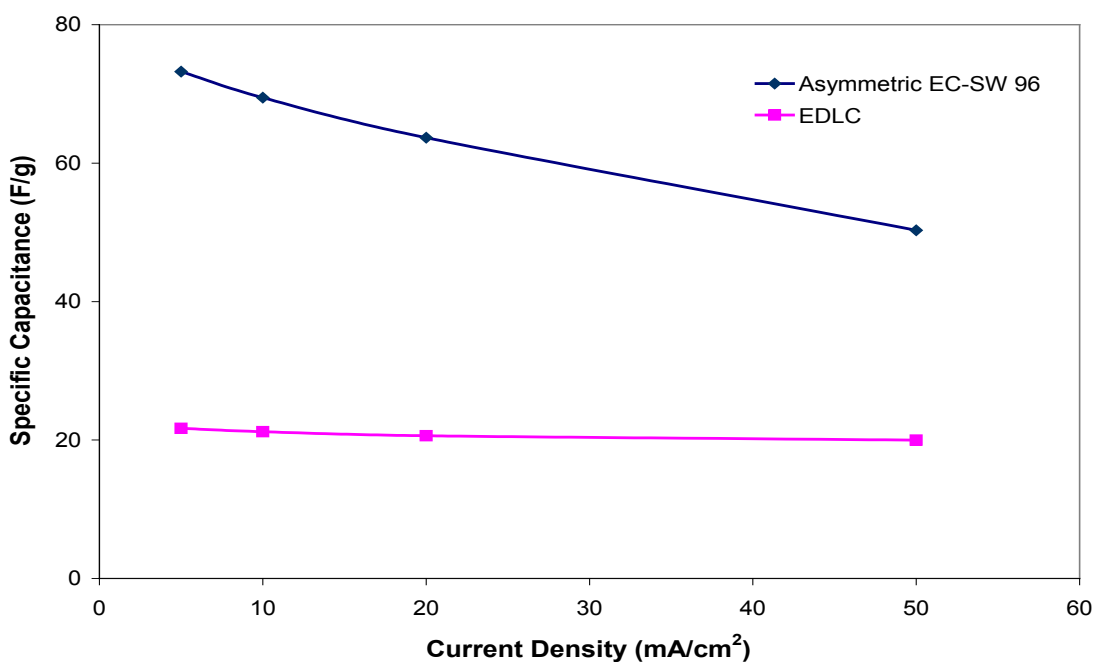


Figure C.24. Specific capacitance as a function of discharge current density of SW 96 and EDLC (95 wt% Ketjenblack EC-600JD electrodes).

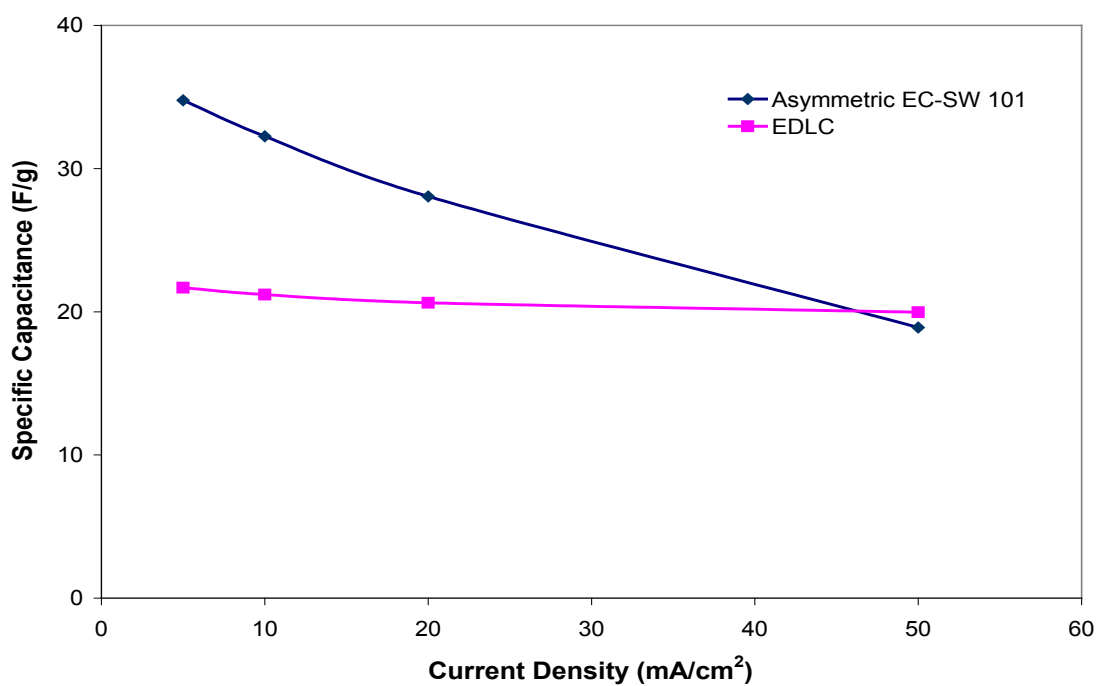


Figure C.25. Specific capacitance as a function of discharge current density of SW 101 and EDLC (95 wt% Ketjenblack EC-600JD electrodes).

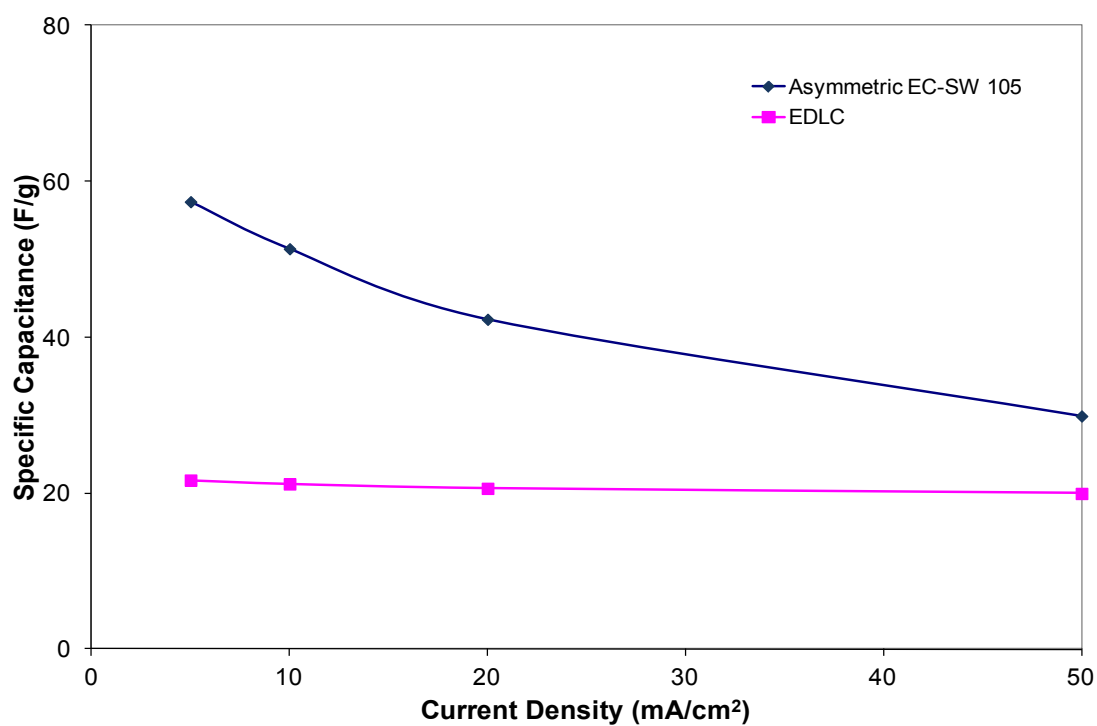


Figure C.26. Specific capacitance as a function of discharge current density of SW 105 and EDLC (95 wt% Ketjenblack EC-600JD electrodes).

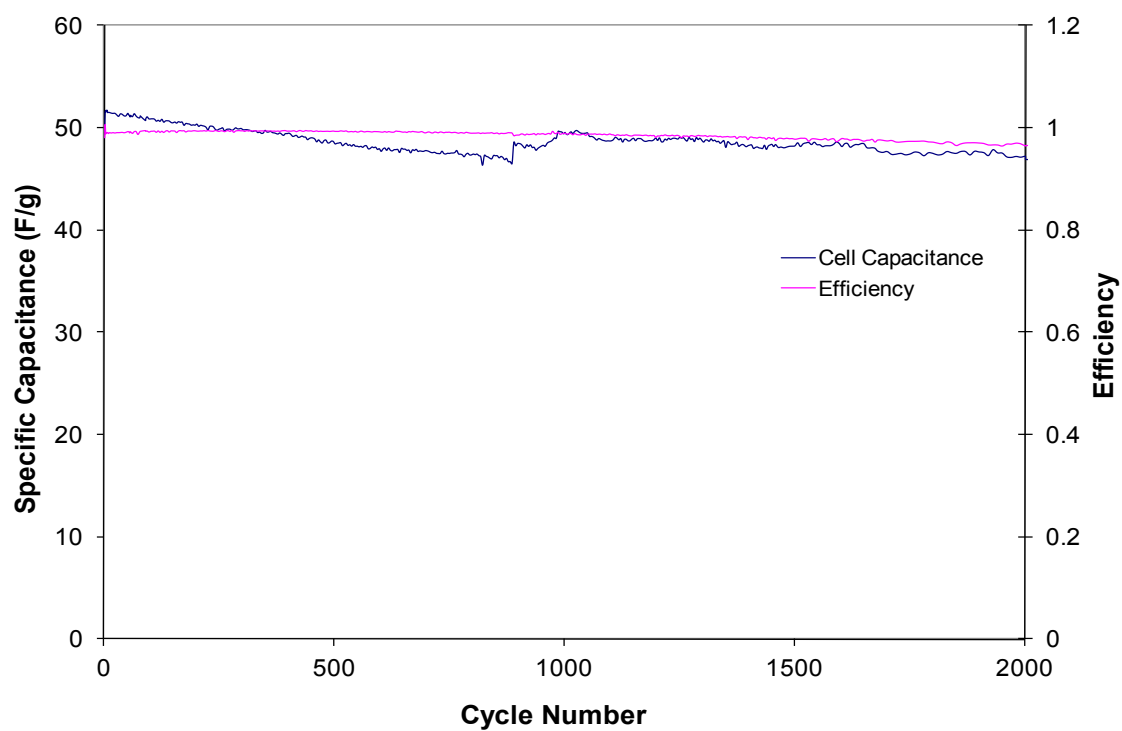


Figure C.27. Specific capacitance and efficiency as a function of cycle number of SW 105 (mass ratio of 12.87) cycled at 10 mA/cm^2 .

Appendix D Permission of Reprint

The material in the following paper was reproduced in Figure 1.1.

RightsLink - Your Account

Page 1 of 4

ELSEVIER LICENSE TERMS AND CONDITIONS

Nov 15, 2011

This is a License Agreement between Wen Nee Yeo ("You") and Elsevier ("Elsevier") provided by Copyright Clearance Center ("CCC"). The license consists of your order details, the terms and conditions provided by Elsevier, and the payment terms and conditions.

All payments must be made in full to CCC. For payment instructions, please see information listed at the bottom of this form.

Supplier	Elsevier Limited The Boulevard, Langford Lane Kidlington, Oxford, OX5 1GB, UK
Registered Company Number	1982084
Customer name	Wen Nee Yeo
Customer address	2102G Woodmar Dr Houghton, MI 49931
License number	2777660739295
License date	Oct 28, 2011
Licensed content publisher	Elsevier
Licensed content publication	Electrochemistry Communications
Licensed content title	Development and implementation of a high temperature electrochemical cell for lithium batteries
Licensed content author	David Muñoz-Rojas, Jean-Bernard Leriche, Charles Delacourt, Philippe Poizot, Ma Rosa Palacin, Jean-Marie Tarascon
Licensed content date	April 2007
Licensed content volume number	9
Licensed content issue number	4
Number of pages	5
Start Page	708
End Page	712
Type of Use	reuse in a thesis/dissertation
Portion	figures/tables/illustrations
Number of figures/tables/illustrations	1
Format	both print and electronic
Are you the author of this Elsevier article?	No
Will you be translating?	No
Order reference number	
Title of your thesis/dissertation	DEVELOPMENT AND TESTING OF AN ASYMMETRIC CAPACITOR WITH A NICKEL-CARBON FOAM POSITIVE ELECTRODE

<https://s100.copyright.com/MyAccount/viewPrintableLicenseDetails?licenseOID=20111...> 11/15/2011

Expected completion date	Dec 2011
Estimated size (number of pages)	150
Elsevier VAT number	GB 494 6272 12
Permissions price	0.00 USD
VAT/Local Sales Tax	0.0 USD / 0.0 GBP
Total	0.00 USD
Terms and Conditions	

INTRODUCTION

1. The publisher for this copyrighted material is Elsevier. By clicking "accept" in connection with completing this licensing transaction, you agree that the following terms and conditions apply to this transaction (along with the Billing and Payment terms and conditions established by Copyright Clearance Center, Inc. ("CCC"), at the time that you opened your Rightslink account and that are available at any time at <http://myaccount.copyright.com>).

GENERAL TERMS

2. Elsevier hereby grants you permission to reproduce the aforementioned material subject to the terms and conditions indicated.
3. Acknowledgement: If any part of the material to be used (for example, figures) has appeared in our publication with credit or acknowledgement to another source, permission must also be sought from that source. If such permission is not obtained then that material may not be included in your publication/copies. Suitable acknowledgement to the source must be made, either as a footnote or in a reference list at the end of your publication, as follows:
 "Reprinted from Publication title, Vol /edition number, Author(s), Title of article / title of chapter, Pages No., Copyright (Year), with permission from Elsevier [OR APPLICABLE SOCIETY COPYRIGHT OWNER]." Also Lancet special credit -
 "Reprinted from The Lancet, Vol. number, Author(s), Title of article, Pages No., Copyright (Year), with permission from Elsevier."
4. Reproduction of this material is confined to the purpose and/or media for which permission is hereby given.
5. Altering/Modifying Material: Not Permitted. However figures and illustrations may be altered/adapted minimally to serve your work. Any other abbreviations, additions, deletions and/or any other alterations shall be made only with prior written authorization of Elsevier Ltd. (Please contact Elsevier at permissions@elsevier.com)
6. If the permission fee for the requested use of our material is waived in this instance, please be advised that your future requests for Elsevier materials may attract a fee.
7. Reservation of Rights: Publisher reserves all rights not specifically granted in the combination of (i) the license details provided by you and accepted in the course of this licensing transaction, (ii) these terms and conditions and (iii) CCC's Billing and Payment terms and conditions.
8. License Contingent Upon Payment: While you may exercise the rights licensed immediately upon issuance of the license at the end of the licensing process for the transaction, provided that you have disclosed complete and accurate details of your proposed use, no license is finally effective unless and until full payment is received from you (either by publisher or by CCC) as provided in CCC's Billing and Payment terms and conditions. If full payment is not received on a timely basis, then any license preliminarily granted shall be deemed automatically revoked and shall be void as if never granted. Further, in the event that you breach any of these terms and conditions or any of CCC's Billing and Payment terms and conditions, the license is automatically revoked and shall be void as if never granted. Use of materials as described in a revoked license, as well as any use of the materials beyond the scope of an unrevoked license, may constitute copyright infringement and publisher reserves the right to take any and all action to protect its copyright in the materials.
9. Warranties: Publisher makes no representations or warranties with respect to the licensed material.
10. Indemnity: You hereby indemnify and agree to hold harmless publisher and CCC, and their respective officers, directors, employees and agents, from and against any and all claims arising out of your use of the licensed material other than as specifically authorized pursuant to this license.
11. No Transfer of License: This license is personal to you and may not be sublicensed, assigned, or transferred by you to any other person without publisher's written permission.
12. No Amendment Except in Writing: This license may not be amended except in a writing signed by both parties (or, in the case of publisher, by CCC on publisher's behalf).
13. Objection to Contrary Terms: Publisher hereby objects to any terms contained in any purchase order, acknowledgment, check endorsement or other writing prepared by you, which terms are inconsistent with these terms and conditions or CCC's Billing and Payment terms and conditions. These terms and conditions, together with CCC's

Billing and Payment terms and conditions (which are incorporated herein), comprise the entire agreement between you and publisher (and CCC) concerning this licensing transaction. In the event of any conflict between your obligations established by these terms and conditions and those established by CCC's Billing and Payment terms and conditions, these terms and conditions shall control.

14. **Revocation:** Elsevier or Copyright Clearance Center may deny the permissions described in this License at their sole discretion, for any reason or no reason, with a full refund payable to you. Notice of such denial will be made using the contact information provided by you. Failure to receive such notice will not alter or invalidate the denial. In no event will Elsevier or Copyright Clearance Center be responsible or liable for any costs, expenses or damage incurred by you as a result of a denial of your permission request, other than a refund of the amount(s) paid by you to Elsevier and/or Copyright Clearance Center for denied permissions.

LIMITED LICENSE

The following terms and conditions apply only to specific license types:

15. **Translation:** This permission is granted for non-exclusive world **English** rights only unless your license was granted for translation rights. If you licensed translation rights you may only translate this content into the languages you requested. A professional translator must perform all translations and reproduce the content word for word preserving the integrity of the article. If this license is to re-use 1 or 2 figures then permission is granted for non-exclusive world rights in all languages.

16. **Website:** The following terms and conditions apply to electronic reserve and author websites:

Electronic reserve: If licensed material is to be posted to website, the web site is to be password-protected and made available only to bona fide students registered on a relevant course if:

This license was made in connection with a course,

This permission is granted for 1 year only. You may obtain a license for future website posting,

All content posted to the web site must maintain the copyright information line on the bottom of each image,

A hyper-text must be included to the Homepage of the journal from which you are licensing at

<http://www.sciencedirect.com/science/journal/xxxxx> or the Elsevier homepage for books at <http://www.elsevier.com> , and

Central Storage: This license does not include permission for a scanned version of the material to be stored in a central repository such as that provided by Heron/XanEdu.

17. **Author website** for journals with the following additional clauses:

All content posted to the web site must maintain the copyright information line on the bottom of each image, and

the permission granted is limited to the personal version of your paper. You are not allowed to download and post the published electronic version of your article (whether PDF or HTML, proof or final version), nor may you scan the printed edition to create an electronic version,

A hyper-text must be included to the Homepage of the journal from which you are licensing at

<http://www.sciencedirect.com/science/journal/xxxxx> . As part of our normal production process, you will receive an e-mail notice when your article appears on Elsevier's online service ScienceDirect (www.sciencedirect.com). That e-mail will include the article's Digital Object Identifier (DOI). This number provides the electronic link to the published article and should be included in the posting of your personal version. We ask that you wait until you receive this e-mail and have the DOI to do any posting.

Central Storage: This license does not include permission for a scanned version of the material to be stored in a central repository such as that provided by Heron/XanEdu.

18. **Author website** for books with the following additional clauses:

Authors are permitted to place a brief summary of their work online only.

A hyper-text must be included to the Elsevier homepage at <http://www.elsevier.com>

All content posted to the web site must maintain the copyright information line on the bottom of each image

You are not allowed to download and post the published electronic version of your chapter, nor may you scan the printed edition to create an electronic version.

Central Storage: This license does not include permission for a scanned version of the material to be stored in a central repository such as that provided by Heron/XanEdu.

19. **Website** (regular and for author): A hyper-text must be included to the Homepage of the journal from which you are licensing at <http://www.sciencedirect.com/science/journal/xxxxx> or for books to the Elsevier homepage at <http://www.elsevier.com>

20. **Thesis/Dissertation:** If your license is for use in a thesis/dissertation your thesis may be submitted to your institution in either print or electronic form. Should your thesis be published commercially, please reapply for permission. These requirements include permission for the Library and Archives of Canada to supply single copies, on demand, of the complete thesis and include permission for UMI to supply single copies, on demand, of the complete thesis. Should your thesis be published commercially, please reapply for permission.

21. Other Conditions:

v1.6

If you would like to pay for this license now, please remit this license along with your payment made payable to "COPYRIGHT CLEARANCE CENTER" otherwise you will be invoiced within 48 hours of the license date. Payment should be in the form of a check or money order referencing your account number and this invoice number RLNK0.

Once you receive your invoice for this order, you may pay your invoice by credit card. Please follow instructions provided at that time.

Make Payment To:
Copyright Clearance Center
Dept 001
P.O. Box 843006
Boston, MA 02284-3006

For suggestions or comments regarding this order, contact RightsLink Customer Support:
customercare@copyright.com or +1-877-622-5543 (toll free in the US) or +1-978-646-2777.

Gratis licenses (referencing \$0 in the Total field) are free. Please retain this printable license for your reference. No payment is required.

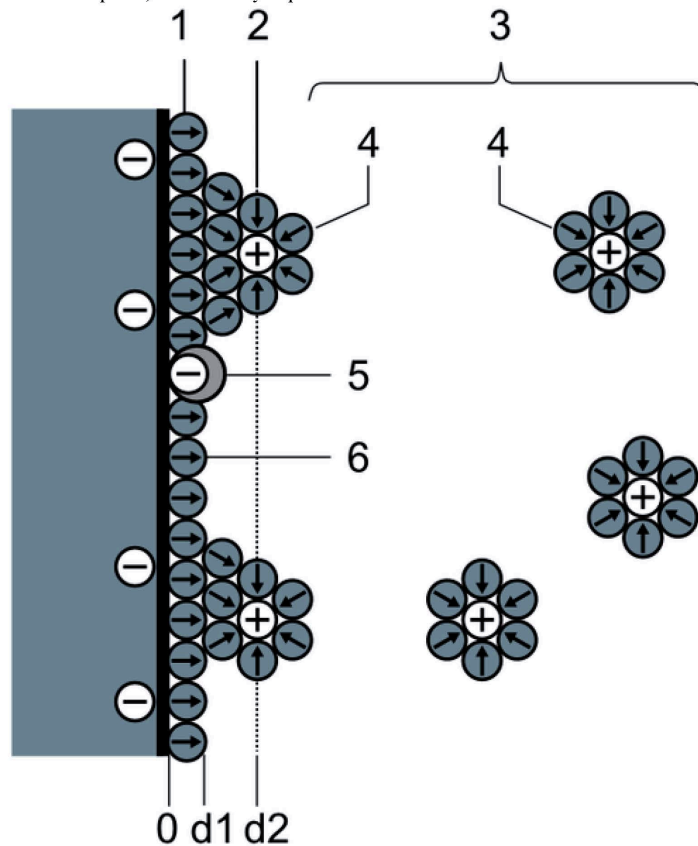
The material in the following paper was reproduced in Figure 2.2.

File:Electric double-layer (BMD model) NT.PNG - Wikipedia, the free encyclopedia

Page 1 of 3

File:Electric double-layer (BMD model) NT.PNG

From Wikipedia, the free encyclopedia



Size of this preview: 506 × 600 pixels. Other resolutions: 202 × 240 pixels.
Full resolution (540 × 640 pixels, file size: 61 KB, MIME type: image/png)



This is a file from the Wikimedia Commons
(https://commons.wikimedia.org/wiki/Main_Page) . Information from its **description page**
there ([https://commons.wikimedia.org/wiki/File:Electric_double-layer_\(BMD_model\)_NT.PNG](https://commons.wikimedia.org/wiki/File:Electric_double-layer_(BMD_model)_NT.PNG)) is shown below.

Commons is a freely licensed media file repository. You can help
(<https://commons.wikimedia.org/wiki/Commons:Welcome>) .

[http://en.wikipedia.org/wiki/File:Electric_double-layer_\(BMD_model\)_NT.PNG](http://en.wikipedia.org/wiki/File:Electric_double-layer_(BMD_model)_NT.PNG)

11/15/2011



This diagram image could be recreated **using vector graphics as an SVG file**. This has several advantages; see Commons:Media for cleanup for more information. If an SVG form of this image is already available, please upload it. After uploading an SVG, replace this template with `{{vector version available|new image name.svg}}`.

Summary

Description **English:** Electric double-layer (BMD model) No text 1.IHP（Inner Helmholtz Layer） 2.OHP（Outer Helmholtz Layer） 3.Diffusion layer 4.Solvated ions 5.Peculiar adsorptive ions 6.Solvent molecule

Date

2008/08/02 (ref:岡村勉夫著 『電気二重層キャパシタと蓄電システム』 日刊工業新聞社 2001年2月28日第2版第1刷 ISBN 4526-047139)

Source

Own work

Author

Tosaka

Permission

(Reusing this file) See below.

Licensing

I, the copyright holder of this work, hereby publish it under the following license:

This file is licensed under the Creative Commons Attribution 3.0 Unported (<http://creativecommons.org/licenses/by/3.0/deed.en>) license.



You are free:

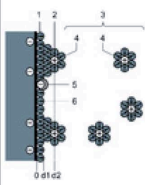
- **to share** – to copy, distribute and transmit the work
- **to remix** – to adapt the work

Under the following conditions:

- **attribution** – You must attribute the work in the manner specified by the author or licensor (but not in any way that suggests that they endorse you or your use of the work).

File history

Click on a date/time to view the file as it appeared at that time.

	Date/Time	Thumbnail	Dimensions	User	Comment
current	21:40, 1 August 2008		540 × 640 (61 KB)	Tosaka	{{{Information Description={{en 1=Electric double-layer (BMD model) No text 1.IHP (Inner Helmholtz Layer) 2.OHP (Outer Helmholtz Layer) 3.Diffusion layer 4.Solvated ions 5.Peculiar adsorptive ions 6.Solvent molecule}}} Source=Own work by uploader A)

File usage

The following pages on the English Wikipedia link to this file (pages on other projects are not listed):

- Double layer (interfacial)

Global file usage

The following other wikis use this file:

- Usage on de.wikipedia.org
 - Doppelschichtkondensator
 - Lithium-Ionen-Kondensator
- Usage on it.wikipedia.org
 - Chimica delle interfasi
 - Doppio strato elettrico
 - Corrente capacitiva

Retrieved from "http://en.wikipedia.org/wiki/File:Electric_double-layer_(BMD_model)_NT.PNG"

The material in the following paper was reproduced in Figure 2.5.

RightsLink - Your Account

Page 1 of 3

SPRINGER LICENSE TERMS AND CONDITIONS

Nov 15, 2011

This is a License Agreement between Wen Nee Yeo ("You") and Springer ("Springer") provided by Copyright Clearance Center ("CCC"). The license consists of your order details, the terms and conditions provided by Springer, and the payment terms and conditions.

All payments must be made in full to CCC. For payment instructions, please see information listed at the bottom of this form.

License Number	2777670730327
License date	Oct 28, 2011
Licensed content publisher	Springer
Licensed content publication	Journal of Solid State Electrochemistry
Licensed content title	A nonstoichiometric structural model to characterize changes in the nickel hydroxide electrode during cycling
Licensed content author	Venkat Srinivasan
Licensed content date	Feb 1, 2005
Volume number	9
Issue number	2
Type of Use	Thesis/Dissertation
Portion	Figures
Author of this Springer article	No
Order reference number	
Title of your thesis / dissertation	DEVELOPMENT AND TESTING OF AN ASYMMETRIC CAPACITOR WITH A NICKEL-CARBON FOAM POSITIVE ELECTRODE
Expected completion date	Dec 2011
Estimated size(pages)	150
Total	0.00 USD

Terms and Conditions

Introduction

The publisher for this copyrighted material is Springer Science + Business Media. By clicking "accept" in connection with completing this licensing transaction, you agree that the following terms and conditions apply to this transaction (along with the Billing and Payment terms and conditions established by Copyright Clearance Center, Inc. ("CCC"), at the time that you opened your Rightslink account and that are available at any time at <http://myaccount.copyright.com>).

Limited License

With reference to your request to reprint in your thesis material on which Springer Science and Business Media control the copyright, permission is granted, free of charge, for the use indicated in your enquiry. Licenses are for one-time use only with a maximum distribution equal to the number that you identified in the licensing process.

This License includes use in an electronic form, provided it is password protected or on the university's intranet, destined to microfilming by UMI and University repository. For any other electronic use, please contact Springer at (permissions.dordrecht@springer.com or permissions.heidelberg@springer.com)

The material can only be used for the purpose of defending your thesis, and with a maximum of 100 extra copies in paper.

<https://s100.copyright.com/MyAccount/viewPrintableLicenseDetails?licenseOID=20111...> 11/15/2011

Although Springer holds copyright to the material and is entitled to negotiate on rights, this license is only valid, provided permission is also obtained from the (co) author (address is given with the article/chapter) and provided it concerns original material which does not carry references to other sources (if material in question appears with credit to another source, authorization from that source is required as well). Permission free of charge on this occasion does not prejudice any rights we might have to charge for reproduction of our copyrighted material in the future.

Altering/Modifying Material: Not Permitted

However figures and illustrations may be altered minimally to serve your work. Any other abbreviations, additions, deletions and/or any other alterations shall be made only with prior written authorization of the author(s) and/or Springer Science + Business Media. (Please contact Springer at permissions.dordrecht@springer.com or permissions.heidelberg@springer.com)

Reservation of Rights

Springer Science + Business Media reserves all rights not specifically granted in the combination of (i) the license details provided by you and accepted in the course of this licensing transaction, (ii) these terms and conditions and (iii) CCC's Billing and Payment terms and conditions.

Copyright Notice:

Please include the following copyright citation referencing the publication in which the material was originally published. Where wording is within brackets, please include verbatim.

"With kind permission from Springer Science+Business Media: <book/journal title, chapter/article title, volume, year of publication, page, name(s) of author(s), figure number(s), and any original (first) copyright notice displayed with material>."

Warranties: Springer Science + Business Media makes no representations or warranties with respect to the licensed material.

Indemnity

You hereby indemnify and agree to hold harmless Springer Science + Business Media and CCC, and their respective officers, directors, employees and agents, from and against any and all claims arising out of your use of the licensed material other than as specifically authorized pursuant to this license.

No Transfer of License

This license is personal to you and may not be sublicensed, assigned, or transferred by you to any other person without Springer Science + Business Media's written permission.

No Amendment Except in Writing

This license may not be amended except in a writing signed by both parties (or, in the case of Springer Science + Business Media, by CCC on Springer Science + Business Media's behalf).

Objection to Contrary Terms

Springer Science + Business Media hereby objects to any terms contained in any purchase order, acknowledgment, check endorsement or other writing prepared by you, which terms are inconsistent with these terms and conditions or CCC's Billing and Payment terms and conditions. These terms and conditions, together with CCC's Billing and Payment terms and conditions (which are incorporated herein), comprise the entire agreement between you and Springer Science + Business Media (and CCC) concerning this licensing transaction. In the event of any conflict between your obligations established by these terms and conditions and those established by CCC's Billing and Payment terms and conditions, these terms and conditions shall control.

Jurisdiction

All disputes that may arise in connection with this present License, or the breach thereof, shall be settled exclusively by the country's law in which the work was originally published.

Other terms and conditions:

v1.2

If you would like to pay for this license now, please remit this license along with your payment made payable to "COPYRIGHT CLEARANCE CENTER" otherwise you will be invoiced within 48 hours of the license date. Payment should be in the form of a check or money order referencing your account number and this invoice number RLNK0.

Once you receive your invoice for this order, you may pay your invoice by credit card. Please follow instructions provided at that time.

Make Payment To:
Copyright Clearance Center
Dept 001
P.O. Box 843006

Boston, MA 02284-3006

For suggestions or comments regarding this order, contact RightsLink Customer Support:
customercare@copyright.com or +1-877-622-5543 (toll free in the US) or +1-978-646-2777.

Gratis licenses (referencing \$0 in the Total field) are free. Please retain this printable license for your reference. No payment is required.
